universität wien

DIPLOMARBEIT

VPAC receptors as target for anti-cancer drug delivery

angestrebter akademischer Grad

Magistra der Naturwissenschaften (Mag.rer.nat.)

Verfasserin:	Raphaela Elisabeth Kaisler
Matrikel-Nummer:	0301555
Studienrichtung (lt. Studienblatt):	A490
Betreuer:	a.o. Univ.Prof. Dr. Wilhelm Mosgöller

Wien, am 04.02.2008

Acknowledgement

I am very grateful to a.o. Univ.Prof. Dr. Wilhelm Mosgöller for supervising my work in a helpful and friendly way.

Further I thank my colleagues Anna Ortner and Sigrid Hensler for the nice atmosphere and their suggestions and hints which helped me to perform my tasks.
Special thanks go to a.o. Univ.Prof. Dr. Gottfried Köhler who offered me a fruitful collaboration at the Max F. Perutz laboratories, Dr. Bohrgasse 9, A-1030 Vienna Austria, to learn and perform Fluorescence Correlation Spectroscopy (FCS) at his lab.

I also thank Univ. Prof. Dr. Michael Miksche, head of institute, for working at the Institute of Cancer Research, Clinic internal medicine-1 (KIM-1) Medical University, Borschkegasse 8a, A-1090 Vienna Austria.

I am grateful that most peptides were synthesised and sponsored from the company piCHEM, Graz, Austria.

Further I thank Ruth Prassl (Institute of Biophysics and Nanosystems Research, Academy of Sciences, Graz, Austria) for the synthesis of liposomes and also Andreas Zimmer (Institute of Pharmacological Sciences, University Graz, Austria) for the production of proticles.

Great thanks go to Mrs. Maria Eisenbauer from tissue culture facility at the IKF, who provided me some of the cell lines and culture medium. She always helped me with cell culture questions. Further I thank a.o. Univ.Prof. Brigitte Marian who gave me some of the cell lines for this work. A great “thank you” to DI Dr. Chantal Rodgarkia-Dara who supported me in western blots and helped me many times with practical hints.

I also want to thank my parents, who supported me and enabled the education at the university and perform this work.

Index of Content

1 Introduction

1.1 VIP and PACAP

Vasoactive intestine peptide (VIP) was first isolated from porcine small intestine in the 1790s by Said and Mutt (1970; 1972). Vasoactive intestinal peptide (VIP) and pituiatary adenylate cyclase activating polypeptide (PACAP) belong to the same superfamiliy of structually releated growth hormone peptides (fig.1). This familiy also includes secretin, glucagon, growth hormon releasing factor (GRF) and the glucagon-like peptide-1 and 2 (GLP-1, GLP-2). This familiy of peptides has a common duplication of an anchestral gene, six genes encode nine bioactive hormons (Sherwood et al. 2000).

Pituitary adenylate cyclase activating peptide (PACAP) was first isolated from ovine hypothalamic tissue by Miyata et al. (1989). PACAP consists of 38 amino acids residues (PACAP-38) and is C-terminally amidated. It has the ability to stimulate adenlyate cyclase in cultured rat anterior pituitary cells.

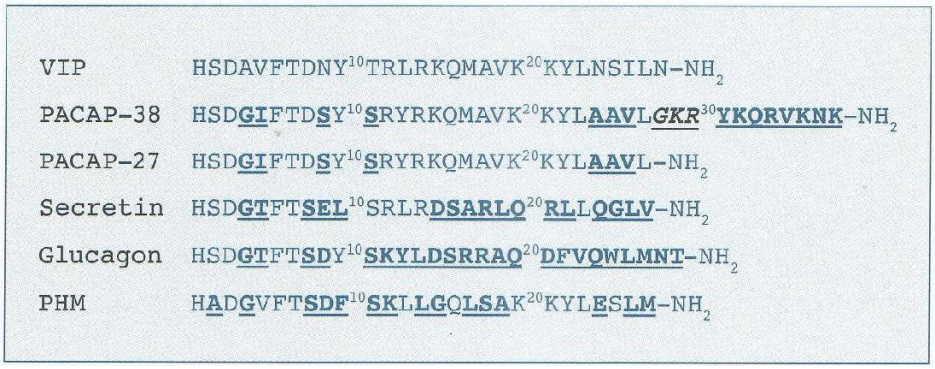

Figure 1. Human Amino acid sequence of the different members of the PACAP-VIP-GRF-glucagon superfamily. Underlined residues indicate amino acids different from those of VIP. In PACAP-38, GKR (Gly^{28}-Lys^{29}-Arg^{30}) is the internal cleavage- amidation site. [from (Bachem 2005)]

1.1.1 Cellular synthesis

VIP is a 28 amino acid long peptide which is synthesied as a precourser peptide of 170 amino acids containing a VIP-related peptide called PHM (fig.2).

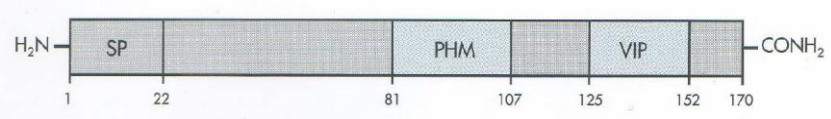

Figure 2. Schematic illustration of human prepro-VIP, and the localisation SP (signal pepide), mature PHM and VIP sequences. Amino acid numbers are shown below. [from (Bachem 2005)]

Posttranslational modifications occur in the endoplasmatic reticulum and by signal peptidase to a 148 aa pro-VIP. Pro-VIP is cleaved by the trypsin-like peptidase to VIP-

GRK (prepro-$VIP_{125-155}$) and PHI/PHM-GRK (prepro-VIP_{81-110}) and these precursers are cleaved by carboxypeptidase-B-like enzyme to VIP-G and PHI/PHM-G. Finally the peptide fragments are metabolized by an amidation enzyme and results in a biologically active C-terminally amidated VIP and PHI/PHM, which is released as a secretory vesicle (fig.3).

PROCESSING OF preproVIP

PreproVIP (170 aa)	
↓	signal peptidase
ProVIP (149 aa)	
↓	trypsin-like enzyme
VIP-GKR (31 aa)	
+ PHM-GKR (30 aa)	
↓	carboxypeptidase B-like enzymes
VIP-G (29 aa)	
+ PHM-G (28 aa)	
↓	amidation enzyme
VIP-NH_2 (28 aa)	
+ PHM-NH_2 (27 aa)	

Figure 3. Processing steps from prepro-VIP to 28 amino acids long VIP. The peptides substrates and products are indicated on the left and the number of amino acids is indicated in parentheses. The processing enzymes are shown on the right. [from (Moody 1996)]

VIP precursers can also be processd by an alternative splicing pathway. In this route the normal cleaving site after PHI remains uncleaved, resulting in a C-terminally extended form termed PHV (peptide with N-terminal histidine and C-terminal valine).

PACAP occures in two biological active stages, PACAP-38 and an alternative splice variant corresponding to its N-terminal 27 amino acids (PACAP-27). PACAP-38 sequence contains an internal cleavage-amidation site (Gly^{28}-Lys^{29}-Arg^{30}) which can be used to generate PACAP-27 (fig.4). PACAP-38 is the prodominant form, but the distribution and ratio of PACAP-38/-27 varies between tissues especially in the central nervous system (CNS), adrenal and testis (Sherwood et al. 2000).

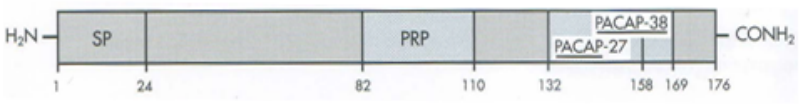

Figure 4. Schematic illustration of the general organisation of human prepro-PACAP, and the localisation of mature PRP; PACAP-27 and PACAP-38 sequence. Amino acid numbers are shown below; SP: signal peptide. [from (Bachem 2005)]

PACAP is hightly conserved during evolution, its amino acid sequence is identical in rat, sheep and human. It differs in frogs and some fishes, but with a complementarity of 86-92% (Sherwood et al. 2000). In mammals PACAP has a strong similarity with the VIP precurser. The posttranslational cleavage site of the 176 amino acid precurser (prepro-PACAP) results in the following peptides: PACAP-38, PACAP-27 and the 29 amino acid PACAP-relates peptide (PRP) which has some structure homology to PACAP-27 (fig.4). The N-terminal 28 amino acid sequence of PACAP-38 showes considerable sequence homology (68%) with VIP (fig.1), but its adenlyate cyclase stimulating activity is 1000 times greater than VIP.

As shown by circular dichroism and nuclear magnetic resonance, the N-terminus of VIP and PACAP-27 is essential for their biological activity (Christophe et al. 1988). The analyses of Christophe et al. revealed an alpha-helical structure of the amino acids 15-28 and two beta-turns at the position 1-4 and 6-10.

1.1.2 Biological activity

VIP has many important functions in cellular processes. It acts as neuropeptide in many tissues additionally to the intestine. It relaxes smooth muscles in blood vessel and the gut. The alternatively spliced peptide is as potent as VIP in relaxing smooth muscle (Moody 1996). VIP and PACAP can be a stimulator of mucose secretion.

In the nervous sytem VIP acts as neuromodulator, it was suggested to be associated with the “visceral forebrain system” that influences and temporarily controls cardiovascular, respiratory and gastrointestinal functions. In the endocrine system VIP activates hormone relase, like VIP released prolactin (PRL), luteinzing hormone (LH) and growth hormone (GH) from the pituitary gland. It acts on the pancras to release either insulin or glucagon, depending on the glucose level. VIP also functions on the exocrine pancreas to increase the bicarbonate output and acts on non-neuronal tissue such as the gonads and some immune cells. During embryogenesis, VIP is expressed in the embryonic brain and has trophic and mitogenic effects (Sherwood et al. 2000).

Like VIP, PACAP is involved in multiple biological processes including reproduction, development, growth, cardiovascular, respiratory and digestive function, immune response and circadian rhythms (Vaudry et al. 2000).

1.1.3 Receptors

VIP and the alternative splicing variants are selectively binding to surface membrane receptors. They belong to the large family of class II G-protein coupled receptors (GPCR), which have a common structure of seven transmembrane domains (7TM). These domains are linked together by three extracellular (EC1, EC2, EC3) and three intracellular (IC1, IC2, IC3) oligopeptide loops. The polypeptide has a long amino-terminal extracellular domain and an intracellular carboxyl terminus. GPCR share several important properties, the most important is the large N-terminal extracellular domain which contains 10 highly conserved amino acids including six cysteins, a putative N-terminal leader sequence and several potential N-glycosylation sites. G-protein coupled receptors trigger mainly the adenlyate cyclase pathway via stimulatory G_s-proteins (G_s). The stimulatory G_q-proteins (G_q) activate the inositol phospholipid signalling pathway (PLC/PI). There are three types of receptors which can interact with VIP and PACAP. According to the Union of Pharmacology (UIPHAR) the nomenclature of these human VPAC receptors (VIP/PACAP) has been classified in three subtypes: $VPAC_1$, $VPAC_2$ and PAC_1 (Harmar et al. 1998; Laburthe and Couvineau 2002).

1.1.3.1 $VPAC_1$

The first recombinant receptor for VIP and PACAP was isolated from rat lung by Ishihara et. al (2002), the human homologue has also been cloned and expressed in cell lines. The gene for the $VPAC_1$ is located on human chromosome 3p22, it has 13 exons ranging in the size from 42-1400bp. The receptor consists of 457 amino acid residues and is also known as VIP_1 or VIP/PACAP type II or PVR_2. $VPAC_1$ receptor has a high affinity for VIP and PACAP **(**IC_{50}, 1nM), low affinity for PHI, PHV (IC_{50}, 100nM, 3000nM) and secretin (IC_{50}, 1500nM) which differs from rat $VPAC_1$ affinity. Signal transduction primarily occurs via the adenlyate cyclase pathway.

Splice variants of $VPAC_1$ were recently discovered by Bokaei et al. (2006) where two novel human 5TM VPAC receptor isoforms are described. The isoforms are differently expressed in peripheral blood mononuclear and cord blood cells and in malignant hematopoietic-and epithelial-derived cancer cell lines. Five transmembrane (5TM) isoforms lack a G-protein binding site and therefore have a significantly decreased lower cAMP response production as to VIP.

$VPAC_1$ is found in certain regions in the brain, especially in the cerebral cortex and hippocampus and predominantly expressed in the peripheral tissue such as liver, lung and intestine (Ishihara et al. 1992; Usdin et al. 1994). $VPAC_1$ is also expressed by resting T lymphocytes and peripheral blood monocytes (Delgado et al. 1996).

1.1.3.2 $VPAC_2$

A second receptor that responds to VIP and PACAP with high affinity was first cloned from the rat olfactory bulb by Lutz et al. (1993). The receptor $VPAC_2$ is also known as VIP-R_2 or VIP/PACAP type III or PVR_3. $VPAC_2$ consists of 460 amino acid residues, the gene is located on chromosome 7q36.3 and it contains of 13 exons. Rat and human $VPAC_2$ recognize VIP (IC_{50}, 3-4nM), PHI and PHV (IC_{50}, 10-30nM) and PACAP-27 (IC_{50}, 10nM) and PACAP-38 (IC_{50}, 30mM). The receptors also recognize GRF and secretin with a very low affinity (IC_{50}, 5000-30.000nM). Ligand binding to $VPAC_2$ results in the preferential activation of adenlyate cyclase.

$VPAC_2$ expression is found in the CNS in high concentrations in the suprachiasmatic nucleus (SCN) and thalamus, in lower concentration in the hippocampus, brainstem, spinal cord and dorsal root ganglion (Sheward et al. 1995; Usdin et al. 1994). $VPAC_2$ is also distributed in several peripheral tissues, including pancreas, skeletal muscle and smooth muscles, kidney, stomach, heart and testis (Adamou et al. 1995; Krempels et al. 1995; Wei and Mojsov 1996).

1.1.3.3 PAC_1

A third receptor subtype was isolated by Pisegna and Wank (1993) from rat pancreatic acinar carcinoma cell line AR4-2J. This PACAP preferring receptor subtype is termed PAC_1 also known as VIP/PACAP type I or PVR_1. The receptor shows a high affinity for PACAP-27 and PACAP-38 (IC_{50}, 1nM) but a much lower affinity to VIP (IC_{50}, 1000nM), with very low affinities it also binds PHI, PHV, secretin and GRF. The PAC_1 gene is located on chromosome 7p14 and encodes 495 amino acids. Unlike to $VPAC_1$ and $VPAC_2$, PAC_1 has several splice variants without systematic nomenclature. PAC_1 receptors prefer both, the adenlyate cyclase (AC) and the phospholipase C (PLC) signalling pathway for signal transduction. The alternative splicing variants contain or lack two exons (hip and hop) in the third intracellular domain, therefore six alternative splice variants can occur. These have different signal transduction pathways. A splice

variant of PAC_1 in the third cytoplasmatic loop, hop2, was suggested to be involved in VIP-related neuroprotection in cell culture. VIP protects cells expressing hop2 from oxidative stress and mediates cytoprotective effects (Pilzer and Gozes 2006).
The receptor is predominantly expressed in the CNS, most abundantly in the olfactory bulb, thalamus, hypothalamus and granules cells of the cerebellum (Hashimoto et al. 1996; Spengler et al. 1993). It is also found in the adrenal medulla (Sundler et al. 1996).

1.1.3.4 Receptor selectivity

Site directed mutagenesis studies showed that the N-terminal ectodomain (N-ted) of VPAC receptor plays a crucial role in ligand binding. The physical interaction domains of VIP and $VPAC_1$ are the side chains at position 6, 22, 24 which are in direct contact with amino acids in the receptor´s N-ted domain. Short consensus repeats (SCR) which lie towards the N-terminus of the cell surface receptors play a crucial structural role. They are involved in ligand recognition. The N-terminal domain of VIP His^1-Phe^6 is largely disordered in solution whereas the C-terminal Ser^{25}-Asn^{28} are very flexible and close to a helical conformation state which was discovered by NMR studies (Laburthe et al. 2007). The author described a “two domain model” for VPAC receptors binding, where VIP is sandwiched between N-ted and the core receptor. The central part and carboxyl terminal of VIP bind to the receptor and peptide amino terminal segments docks to the heptahelical receptor core. The N-ted domain ensured receptor affinity and positions the peptide´s N-terminus to the receptor core for activation. Additional to this model a new mechanism “hidden agonist within the N-ted” was suggested recently (Dong et al. 2006) where N-ted is still bound to the ligand but exposes a hidden epitope that is present within the N-ted domain of receptors. The N-ted epitope becomes an agonist by activating the receptor and interacting with the heptahelical core of the receptor.
PAC_1 receptors with the N-ted domain are selective and specific for the agonist PACAP, while splice variants which delete the N-ted sequence are less specific (Laburthe and Couvineau 2002).

1.1.3.5 Receptor recycling

Unstimulated cells show slow endocytosis of receptors from the surface into endosomes, whereas agonist-stimulated cells dramatically increase their endocytosis

rate. After endocytosis and ligand detachment, the receptor can be recycled back to the membrane or to a smaller extent it can be routed to lysosomes. G-protein coupled receptors are extremely temperature and energy dependent, temperatures below 16°C prevents endocytosis. Agonist stimulated accumulation of GPCR occurs in clathrin-coated pits after budding from the cell surface to form clathrin-coated vesicles. The reduction of surface receptors is termed internalisation or sequestration, which occurs either as endocytosis or recycling or a combination of both. The receptor density often decreases after the agonist concentration has been elevated for some time. Ligand binding leads to the phosphorylation at different intracellular sites by G-protein kinases (GRK). The kinase recruits the cytosolic protein β-arrestin which uncouples the G-protein (G_s). The phosphorylations are involved in the receptor desensitisation which is very rapidly to generate a second messenger. Early endosomes determine the fate of endocytosed receptor, with recycling to the plasma membrane or degradation. Desensitisation is described as loss of functional response due to receptor internalisation, which can be short-time (seconds-minutes) or long-time (hours). The recovery of functional responses after desensitisation is called resensitisation. Also ubiquitination in endocytosis and degradation of receptor via lysosomal pathway can occur. Usually there is a balance between de-and resensitisation (Koenig and Edwardson 1997).

$VPAC_1$ receptor signalling, desensitisation and sequestration are regulated by phosphorylation of GRKs. A dose-depending increase of cAMP occurs within 5-10 min and followed by a complete desensitisation after 20min (Laburthe et al. 2002; Shetzline et al. 2002). The desensitisation of VPAC receptor activity is associated with a drop of the VIP induced cAMP generation. Dependent on time and concentration VIP desensitisation occurs, the loss of response to VIP is related to a disappearance of the cell surface receptors, this is partly reversible. The internalisation of VIP reaches a maximum after 60min, the rate of receptor occupancy increases with VIP concentration whereas the rate of internalisation remains constant. The internalised receptor remains functionally, undegraded receptors recycle back to the surface within a half-time of 10min from the endosomal vesicles. The ligand appears degraded in vesicles whereas the recycled receptor is coupled again to the adenlyate cyclase components (Rosselin et al. 1988).

In blood serum VIP has a half-life time of less than one minute (Domschke et al. 1978), therefore a new strategy to enhance full length VIP survival for specific targeting was developed (fig.5). A [Arg^{8}]-VIP-dye analogue is described to increase stability towards proteolytic degradation with a longer half-life *in vivo* (Bhargava et al. 2002).

Liposomes can be used to deliver helical folded VIP to target destination and release free VIP at VPAC cell surface receptors (Rubinstein 2005; Sejourne et al. 1997; Sethi et al. 2005; Stark et al. 2007). An advantage for liposome application is the protective envelope of liposomes for VIP degradation by proteases.

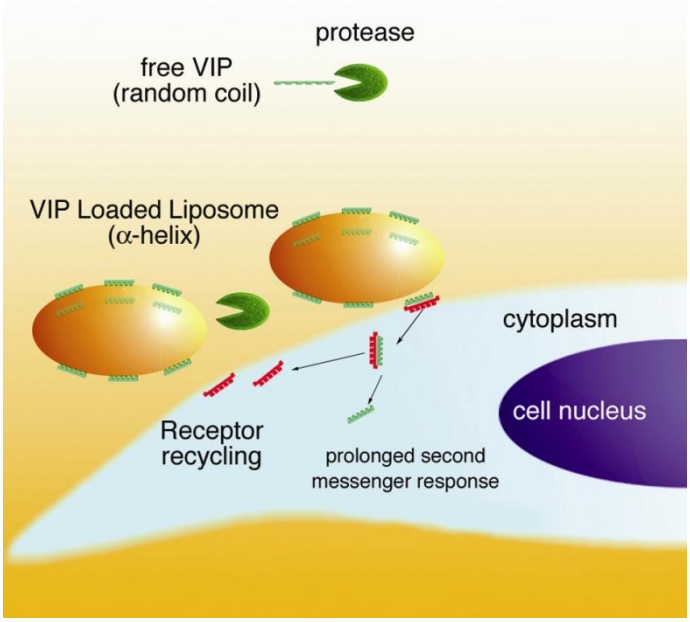

Figure 5. Schematic model of cell entry behaviour of liposomes, and free VIP. Free random coiled VIP can be degraded by proteases. VIP in liposomes is folded in a α-helix, this is the preferred form for receptor recognition, it is protected from endogenous proteases in the cytosol. After binding, the ligand-receptor complex is internalised into the cell thereby triggering signal transduction via G-proteins and second messengers. VPAC receptors are recycled back to the cell surface and can be again loaded with the ligand. [from (Hajos F 2008)]

1.1.4 Synthetic VIP analogues

Several potent VIP analogues were tested *in vitro* and *in vivo*. For example a hybrid combing a sequence of VIP and a sequence of neurotensin, [neurotensin(6-11)VIP(7-28)] termed VIPhyb. It acts as an antagonist to VIP (Gozes and Brenneman 1989; Hill et al. 1991). (N-steryl,Nle^{17})VIPhyb called (SN)VIPhyb was described as anti-proliferative factor in breast cancer cells (Moody et al. 2001). Inhibiting growth promoting actions of VIP where shown in mouse embryos (Gressens et al. 1993) and on various cell lines (Lilling et al. 1994; Wollman et al. 1993). Gozes et. al (1989; 1991) found other cell lines where it is no inhibition. A lipophilic analogue of VIP, (steryl-Nle^{17}-VIP), has

been reported to enhance survival of neurons in culture with 100-fold greater potency than VIP (Gozes et al. 1994) and also to be neuroprotective in animals models of Alzheimer´s disease (Gozes et al. 1996).

1.1.4.1 $VPAC_1$ selective analogues

Two highly selective agonists have been described, one is the VIP/GFR hybrid [Lys^{15},Arg^{16},Leu^{27}]VIP(1-7)-GRF(8-27)-NH_2 (IC_{50}, 1nM) first designed by Gourlet et al. (1997b) as a selective $VPAC_1$ agonist which does not interact with the GRF receptor. He also discovered a selective agonist for $VPAC_1$ and secretin receptor if changing Ser^{16} to Arg^{16} of secretin, it was used as a highly selective $VPAC_1$ agonist in the brain (IC_{50}, 2nM). A VIP analogue, ($Ala^{11,22,18}$)-VIP (Nicole et al. 2000), which was designed after a complete alanine-scan of VIP (table 1) is the most potent $VPAC_1$ selective agonist to date. Also a selective antagonist for $VPAC_1$ was discovered by Gourlet et. al (1997b), [Acetyl-His^1, D-Phe^2, Lys^{15}, Arg^{16}]VIP(3-7)GRF(8-27)-NH_2 or PG-97-269, of which the antagonistic properties is mostly related to D-Phe at position 2 instead of an serine in VIP.

1.1.4.2 $VPAC_2$ selective analogues

$VPAC_2$ specificity is also mediated by the receptor´s N-ted domain, but also transmembrane segment 5 and extracellular loop 3 are important of peptide agonist recognition which was shown by Juarranz et. al (1999). Two highly selective cyclic $VPAC_2$ peptides, Ro-25-1553(Gourlet et al. 1997c)1997c) which consist of Ac-His^1[Glu^8, Lys^{12}, Nle^{17}, Ala^{19}, Asp^{25}, Leu^{26}, $Lys^{27,28}$, $Gly^{29,30}$, Thr^{31}]-NH_2VIP(cyclo21-25) and Ro-25-1392 (Xia et al. 1997) which is composed of Ac-His^1-[Glu^8,OCH_3-Tyr^{10},Lys^{12},Nle^{17},Ala^{19},Asp^{25},Leu^{26},$Lys^{27,28}$]-VIP (cyclo 21-25), have been described. A peptide fragment of VIP, $VIP_{4-28,}$ acts as an endogenous $VPAC_1$ agonist and $VPAC_2$ antagonist previously described by Goetzl et. al (1989). Recently a selective $VPAC_2$ antagonist, PG-99-465, has been synthesized and described by Robberecht and his group (Grant et al. 2006; Vanneste et al. 2004), which acts on expressed $VPAC_1$ receptors on the endothelium, $VPAC_2$ on the outer layers and NPR-C receptor throughout the artery.

1.1.4.3 PAC_1 selective analogues

Maxadilan, a 61 amino acid peptide from sand flies, which has no homology to PACAP, activates the PAC_1 receptor and has a high binding affinity (IC_{50}, 1-3nM). It is not interacting with $VPAC_1$ and $VPAC_2$ receptors (Moro and Lerner 1997). The fragment PACAP-27 (aa 6-38) is a potent antagonist for PAC_1, it does not interact with $VPAC_1$ but it has a significant affinity for $VPAC_2$ (Dickinson et al. 1997).

Receptor	Agonist	Reference	Antagonist	Reference
$VPAC_1$	$(Ala^{11,22,28})$-VIP	(Nicole et al. 2000)	PG-97-269	(Gourlet et al. 1997a)
$VPAC_2$	Ro25-1392	(Xia et al. 1997)	PG-99-465	(Vanneste et al. 2004)
PAC_1	Maxadilan	(Moro and Lerner 1997)	Maxadilan Δ24-42 Maxadilan Δ24-43	(Moro et al. 1999) (Uchida et al. 1998)

Table 1. Instrumental agonists and antagonists of VPAC receptors. [modified from (Harmar, Arimura et al. 1998)]

1.1.5 Signal transduction pathway

After the ligand-receptor complex is internalised, signal transduction occurs. Typically it alters gene transcription and cellular function. VIP signalling utilizes mainly G_s and adenlyate cyclase and cAMP as second messenger. VIP also activates the inositol phospholipid signalling pathway (PLC/PI) pathway which releases calcium. PACAP mainly stimulates G_q and transduces the signal via the PLC/PI pathway.

In the unstimulated state, the receptor and the G protein are both inactive. Specific binding of an extracellular ligand, changes the conformation of the receptor, this alters the conformation of the G protein bound to the receptor. The alteration of the α subunit of the G protein allows it to exchange its GDP for GTP. The G protein breaks up into two active components, an α subunit and a βγ complex. Both can regulate the activity of target proteins in the plasma membrane. The receptor stays active while the external signal molecule is bound to it, and it can therefore catalyze the activation of many molecules of G protein. After ligand binding the ligand-receptor complex (VIP-$VPAC_{1/2}$; PACAP-PAC_1) is engulfed into the cell via endocytosis. The G-protein α subunit activates its target protein, it shuts itself off by hydrolyzing its bound GTP to GDP. This inactivates the α subunit, which dissociates from the target protein and

reassociates with a βγ complex to reform an inactive G protein. Binding to the target protein or to a membrane-bound protein usually stimulates the GTPase activity of the α subunit; this stimulation significantly enhances the inactivation. Gα activates the enzyme adenlyate cyclase (AC) which catalyzed adenosine triphosphate (ATP) to cyclic AMP (cAMP) through a cyclisation reaction that removes two phosphate groups as pyrophosphate (PP_i); a pyrophosphatase drives this synthesis by hydrolyzing the released pyrophosphate to phosphate. Cyclic AMP is unstable in the cell, because it is itself hydrolyzed by a specific phosphodiesterase to form 5'-AMP. The binding of cyclic AMP to the regulatory subunits of cAMP-depending protein kinase (PKA) induces a conformational change, thereby activating the kinase activity of the catalytic subunits. The release of the catalytic subunits requires the binding of more than two cAMP molecules to the regulatory subunits in the tetramer. This requirement greatly limits the response of the kinase to changes in cAMP concentration. Mammalian cells have at least two types of PKAs: type I is mainly in the cytosol, whereas type II is bound via its regulatory subunit and special anchoring proteins to the plasma membrane, nuclear membrane, mitochondrial outer membrane, and microtubules. In all cases, however, once the catalytic subunits are detached and active, they can migrate into the nucleus (where they can phosphorylate gene regulatory proteins), while the regulatory subunits remain in the cytoplasm. The three-dimensional structure of the protein kinase domain of the PKA catalytic subunit is able to phosphorylate the CREB gene regulatory protein. Once phosphorylated, CREB recruits the coactivator CBP, which stimulates the gene transcription for c-fos, c-jun, c-myc and vascular endothelial growth factor (VEGF), etc.. This signalling pathway controls different processes in cells, like hormone synthesis in endocrine brain cells for the production of proteins required for long-term memory in the brain.

The alternative pathway which is predominantly activated by PACAP interacts with G_q. The activated receptor stimulates the plasma membrane bound enzyme phospholipase C-β via a G_q protein. Depending on the isoform of the enzyme, it may be activated by the α subunit of G_q, by the βγ complex of another G protein, or by both. Two intracellular messenger molecules are produced when $PI(4,5)P_2$ is hydrolyzed by the activated phospholipase C-β. Inositol 1,4,5-triphosphate (IP_3) diffuses through the cytosol and releases Ca^{2+} from the endoplasmic reticulum by binding to and opening

IP_3-gated Ca^{2+}-release channels in the endoplasmic reticulum membrane. The large electrochemical gradient for Ca^{2+} across this membrane causes Ca^{2+} to escape into the cytosol. Diacylglycerol remains in the plasma membrane and, together with phosphatidylserine and Ca^{2+}, helps to activate the enzyme protein kinase C, which is recruited from the cytosol to the cytosolic face of the plasma membrane [fig.6, (Alberts B 2002)].

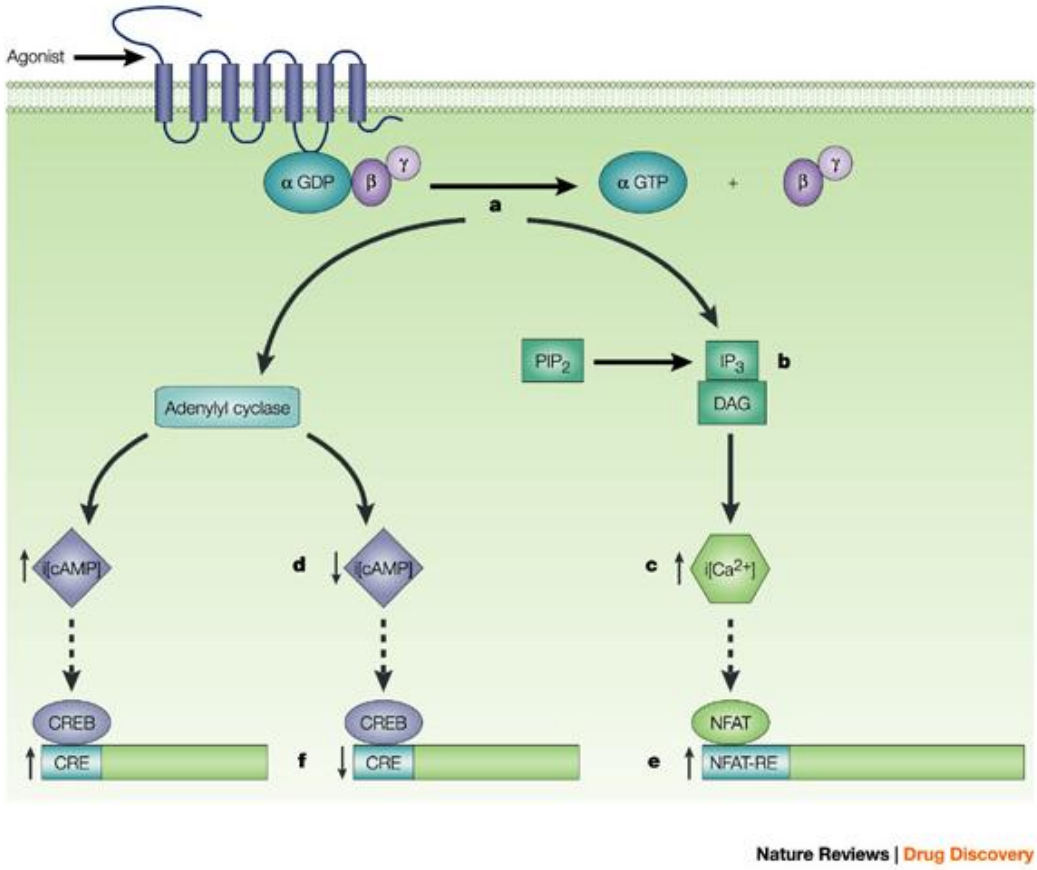

Figure 6. GPCR signalling cascade. The initial stage of GPCR activation occurs via agonist-induced conformational changes in the receptor to form an active agonist–receptor complex that is able to interact with heterotrimeric G-proteins and facilitate its activation via exchange of GDP for GTP at the subunit. (a). Following G-protein activation, the dissociated subunit and dimers modulate activity of effector proteins that control the level of intracellular signalling molecules. Levels of phosphatidylinositol biphosphate (PIP_2) and inositol triphosphate (IP_3, b) changes in the levels of the intracellular signalling molecules Ca^{2+} (c). G-protein subunit activation of adenylyl cyclase leads to cAMP increase (d). Finally, changes in the levels of these signalling molecules produce alterations in gene transcription or protein activity and result in the observed functional response of the cell; transcription factors such as CREB (cAMP response element binding protein) and reporter genes under the control of appropriate upstream elements (e and f). CRE, cAMP regulatory element, NFAT-RE, Nuclear factor of activated T-cells response element and DAG, diacylglycerol. [from (Williams 2004)]

1.2 VIP and Cancer

VIP has important effects which include cell growth and differentiation of neuronal survival, early ontogeny and developmental functions. VIP can be stimulatory or inhibitory on cell growth (Muller et al. 1995) as well as normal tissues, to exert neuroprotective activity and requires glial cells secreting neuroprotective proteins (Gozes and Brenneman 2000). Also in cancer cells VIP plays a important role in stimulation and inhibition of cell growth of lung and breast cancer (Moody et al. 1998), but VIP behaves like a growth factor in the CNS as integrative regulator during development, neurogenesis and embryogenesis (Moody et al. 2003). VIP acts on pancreatic duct cells and mediates bicarbonate secretion (Jiang et al. 1997). The peptide also inhibits excessive growth stimulation of small cell lung cancer (SCLC) cells, this indicates an anti-proliferative effect of VIP (Maruno et al. 1998; Moody 1996).

Table 2. **VPAC receptor expression pattern of physical tissue.** *, indicates the dominant receptor; ?, receptor tested but not sure; blank, VPAC receptor subtypes are not analysed.

PHYSICALY TISSUE EXPRESSION							
Organ/ Tissue	**Receptor**		**Reference**	**Organ/ Tissue**	**Receptor**		**Reference**
	VPAC	**PAC_1**			**VPAC**	**PAC_1**	
Colon mucosa	$VPAC_1$		(Reubi et al. 1999)	seminal vesicle smooth muscle	$VPAC_2$		(Reubi 2000)
colorectal/gastric mucosa	$VPAC_1$		(Reubi 2000)	smooth muscle	VPAC		(Reubi et al. 1999)
stomach	$VPAC_2$		(Adamou et al. 1995)	smooth muscle	$VPAC_2$		(Schulz et al. 2004)
	$VPAC_2$		(Schulz et al. 2004)	smooth muscle	$VPAC_2$		(Reubi 2003)
stomach smooth muscle	$VPAC_2$		(Reubi 2000)	skeletal muscle	$VPAC_2$		(Adamou et al. 1995)
stomach mucosa	$VPAC_1$		(Reubi 2000)	heart	$VPAC_2$		(Adamou et al. 1995)
intestine	$VPAC_1$		(Ishihara et al. 1992)	blood vessels	$VPAC_{1/2*}$		(Reubi 2000)
PNS myentric plexus (colon wall)		PAC_1	(Reubi 2000)	blood vessels	$VPAC_2$		(Schulz et al. 2004)
Lung acini	$VPAC_{1,2?}$		(Reubi 2000)	monocytes	$VPAC_{1/2}$		(Kojima et al. 2005)
Lung acini	$VPAC_1$		(Reubi et al. 2000)	ateries/(veins)	$VPAC_2$		(Reubi 2003)
Airway epithel, bronchus	$VPAC_1$		(Busto et al. 2003)	vessels	$VPAC_2$		(Reubi et al. 1999)
lung	$VPAC_1$		(Ishihara et al. 1992)	liver	$VPAC_1$		(Ishihara et al. 1992)
Uterus glands	$VPAC_{1,2?}$	PAC_1	(Reubi 2000)	hepatocytes	$VPAC_1$		(Reubi et al. 2000)
Uterus stroma	$VPAC_1$		(Reubi 2000)	hepatocytes	$VPAC_1$		(Reubi 2000)
Breast	$VPAC_1$		(Dagar et al. 2001)	kidney	$VPAC_2$		(Adamou et al. 1995)
breast lobulus/duct	$VPAC_1$		(Reubi 2000)	kidney glomeruli	$VPAC_1$		(Reubi 2000)
breast lobulus/duct	$VPAC_1$		(Reubi et al. 2000)	Prostate glands	$VPAC_1$		(Reubi et al. 2000)
Microglia	$VPAC_1$		(Delgado et al. 2003)	Prostate glands	$VPAC_1$		(Reubi 2000)
	$VPAC_1$		(Delgado 2002)	Prostate stroma	$VPAC_2$		(Reubi 2000)
	$VPAC_1$		(Kim et al. 2000)	Prostate epithelial cell culture	$VPAC_{1/2}$		(Juarranz et al. 2001)

T cell	$VPAC_1$		(Delgado et al. 1996)	Lymphnodes	$VPAC_1$		(Reubi 2000)
neuron	$VPAC_{1/2*}$		(Gressens et al. 1993)	Lymphnodes	$VPAC_1$		(Reubi et al. 2000)
myenteric neurons	$VPAC_1$	PAC_1	(Schulz et al. 2004)	GALT	$VPAC_1$	PAC_1	(Reubi 2000)
neuroendocrinal cell	$VPAC_2$	PAC_1	(Schulz et al. 2004)	Spleen PALS	$VPAC_1$		(Reubi 2000)
cerebal cortex	$VPAC_1$		(Ishihara et al. 1992)	Thyroid follicle	$VPAC_1$		(Reubi 2000)
hippocampus	$VPAC_1$		(Ishihara et al. 1992)	Parotis gland	$VPAC_1$		(Reubi 2000)
thalamus	$VPAC_2$		(Sheward et al. 1995)	Adipose tissue	$VPAC_2$		(Adamou et al. 1995)
Suprachiasmaticus nucleus (SCN)	$VPAC_2$		(Sheward et al. 1995)	testis	$VPAC_2$		(Adamou et al. 1995)
adreanal medulla	$VPAC_{1?}$	PAC_1	(Reubi 2000)	Bladder/Ureter urothelium	$VPAC_1$		(Reubi 2000)
adreanal medulla		PAC_1	(Reubi et al. 2000)				
Pancreas	$VPAC_2$		(Adamou et al. 1995)				
Pancreas	$VPAC_2$		Jiang et al., 1997, CR				
Pancreas acini		$PAC_{1?}$	(Reubi 2000)				
Pancreas duct	$VPAC_1$		(Reubi et al. 2000)				
Pancreas duct	$VPAC_1$		(Reubi 2000)				
Mucosa	$VPAC_1$		(Schulz et al. 2004)				
Mucosa	VPAC		(Reubi et al. 1999)				

1.2.1 VPAC expression pattern of tumour cells

Reubi et. al (2000) performed several *in vitro* receptor autoradiography studies with ^{125}I-VIP or ^{125}I-PACAP in tissue sections. The $VPAC_1$ receptor is expressed in a wide variety of tissues including liver, breast, kidney, prostate, ureter, bladder, pancreatic ducts, gastrointestinal mucosa, lung, thyroid, adipose and lymphoid tissue, whereas the $VPAC_2$ receptor is predominantly found in smooth muscles and blood vessels. The PAC_1 receptor is distributed in adrenal medulla.

$VPAC_1$ receptors are also expressed in human tumours including breast, prostate, pancreas, lung, colon, stomach, liver and bladder carcinomas, lymphomas and meningeomas. Leiomyomas express preferentially $VPAC_2$. Glial tumours, pituitary adenomas, neuroblastomas, paragangliomas, pheochromocytomas, endometrial carcinomas, preferentially express PAC_1. Other researchers investigated the expression pattern of tumour tissue and cell lines as seen in table 3.

Table 3. VPAC receptor expression pattern of tumour tissue. *, indicates the dominant receptor; ?, receptor tested but not sure; blank, VPAC receptor subtypes are not analysed.

TUMOUR TISSUE							
Organ/ Tissue	**Receptor**		**Reference**	**Organ/ Tissue**	**Receptor**		**Reference**
	$VPAC_{1/2}$	**PAC_1**			**$VPAC_{1/2}$**	**PAC_1**	
Colon Carcinoma HT-29	VPAC		(Bellan et al. 1992)	Sup T1 cell lymphoblastom	$VPAC_2$		(Igarashi et al. 2002)
	VPAC		(Ou et al. 2005)	neuroblastoma	VPAC		(Virgolini et al. 1994b)
HT-29,SW430,DLD-1, Caco-2	VPAC		(Lelievre et al. 1998)	neuroblastoma	VPAC		(Lilling et al. 1994)
HCT-15	$VPAC_1$		(Moody et al. 2001)	neuroblastoma	VPAC		(Wollman et al. 1993)
HCT-15	VPAC		(Levy et al. 2002)	neuroblastoma	$VPAC_{1/2}$		(Reubi 2003)
gastroinestinal tact tumour	VPAC		(Virgolini et al. 1996)	neuroendrocrinial tumour	$VPAC_{1/2}$		(Warner and O'Dorisio T 2002)
	VPAC		(Virgolini et al. 1994a)	ACTH-prod. Hypophyseal adenoma	VPAC		(Virgolini et al. 1994b)
intestinal endocrine carcinoma	VPAC		(Virgolini et al. 1996)	medulloblastoma	$VPAC_{1/2}$		(Reubi 2003)
	VPAC		(Ishihara et al. 1992)	meningoma	$VPAC_1$	PAC_1	(Schulz et al. 2004)
	VPAC		(Adamou et al. 1995)	Meningoma	$VPAC_1$		(Reubi 2000)
	VPAC		(Virgolini et al. 1994b)	meningoma	$VPAC_{1/2}$		(Reubi 2003)
gastric carcinoma	$VPAC_1$		(Reubi 2003)	Pituitary Adenoma	$VPAC_{1/2?}$	PAC_1	(Reubi 2000)
	$VPAC_1$		(Reubi 2000)	Pituitary Adenoma	$VPAC_1$		(Schulz et al. 2004)
Colon carcinoma	$VPAC_1$		(Reubi 2000)	glioblastoma	$VPAC_{1/2}$	PAC_1	(Schulz et al. 2004)
			(Reubi et al. 2000)	Glioma	$VPAC_{1/2?}$	PAC_1	(Reubi 2000)
colorectal carcinoma		$PAC_{1?}$	(Schulz et al. 2004)	CNS cancer	$VPAC_1$		(Moody et al. 2001)
	$VPAC_1$		(Reubi 2003)	Pheochromocytomas	$VPAC_{1/2?}$	PAC_1	(Reubi 2000)
gastric colorectal tumour	$VPAC_1$		(Reubi et al. 1999)	Pheochromocytomas	$VPAC_1$	PAC_1	(Reubi et al. 2000)
gut cariniod, gastrinoma,	$VPAC_{1/2}$		(Reubi 2003)	Paraganglia tumour	$VPAC_{1/2?}$	PAC_1	(Reubi 2000)

insulinmoma	VPAC		(Virgolini et al. 1994a)	Paraganglia tumour	$VPAC_1$	PAC_1	(Reubi 2000)
	VPAC		(Virgolini et al. 1996)	Pheochromocytomas	VPAC		(Virgolini et al. 1996)
	VPAC		(Virgolini et al. 1994b)	Pheochromocytomas	VPAC		(Virgolini et al. 1994b)
	$VPAC_{2?}$		(Schulz et al. 2004)	ductal pancreas carcinoma	$VPAC_1$		(Reubi 2000)
stomach carcinoma	$VPAC_{2?}$	$PAC_{1?}$	(Schulz et al. 2004)	Pancreatic Adenocarcinoma	VPAC		(Estival et al. 1983)
NSCLC	$VPAC_1$		(Moody et al. 2003)	PANC-1	$VPAC_{1/2}$		(Estival et al. 1983)
	$VPAC_1$		(Reubi 2000)	Pancreatic adenocarcinoma (Capan-1/2, Su.86.86, BxPC-3,MDA Panc-3, AsPC-1, Hs766T, Panc-1)	$VPAC_1$		(Jiang et al. 1997)
	$VPAC_1$		(Reubi 2000)	exocrine pancreatic tumour	$VPAC_1$		(Reubi 2003)
	$VPAC_1$		(Moody et al. 2001)	pancreas cancer	$VPAC_1$		(Virgolini et al. 1994a)
	$VPAC_1$		(Reubi 2003)	pancreas cancer	$VPAC_1$		(Schulz, et al. 2004)
SCLC	$VPAC_{1/2}$		(Reubi 2003)	Leiomyoma	$VPAC_2$		(Reubi 2003)
SCLC	VPAC		(Virgolini et al. 1994b)	Leiomyoma	$VPAC_2$		(Reubi et al. 2000)
SCLC (NCI-H345)	$VPAC_2$		(Moody et al. 2003)	Leiomyoma	$VPAC_2$		(Reubi 2000)
SCLC	$VPAC_1$		(Moody et al. 2003)	leukemia	$VPAC_1$		(Moody et al. 2001)
Lung cancer SCLC	VPAC		(Maruno et al. 1998)	liver carcinoma		$PAC_{1?}$	(Schulz et al. 2004)
Lung carcinoma (SCLC, NSCLC)	$VPAC_{1/2}$		(Busto et al. 2003)	liver carcinoma			(Warner and O'Dorisio T 2002)
bronchi, pulmonary ateries carconoma	$VPAC_{1?,2}$		(Schmidt et al. 2001)	liver metasatsis	VPAC		(Virgolini et al. 1996)
Lung epithelial carcinoma	$VPAC_2$		(Busto et al. 2003)	hepatocellular carcinoma	$VPAC_1$		(Reubi et al. 2000)
lung metastasis	VPAC		(Virgolini et al. 1996)		$VPAC_1$		(Reubi 2000)

lung cancer (NCI-H1299)	$VPAC_1$		(Moody et al. 2004)	hepatocellular carcinoma	$VPAC_1$		(Reubi 2003)
lung carcinoma cell line (SW-900, Calu-1)	VPAC		(Laburthe et al. 1981)	Kidney carcinoma COS-7 cell line	$VPAC_{1,2}$		(Virgolini et al. 1996)
endometrial carcinoma	$VPAC_{1/2?}$	PAC_1	(Reubi 2000)	kidney cancer	$VPAC_{1,2}$		(Warner and O'Dorisio T 2002)
endometrial carcinoma	$VPAC_1$	PAC_1	(Reubi et al. 2000)	renal carcinoma	$VPAC_1$		(Reubi 2003)
endometrial carcinoma	$VPAC_{1/2}$		(Reubi 2003)	renal cancer	$VPAC_1$		(Moody et al. 2001)
Ovarian cancer	$VPAC_1$		(Moody et al. 2001)	Prostate carcinoma	$VPAC_1$		(Reubi et al. 2000)
Ovarian carcinoma	$VPAC_1$		(Reubi 2003)	Prostate carcinoma	$VPAC_1$		(Reubi 2000)
Uterine adenocarcinoma	$VPAC_1$		(Ichikawa et al. 1996)	prosate carcinoma	$VPAC_1$		(Reubi 2003)
Breast cancer	$VPAC_1$		(Dagar et al. 2001)	prostate cancer	$VPAC_1$	$PAC_{1?}$	(Schulz et al. 2004)
breast cancer T47D	$VPAC_1$		(Igarashi et al. 2002)	prostate cancer	$VPAC_1$		(Moody et al. 2001)
breast cancer	$VPAC_{1*/2}$	PAC_1	(Schulz et al. 2004)	Non-Hodgekin lymphomas	$VPAC_1$		(Reubi 2000)
breast cancer	$VPAC_1$		(Reubi et al. 2002)	Non-Hodgekin lymphomas	$VPAC_1$		(Reubi et al. 2000)
breast cancer (BT-20, MCF-7, MDA-MB-231, SK BR-3, ZR-75-1)	VPAC		(Zia et al. 1996)	lymphoma	$VPAC_{1/2}$		(Reubi 2003)
breast cancer (MCF-7, T47D)	$VPAC_1$		(Moody et al. 2000)	thyroid carcinoma		$PAC_{1?}$	(Schulz et al. 2004)
ductal/ lobular breast cancer	$VPAC_1$		(Reubi 2000)	thyroid carcinoma	VPAC		(Virgolini et al. 1994b)
ductal/ lobular breast cancer	$VPAC_1$		(Reubi et al. 2000)	thyroid carcinoma	VPAC		(Warner and O'Dorisio T 2002)
breast carcinoma	$VPAC_1$		(Reubi 2003)	carcinoid cancer	$VPAC_{2?}$		(Schulz et al. 2004)

ductal breast cancer	$VPAC_{1/2}$		(Virgolini et al. 1994b)	carcinoid carcinoma	VPAC		(Virgolini et al. 1994b)
esophageal cracinoma	$VPAC_1$		(Reubi 2003)		VPAC		(Virgolini et al. 1996)
urothelial carcinoma (bladder)	$VPAC_1$		(Reubi 2000)				
urinary bladder carcinoma	$VPAC_1$		(Reubi 2003)				

1.2.1.1 $VPAC_1$-specific ligand

The most important amino acids for $VPAC_1$ affinity are His^1, Asp^3, Phe^6, $Arg^{12,14}$ and Leu^{23}. Furthermore Asn^{24} is a very important amino acid at this position for human $VPAC_1$ high affinity (Ito et al. 2001). Substitution of Ala at positions 1, 3, 6, 12, 14 and 23 of VIP reduces binding affinity to human $VPAC_1$ receptors over 50-fold. Also a substitution of Ala at positions 5, 7, 10, 15, 16, 20, 22 and 26 reduces binding affinity 5-50 times. Most amino acids for $VPAC_1$ receptor binding are identical in PACAP-27, nine amino acids which are different are $Ala^{2,8,9,11,19,24,25,27,\ 28}$ to determine a high affinity for $VPAC_1$ and enhanced metabolic activity. Nicole et. al (2000) and his group developed a VIP analogue $Ala^{(11,22,28)}$-VIP (>1000-fold) highly selective for $VPAC_1$.

Because Virgolini and her group showed that ^{123}I-VIP and ^{123}I-OCT (somatostatin analogues octreotide) targets VPAC expressing tumours (Vanneste et al. 2004; Virgolini et al. 1994a; 1996; 1994b), and because upon systemic administration not only tumour targeting but also vasorelaxation via $VPAC_2$ occurred. The advantage of a $VPAC_1$ specific analogue could be to circumvent $VPAC_2$ mediated vasorelaxation and specifically target $VPAC_1$ expressing cancer cells.

1.2.2 VPAC receptors as cell entry point for drug delivery

Peptide receptors as molecular targets for cancer diagnosis and therapy were previously known. Reubi and his group (2000) summarized the significance of peptides and their receptors in cancer. In cancer overexpressed G-protein coupled receptors can internalise into the cell together with their specifically bound ligands. Ligands may function as pharmacophor (e.g. radiotracer), these internalisation may accumulate radiotracer in the cell as the target. The strategy can be used for peptides linked to cytotoxic drugs or radioactive isotopes. Small and hydrophilic peptides penetrate the tissue well, this permits rapid access to the tumour site after systemic application. Typically peptides will not cross the blood-brain-barrier and do not enter the brain in a significant amount.

An 8-20 amino acid long peptide provide an adequate attachment site for a chelator molecule like dietyhlenetriaminopentaacetic acid (DTPA) or 1,4,7,10-tetraazacyclododecane-1,4,7,10-tetraacetic acid (DOTA), which accept certain types of metallic radioisotopes (Reubi 2003).

VPAC receptors as entry point for drugs were previously shown by Moody et. al (2001). They investigated the VPAC receptor antagonist VIPhyb or (SN)VIPhyb, with or without conjugated chemotherapeutic drugs like taxol, to inhibit growth of breast cancer cells.

Ellipticine is a topoisomerase II inhibitor, it causes double strand breaks in the DNA. Also topoisomerase I inhibitors cause single strand breaks in DNA, and are used as treatment for lung cancer patients. Moody developed VIP-ellipticine conjugates, VIP-ALALA-ellipticine and VIP-LALA-ellipticine, which are coupled to the C-terminus of VIP and are cytotoxic for lung cancer cells. VIP-ellipticine conjugates function as $VPAC_1$ agonist and after internalisation it elevates cAMP. VIP conjugates targeted to $VPAC_1$ can increase the selectivity of drug delivery, however we have to expect that also normal cells which express the receptor are treated. The advantage of peptide chemotherapeutic agents is that the peptide acts as a prodrug, which means that the inactive prodrug is delivered and recognizes the VPAC as the target. Because of the high density of receptors at the cell surface, appreciable amounts of the prodrug are internalised into the cells and elicit its function (Moody et al. 2004).

Another approach was performed by Ou et. al (2005), they investigated radioiodinated antisense oligonuclide mediated by the VPAC receptors. A 15-mer phosphorothioate antisense oligonuclide (ASON) is complimentary to the start region of c-myc oncogene mRNA, which was radioiodinated to enhance anti-tumour activity. VIP covalently bound to polylysine (VIP-^{131}I-ASON) was used as a carrier to deliver the oligonucleotide to the VPAC positive tumour cells. VIP-polylysine carrier greatly increased HT-29 tumour uptake of ASON. Treatment with VIP-^{131}I-ASON complexes results in tumour growth delay in human colon cancer in an animal model.

1.2.2.1 VIP-Hematoporphyrin for PDT

Photodynamic therapy (PDT) is a therapeutic modality for treatment of cancer diseases and non-oncological disorders first described in the early 1970s. This approach is based on systemic administration and selective accumulation of a photo-sensitiser in tumour tissue. Typical photo-sensitisers belong to following chemical classes: phthalocyanine, porphyrin, porphyrin-oligomer, chlorine, porphycene, chlorophyll a derivates, phenantroperylenequinone. All molecule classes have different targets in the cell. Typically targets are mitochondria, ER, Golgi apparatus, lysosomes, endosomes and

plasma membrane. The light absorption spectrum depends on the photo-sensitiser, usually it is between 600-800nm. After irradiation the photo-sensitiser transforms from its ground singlet state into an excited singlet state. It can decay back to the ground state by emitting fluorescence. A fraction of the excited singlet state is transformed via intersystem crossing into a relatively long-lived excited triplet state (micro-nanoseconds). This triplet state can either be derived from free radicals or radical ions by hydrogen atom extraction or electron transfer to biological substrates, soluble molecules or oxygen. These radicals can interact with ground state oxygen to produce hydrogen peroxide, hydroxyl radials and superoxide anion radicals (type I reaction, fig.7). As alternative pathway the excited triplet state can be derived from non-radical but highly reactive singlet oxygen ($^1O_2$, type II reaction). The ratio between the two pathways depends on the chemical properties of the photo-sensitiser and the nature of the substrate molecule. Singlet oxygen ($^1O_2$) has a prevalent role in the molecular process initiated by PDT.

The photodamage and cytotoxicity after PDT treatment depends on multiple factors such as photosensitising agent, the localisation at the time of irradiation, total administered dose, total light exposure, light fluency rate, the time between administration and the photo-sensitiser irradiation and the type of tumour with its level of oxygenation. PDT *in vivo* has been shown to reduce the number of clonogenic tumour cells through direct ROS-mediated photodamage (Henderson et al. 1985). PDT has a much lower potential to cause DNA damage compared to X-rays. Typically the photo-sensitisers do not reach the nucleus, because of the short life-time of singlet oxygen ($t_{1/2}$<0,04µs, radius of action <0,02µm). Photoactive components localizing to the mitochondria or ER promote apoptosis upon a certain threshold of oxidative stress, whereas the photo-sensitiser targets either the plasma membrane or lysosomes by delaying or blocking the apoptotic program predisposing the cell to necrosis. Autophagy may be induced by PDT to repair and survive photoinjury to key organelles and turns into cell death signals if the repair fails. Three major morphologies of programmed cell death appear after photosensitisation: apoptosis, necrosis and autophagy. Type I programmed cell death (PCD) is characterized by changes involving nuclear condensation and general cellular shrinking. Type II PCD is distinguished by a lysosomal–dependent digestion of the cell and the presence of autophagy vacuoles

(autophagosomes) while type III PCD is marked by cellular swelling and a rapid loss of cell membrane integrity. These processes are defined as apoptosis, autophagy cell death and necrosis. All pathways are signalling through different death signal molecules, the pathways are interchangeable, therefore specific inhibition of one death signal is not sufficient to block PDT-mediated cell death (Buytaert et al. 2007).

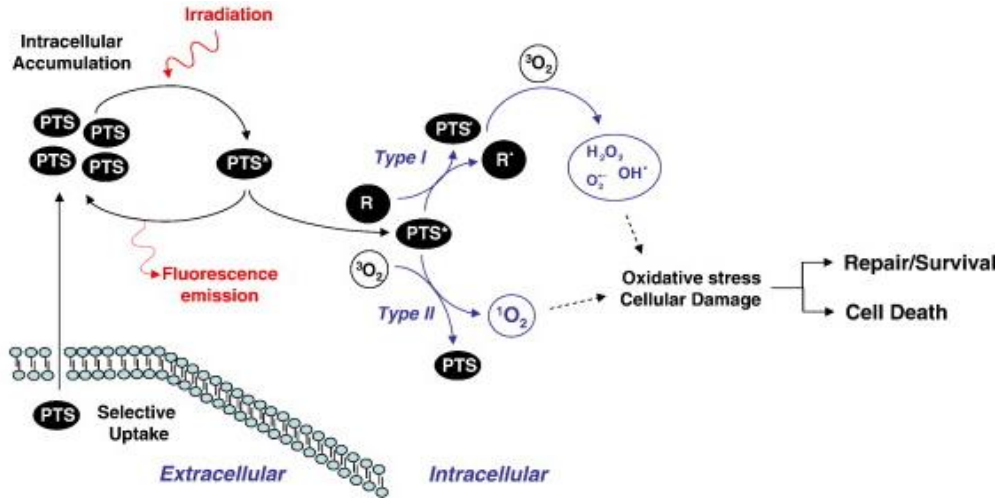

Figure 7. The action mechanism of photosensitising agents in PDT. A photo sensitiser in its singlet ground state (PTS) is excited to higher energy levels (PTS*) upon irradiation and absorption of a photon of the appropriate wavelength. Deactivation occurs either through the emission of fluorescence or via intersystem crossing leading to formation of the excited triplet state (3PTS). Subsequently, energy can be lost in the presence of biological substrates and molecular oxygen ($^3O_2$), via Type I and Type II reactions leading to the formation of free radicals and ROS ($O_2^{\bullet -}$, $HO^{\bullet}$, H_2O_2, and $^1O_2$). These cytotoxic species cause cellular photodamage which can activate a repair mechanism or lead to cell death when the damage is beyond repair capacity. [from (Buytaert et al. 2007)]

Photodynamic therapy offers the advantage of an effective and selective method of destroying diseased tissues without damaging surrounding healthy tissues. One of the aspects of anti-tumour effectiveness of PDT is related to the distribution of photosensitizing drugs. We were interested wheter or not we can link a classical PDT substance. Hematoporphyrin to VIP and use VIP-conjugate as pharmacophore for specific cell targeting.

Hematoporphyrin is a macrocyclic tetrapyrrolic ring system with highly reactive hydroxyl side groups termed porphyrin. Yang et. al (2007) described a PDT assay with a semiconductor laser at 630nm with the energy density of 2, 5, 10, and 20 J/cm. After further culture for 24h, the survival rate of LoVo and CoLo205 cells were analyzed by MTT assay, and the cellular fluorescence intensity of hematoporphyrin derivate luminescene was measured.

The hematpoporphyrin derivate Photofrin®/photosan, also called porfimer natrium, is a porphyrin oligomer with a molecular mass of about 50 kDa. The molecule is excited between 600-700nm. Photofrin® was the first approved photodynamic therapy agent to combat cancer. The intercellular distribution of Photofrin® was observed after 4 houres incubation in malignent MCF-7 and A549 cells. The most intensive signal was found around the nuclear envelope (Saczko et al. 2007).

Photosan is highly sensitve to light, patients treated with porfimer natrium are extra sensitve to light for at least 30 days after treatment. Light includes sunlight, bright indoor lights, and vehicle headlights.

1.2.2.2 VIP-DOTA-Gd

Radio-labelled VIP (^{123}I-VIP or ^{123}I-OCT) was successfully used in the detection of gastrointestinal and breast tumours (Vanneste et al. 2004; Virgolini et al. 1994a; 1996; 1994b), and therapy (Krenning et al. 2004; Virgolini et al. 1998). Peptides can be labelled with various trivalent radiometals for imaging or targeting radionuclide therapy applications (Sosabowski and Mather 2006). 1,4,7,10-tetraazacyclododecane-1,4,7,10-tetraacetic acid (DOTA) is a macrocyclic chelator, almost capable of strongly encapsulating metals used for photon emission tomography (PET). Radioisotopes like ^{111}In, ^{86}Y, ^{90}Y, ^{67}Ga, ^{68}Ga and ^{64}Cu or for ^{99}mTc and ^{188}Re require a chelator like DOTA. VIP conjugation to DOTA with trivalent metallic isotopes forms a stable complex. DOTA is a chelator to quench cytotoxic effects of the trivalent metals (Heppeler et al. 2000).

Gadolinium (Gd) is a non isotopic trivalent metal which is widely used to enhance the contrast of images in magnet resonance imaging (MRI). Unpaired electrons of gadolinium generate electron spin that interfere with the nuclear spin of hydrogen which conditions the paramagnetic effect of gadolinium. The chelates function as extracellular space markers that enhance tissue contrast. The common oxidation state of Gd is 3+ in which the three outer electrons are lost. There are no electrons or orbitals available for covalent binding; therefore free Gd^{3+} is highly toxic. The ionic radius of Gd^{3+} (107,8 pm) is close to that of Ca^{2+} (114 pm) and therefore unchelated Gd inhibits those physiological processes which are depending upon Ca^{2+} influx. To reduce the toxicity for medical applications Gd is chelated. Gd chelates do not diffuse through plasma membranes and therefore is not able to penetrate the blood-brain barrier (BBB).

Macrocyclic chelates such as Gadoteratemeglumine (DOTA-Gd) and Gadoteridol (Gd-HP-DO3A) are more stable than linear molecules like Gadodiamide (Gd-DTPA-BMA) and Gadopentetatedimeglumine (Gd-DPTA). The chemical instability of the chelate can lead to exchanges with other metal ions like $Cu^{2+,}$ Zn^{2+} and Ca^{2+}. Transmetallation between contrast agents and body cations has biological consequences such as accumulation of Gd^{3+} in bones, interaction with metalloenzymes, increased zincuria, interaction with scintigraphic procedures and hence superious hypocalcaemia.

Released free Gd^{3+} of the macrocyclic chelate DOTA-Gd and Gd-HP-DO3A is less than 1%, whereas it is much higher for the linear chelates Gd-DTPA-BMA and Gd-DPTA (35%). Half–life time of macrocyclic chelates (Gd-DOTA $T_{1/2}$ >1 month, Gd-HP-DO3A $T_{1/2}$=3h) differs clearly from linear chelates [(Gd-DTPA $T_{1/2}$=10min, Gd-DTPA-BMA $T_{1/2}$~30s; (Idee et al. 2006)].

VIP-DOTA as chelator of metal ions has good potential to improve the tumour targeting with diagnostic or therapeutic radionuclides. We produced VIP-DOTA-Gd, where DOTA is linked to VIP. We were interested whether or not the construct has potential in tumour cell targeting. Chelate binding of Gd in DOTA does not largely change the molecular size appearance of the VIP-conjugate.

2 Objectives and aims

Two issues arise with the use of VPAC receptors as anti-cancer drug targets. We aimed to investigate the potential of non radioactive labelled VIP tumour targeting.

We expect that VIP-DOTA can internalise Gd at similar rates than radioisotopes. VIP-DOTA internalisation and cytoplasmic accumulation could improve the background signal ratio in clinical imaging applications. The sensitivity and/or specificity of diagnostic and therapeutic procedures could be enhanced.

The second issue in discussion is whether or not $VPAC_1$ receptor can serve as more specific target for delivery of anti-cancer drugs into the cell. We envisioned a specific $VPAC_1$-drug delivery system, with a selective $VPAC_1$ analogue which targets $VPAC_1$ positive tumour cells. The advantage of targeting $VPAC_1$ is to circumvent side effects due to the physiological properties of VIP, i.e. vasodilation and relaxation via $VPAC_2$. Another advantage may be the overexpression of $VPAC_1$ receptors in tumour cells compared to healty tissue.

2.1 Find tumour cells with VPAC receptors

We investigated the expression pattern of 14 tumour cell lines and one endothelial cell line for their $VPAC_1$, $VPAC_2$ and PAC_1 expression pattern by immunohistochemistry (ICC) staining with specific monoclonal and polyclonal antibodies to $VPAC_1$, $VPAC_2$ and PAC_1. Also western blot (WB) was used for the detection of VPAC receptors with these antibodies.

2.2 Select peptide analogues

We were interested in the potential of VIP and a selective $VPAC_1$ agonist to be a carrier for conjugates (drugs), envisioning their applicability in cancer diagnostics.

- The conjugates Cy3 and Fluo linked to VIP (VIP-Cy3, VIP-Fluo) were tested for their potential of internalisation via VPAC receptors into the cell.

- DOTA and DOTA-Gd conjugated to VIP (VIP-DOTA, VIP-DOTA-Gd) were analysed for their potential in MRI diagnostics and the cytotoxicty of Gd in cell culture.

- VIP linked to hematoporphyrin (VIP-PDT) was studied for its potential in photodynamic therapy (PDT).

- The specific $VPAC_1$ agonist ($Ala^{11,22,28}$)-VIP was used to investigate the selective $VPAC_1$ mediated entry into the cell. The peptide was conjugated to FITC which served the visualisation of intracellular conjugates via CLSM.

- Because of the short half-life time of VIP we produced nanosized liposomes and proticles as peptide carriers, designed for VIP delivery. These nanoparticles can protect the peptides from proteolytic degradation. I tested if liposomes and proticles cause a sustained biological response, indicating a protection and release of VIP.

2.3 Test Peptide constructs for internalisation

When envisioning VIP peptide analogues as carriers for cancer cell targeting, the most important step is the internalisation of peptide conjugates into the cell. We analyzed fluorescent VIP conjugates, like VIP-Cy3, VIP-Fluo and ($Ala^{11.22.28}$)-VIP-FITC with confocal laser scanning microscopy (CLSM) and fluorescent correlation spectroscopy (FCS) for their internalisation behaviour.

In addition to the direct visualisation of internalised fluorochromes, we used indirect methods, i.e. ELISA, to visualise the internalisation of peptide conjugates into the cell. Because VIP is internalised to elicit specific biological responses, we can use these responses to show internalisation of non-fluorescing peptide conjugates (i.e. VIP-PDT, VIP-DOTA-Gd). The measuring of the second messenger cAMP by ELISA reveals the internalisation of VIP and VIP conjugates.

2.4 Test Peptide constructs for other effects (proliferation, cytotoxicity)

Aiming at the medical use of peptide conjugates, we were interested in further important aspects like proliferative or cytotoxic properties of the substances. Therefore we investigated all peptide constructs for their proliferation modification and cytotoxicity by MTT assays in cell culture.

The potential of VIP-PDT was analysed in cells, by tests for their reactive oxygen species (ROS) with and without light radiation. Furthermore the PDT conjugate was tested for the potential to induce apoptosis or proliferation in cell culture after treatment with light radiation.

3 Material and Methods

3.1 Cell culture

Cell lines were cultured with different medium supplements at 37°C with 5% CO_2 in the atmosphere in polyethylene 25/75cm^2 Cell Culture Flasks (Corning, Lowell, USA). The medium was changed every second day, therfore cell were washed once with PBS. The aherently growing cells were split at about 90% confluency in subcultivation ratio depending on each cell line. Before splitting, the cells were washed with PBS and incubated with 1x Trypsin-EDTA (PAA, Pasching, Austria) for 2-5min at 37°C with 5%CO_2 in the atmosphere. Afterwards cells were suspended in 5ml medium and centrifuged at 1000rpm for 5min (Rotanta 46 RC, Hettrich Zentrifugen, Tuttlingen, Germany). The pellet was resuspended in 5ml medium and divided depending on their subcultivation ratio and cultured at 37°C 5%CO_2.

Before supplementation of medium, the fetal bovine serum (PAA) was once heat inactivated at 60°C for 15min and stored at -20°C.

Phosphate buffered saline (PBS):

A stock solution of 10x PBS was prepared. All chemicals were purchased by Merck (Darmstadt, Germany).

Table 4. 10x Phosphate buffered saline (PBS).

chemical substances	concentration [M]	concentration [g/l]
$Na_2HPO_4*2H_2O$	92,3 mM	14,4g
KH_2PO_4	14,6 mM	2g
KCl	26,8 mM	2g
NaCl	1,4M	80g

Substances from table 4 were dissolved in l000ml bidest. water to obtain 10x PBS. PBS was adjusted to pH 7,4 and sterile filtrated with 0,22µM filters (Corning, Lowell, USA).

3.1.1 Cell lines

The cell lines used in this project were obtained from the American Type Culture Collection (ATCC, LGC Promochem, Wesel Germany) and the tissue culture facility of the Institute of Cancer Research Vienna (KIM-1 Medical University, Vienna Austria; table 5).

Table 5. Used cell lines

Organ	Tumour cell line	Growth properties	Medium	Reference or ATCC No.
Human prostate carcinoma	LNCaP	adherent, single cells and loosely attached clusters	RPMI 1640	CRL-1740
Human prostata carcinoma	PC-3	adherent	RPMI 1640	CRL-1435
Human pancreas adenocarcinoma	Capan-1	adherent	RPMI 1640	HTB-79
Human pancreas duct epithelioid carcinoma	PANC-1	adherent	DMEM	CRL-1469
Lung carcinoma	A427	adherent	MNP	HTB-53
Human liver hepatocellular carcinoma	Hep3B	adherent	RPMI 1640	HB-8064
Human thyriod adenocarcinoma	SW1736	adherent	RPMI 1640	Inst. Cancer Research
Human glioblastoma	MGC	adherent	MEME	Inst. Cancer Research
Human colorectal carcinoma	HCT-15	adherent	RPMI 1640	CCL-225
Human colorectal carcinoma	HT-29	adherent	RPMI 1640	HTB-38
Human colorectal carcinoma	CaCo-2	adherent	RPMI 1640	HTB-37
Human colorectal carcinoma	HCT-116	adherent	MEME	CCL-247
Human mammary gland, epithelial adenocarcinoma	MCF-7	adherent	DMEM without phenolred modified	HTB-22
Human microvascular endothelial cells	HMEC-1	adherent	DMEM modified	Inst. Cancer Research

LNCaP is a human prostate carcinoma cell line derived from a left supraclavicular lymph node (ATCC Number CRL-1740) of a 50 year old Caucasian male. The epithelial adherent cell line consists of single cells or loosely attached clusters. The cells were cultured with the medium RPMI 1640 at 37°C with 5% CO_2 in the atmosphere, and subcultivated 1:10.

PC3 is a human prostate adenocarcinoma derived from bone, tumour state grad IV (ATCC Number CRL-1435) of a 62 year old Caucasian male. These cells form epithelial adherent clusters. The medium for this cell line was RPMI 1640. The cells were cultured at 37°C, with 5%CO_2 in the atmosphere and subcultivated 1:10.

Capan-1 is a human pancreas adenocarinoma derived from liver (ATCC Number HTB-79) of 40 year old Caucasian male. The cells are epithelial and adherent. The medium for this cell line was RPMI 1640. The cell line was cultured at 37°C, with 5% CO_2 in the atmosphere and subcultivated 1:5.

PANC-1 is a human pancreas duct epithelioid carcinoma cell line (ATCC Number CRL-1469) from a 56 year old Caucasian male. An epithelial adherent cell line cultured with RPMI 1640. Cells grew at 37°C with 5% CO_2 in the atmosphere. The subcultivation ratio was 1:5.

A427 is a human lung carcinoma (ATCC Number HTB-53) from a 52 year old Caucasian male. The epithelial cell line grows adherent. The medium for this cell line was MNP. The cells were cultured at 37°C with 5% CO_2 in the atmosphere and subcultivated 1:5.

Hep3B is a human liver hepatocellular carcinoma (ATCC Number HB-8064) from an 8 year black juvenile. The epithelial cell line grows adherent. The cell line was cultured with RPMI 1640. The cells grew at 37°C with 5%CO_2 in the atmosphere and a subcultivation ratio of 1:2.

SW1736 is a human thyroid adenocarcinoma cell line cultured at the tissue culture facility of the Institute of Cancer Research, Vienna, Austria, from a biopsy. This adherent cell line was cultured with RPMI 1640. The cells grew at 37°C with 5%CO_2 in the atmosphere and a subcultivation ratio of 1:10. SW1736 cells were grown on collagen (Sigma Aldrich, St.Louis, MO) layer coated flasks (85µl Collagen/1616µl PBS for 25cm^2).

MGC is a human glioblastoma cell line. The cell line was initiated at the tissue culture facility of the Institute of Cancer Research, Vienna, Austria from a biopsy. This adherent cell line was cultured with MEME supplemented at 37°C with 5%CO_2 in the atmosphere and subcultivated 1:5.

HCT-15 is a human colorectal adenocarcinoma Duke´s type C (ATCC Number CCL-225) from a male. The cell line is epithelial and adherent. It was cultured with RPMI 1640 at 37°C with 5% CO_2 in the atmosphere and subcultivated1:10.

HT-29 is a human colorectal adenocarcinoma (ATCC Number HTB-38) derived from a 44 year old female Caucasian. Cells were isolated from a primary tumour in 1964 by J. Fogh. The cell line is epithelial and adherent. It was cultured with RPMI 1640 complemented with a final concentration of 10% FBS at 37°C with 5%CO_2 in the atmosphere, and subcultivated 1:10.

CaCo-2 is a human colorectal adenocarcinoma (ATCC Number HTB-37) derived from 72 year old Caucasian male. The cell line is epithelial and adherent. It was cultured with RPMI 1640 at 37°C with 5%CO_2 in the atmosphere. CaCo-2 cells were subcultivated 1:5.

HCT-116 is a human colorectal adenocarcinoma (ATCC Number CCL-247) derived from adult male. The cell line is adherent and was cultured with DMEM modified medium (see chapter 3.1.2.2) at 37°C with 5%CO_2 in the atmosphere, and subcultivated 1:10.

MCF-7 is a human breast mammary gland epithelial adenocarcinoma (ATCC Number HTB-22) derived from pleural effusion of a 69 year old female Caucasian. The cell line is adherent and cultured with DMEM modified medium without phenol red (see chapter 3.1.2.2) and supplemented with 10% FBS. The cells grew at 37°C with 5%CO_2 in the atmosphere, and were subcultivated 1:10.

HMEC-1 is a human microvascular endothelial cell line (Ades et al. 1992) derived from the tissue culture facilities of the Institute of Cancer Research, Vienna, Austria from a biopsy. The cells were grown on collagen (Sigma Aldrich, St.Louis, MO) layer coated flasks (85µl Collagen/1616µl PBS for 25cm^2) at 37°C with 5%CO_2 in the atmosphere. The adherent cell line was cultured with DMEM modified medium (see chapter 3.1.2.2) and subcultivated 1:4.

3.1.2 Cell Culture Medium

3.1.2.1 RPMI 1640

RPMI 1640 (Sigma Aldrich, St.Louis, MO) was complemented with 10% fetal bovine serum (FBS, PAA) 2g/l $NaHCO_3$ (VWR, Vienna, Austria) and 1% Penicillin-Streptomycin (PAA). After addition the solution was sterile filtered 0,22µm filter (Corning) and stored at 4°C for max. 2 weeks.
RPMI 1640 without phenol red (PAA) was used for MTT assays.

3.1.2.2 DMEM

DMEM (Sigma Aldrich) was complemented with 10% FBS (PAA), 3,7g/l $NaHCO_3$ (VWR) and 1% Penicillin-Streptomycin (PAA). After addition the solution was sterile filtered 0,22µm filter (Corning) and stored at 4°C for max. 2 weeks.

Medium for MCF-7 cell line:

DMEM without phenol red (Invitrogen, Carlsbad, USA) was complemented with 10% FBS (PAA) 3,7g/l $NaHCO_3$ (VWR) and a total concentration of 4,5g/l glucose monohydrate (VWR). After addition the solution was sterile filtered 0,22µm filter (Corning). The sterile medium was supplemented with 57,2µl/l of 3,5µM insulin stock (Sigma Aldrich), 2mM L-Glutamine (Sigma) and 1% Penicillin-Streptomycin (PAA) and stored at 4°C up to 2 weeks.

Medium for HMEC-1 cell line:

DMEM (Sigma Aldrich) was supplemented with 10% FBS (PAA) 3,7g/l $NaHCO_3$ (VWR). After addition the solution was sterile filtered 0,22µm filter (Corning). The sterile medium was supplemented with 10µg/ml endothelial growth factor (EGF, Sigma Aldrich) and 24ng/ml hydrocortisone (Sigma Aldrich) and stored at 4°C for one week.

3.1.2.3 MEME

MEME (Sigma Aldrich) was supplemented with 10% FBS (PAA), 2,2g/l $NaHCO_3$ (VWR) and 1% Penicillin-Streptomycin (PAA). After addition the solution was sterile filtered 0,22µm filter (Corning) and stored at 4°C up to 2 weeks.

3.1.2.4 MNP

MEME (Sigma Aldrich) was complemented with 10% FBS (PAA), 2,2g/l $NaHCO_3$ (VWR), 1% Penicillin-Streptomycin (PAA), 2µl/ml pyruvate (Sigma Aldrich) and 1% non-essential amino acids (NEAA, PAA). After addition the solution was sterile filtered 0,22µm filter (Corning) and stored at 4°C for max. 2 weeks.

3.2 Peptides and other Substances

Vasoactive intestinal peptide (VIP), VIP-DOTA with and without gadolinium (VIP-DOTA-Gd), pituitary adenlyate cyclase-activating peptide (PACAP), VIP-hematoporphyrin (VIP-PDT), photosan, VIP-Cy3 and VIP-Fluo were synthesized using FMOC solid-phase peptide synthesis (FMOC-SPPS) and finally purified by RP-HPLC (piCHEM, Graz, Austria). ($Ala^{11,22,28}$)-VIP and ($Ala^{11,22,28}$)-VIP-FITC were produced by Bachem (Bubendorf, Switzerland).

The liposome batch L08I was synthesised by Ruth Prassel (Institute of Biophysics and Nanosystems Research, Academy of Sciences, Graz, Austria). VIP-loaded proticles batch #G (PG) were produced and purified by Andreas Zimmer (Institute of Pharmacological Sciences, University Graz, Austria).

All conjugates were covalently linked to the C-terminus except scrambled VIP, where Cy3 is linked to N-terminus (table.6). Chemical structures of VIP-conjugates are shown in fig.8.

Table 6. Peptides and substances used.

Peptide	Sequence N-C terminus (one letter aa code)	Molecular mass [Da]	conjugate	Produced by
VIP	HSDAVFTDNYTRLRKQMAVK-NH_2	3325,9	-	piCHEM
($Ala^{11,22,28}$)-VIP	HSDAVFTDNY**A**RLRKQ-M(O)-Dip-VKK**A**LNSIL**A**-NH_2	3160,7	-	Bachem
VIP-DOTA	Ac-HSDAVFTDNYTRLRKQM(O) AVKKYLNSILNK(DOTA)-NH_2	3898,4	DOTA	piCHEM
VIP-DOTA-Gd	Ac-HSDAVFTDNYTRLRKQM(O) AVKKYLNSILNK(DOTA[Gd])-NH_2	3994,6	DOTA-Gd	piCHEM
VIP-PDT	HSDAVFTDNYTRLRKQMAVK KYLNSILNK(Haem)-NH_2	4075,0	hematoporphyrin	piCHEM
PACAP	HSDGIFTDSYSRYRKQMAVK KYLAAVLGKRKQRVKNK-NH_2	4531,5	-	piCHEM
Photofrin®	hematoporphyrin oligomer	ca.10.000	-	piCHEM
VIP-Cy3	HSDAVFTDNYTRLRKQ MAVK-K-Cy3	3921,7	Cy3	piCHEM
VIP-Fluo	HSDAVFTDNYTRLRKQ MAVK-K-Fluo	3812,3	Flourescein	piCHEM
$Ala^{(11,22,28)}$-VIP-FITC	HSDAVFTDNY**A**RLRKQ-M(O)-Dip-VKK**A**LNSIL**A**-K-FITC-NH_2	3678,26	FITC	Bachem
Cy3-Scr-VIP	Cy3-AhxYIKKMNRVLAQDN SDATYSVLNTKHLRF-NH	3906,7	Cy3	piCHEM
Et-Cy3-OH	Ethyl-Cy3-OH	629,8	Cy3	piCHEM
Liposome batch L08I	VIP in Lyso-PG:DSPE [PEG200]=11:7,5:1	100nm filter	-	Ruth Prassl
Proticle batch #G	VIP-loaded proticles (Oligonuctleotide:VIP:protamin=1:2:0,6)	100µg/ml	-	Andreas Zimmer

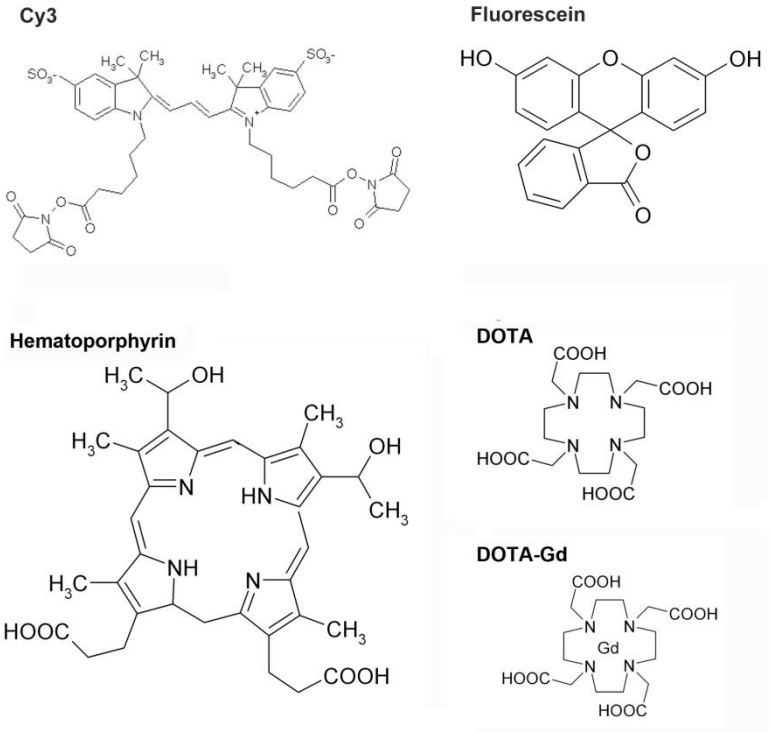

Figure 8. Chemical structure of VIP conjugates used in this study. Cy3 and Fluorescein are fluorescing molecules. DOTA, DOTA chelated to gadolinium (Gd) has an application in MRI diagnostic. All conjugates are linked to the C-terminus of VIP with lysine as linker.

3.3 Western Blot analysis (WB)

Western blot analysis was performed to determine the $VPAC_1$ and $VPAC_2$ expression of the cells. The concentration of protein lysate of all cell lines were analysed to separate on a polyacrylamide gel for SDS-PAGE. Separated proteins were blotted onto nitrocellulose membrane. An immunodetection was done with specific antibodies and were visualised with chemiluminescence on an X-ray films.

Total protein content:

- *RIPA II Buffer:* 50mM TRIS-Cl (Merck), pH 7,4, 500mM NaCl (Sigma Aldrich), 1% Nonidet NP40 (Sigma Aldrich), 0,1% SDS (Roth, Karlsruhe, Germany), 0,05% Natriumazid NaN_3 (Merck).
- 1mM Natriumorthovanadate $NaVO_4$ in PBS

All preparations were done on ice. All cells lines were cultured in $25cm^2$ flask for 2 day at 37°C with 5%CO_2 in the atmosphere. The cells were scraped off with a cell scraper (Corning) in 3ml fresh medium including 1mM $NaVO_4$ (Sigma Aldrich). The flak was washed with PBS, $NaVO_4$ to remove all cells. After centrifugation at 1500rpm for5min,

cells were washed with 3ml PBS, $NaVO_4$. After a centrifugation at 1500rpm for 5min, the pellet was lysed with 100µl RIPA II buffer, 1x Complete Protease inhibitor (Roche Diagonstics, Basel, Switzerland) and $NaVO_4$. Cell lysate was sonicated (Sonoplus Bandelin, Berlin, Germany) 3 times 3s and centrifuged at 1500rpm for 5min. The total protein lysate was stored at -20°C.

Determination of Protein Concentration:

The protein concentration was determined with Bradford assay. A bovine serum albumin (BSA, Pierce, Rockford, USA) standard curve (range 0-8mg/ml) was used to calculate the unknown protein concentration. 1µl RIPA II buffer, 0-8µl BSA, 150µl Coomassie Protein Assay Reagent (Pierce) complemented with bidest. water to reach 160µl in total. 1µl protein lysate, 9µl bidest. water and 150µl Coomassie Protein Assay Reagent (Pierce) were used for determination of protein concentration. Standards and samples absorbance were measured at 595nm with Synergy HT Microplate Reader (BIO-TEK, Vermont, USA).

SDS-PAGE:

- *10x Electrophoresis buffer,* all chemicals were purchased by Merck*:* 14,4% (w/v) glycine, 3% (w/v) TRIS, 1% (w/v) SDS. 1x electrophoresis buffer was diluted 1:10 with dest. water.
- *Resolving gel buffer:* 1,5M TRIS/HCl pH 8,8
- *Stacking gel buffer:* 0,5M TRIS/HCl pH 6,8
- 40% Acrylamide/Bisacrylamide 37,5:1 (2,6% C) (Bio-Rad, Hercules, Canada)
- 10% (w/v) SDS (Sigma Aldrich)
- 10% /w/v) APS (Sigma Aldrich)
- TEMED (Sigma Aldrich)
- *6x SDS-PAGE reducing buffer:* 7ml 1M TRIS (Merck) pH 6,8; 2ml Glycerine (Merck), 1ml Mercaptoethanole (Sigma Aldrich), 1g SDS (Merck); 0,1mg bromphenole blue (Sigma Aldrich). Aliquotes were stored at -20°C.

Table 7. Recipe for a 12% polyacrylamide (PAA) gel.

Amount for 2 gels	**Resolving gel 12%**	**Stacking gel 5%**
40% Acryl/Bisacrylamide	3 ml	0,5 ml
Resolving Buffer pH 8,8	2,5 ml	--------
Stacking Buffer pH 6,8	-------	1,0 ml
bidest. Water	4,5 ml	2,5 ml
degas		
10% SDS	100µl	100µl
10% APS	100µl	100µl
TEMED	4,0µl	8,0µl
Amount	*10,2 ml*	*4,2 ml*

After overlaying the separation gel (tab.7) with 96 % ethanol, the gel was polymerised during 30 minutes. The ethanol was then removed and the stacking gel was polymerised during 30 minutes in the presence of a sample comb 0,75mm (Hoefer SE 260, Amersham, San Francisco, USA).

For denaturing the samples, they were mixed in 1x SDS-PAGE reducing sample buffer, incubated for 5 minutes at 95°C and shortly centrifuged. 20µg/lane of proteins and 5µl/lane of the Page Ruler Prestained Protein Ladder (Fermantas, Ontario, Canada) were loaded onto the gel. The electrophoresis chamber (Hoefer SE 260) was then filled with 1x electrophoresis buffer before separating the proteins at 130V/100mA 1-1,5 hours at room temperature. Once the proteins were separated, the gels were used for western blot.

Blotting:

- *10x blot buffer:* 14,4% (w/v) glycine (144g/l), 3% (w/v) TRIS (30g/l), 0,2% (w/v) SDS (2g/l). All chemicals were purchased by Merck. 1x Blot buffer consisted of 20% (v/v) MeOH and was cooled to 4°C before use.

After electrophoresis the gel was equilibrated in 1x blot buffer. The nitrocellulose membrane (Bio-Rad) was also pre-soaked in the 1x blot buffer. The sandwich of blot, gel, filter paper and fibre pads was constructed in the blotting cassette according to the supplier's instructions (Hoefer TE 22). The electro blotting was performed at 25V/60mA over night at 4°C.

Ponceau staining:

A reversible staining of the proteins on the membrane was performed using 0.5% Ponceau Red S (Sigma Aldrich) in 1% acetic acid (Sigma Aldrich) for 5 minutes. The membrane was then carefully washed with water to reveal the protein bands. Before immunodetection, the ponceau staining was removed during the blocking step.

Immunodetection with antibodies:

- *TPBS buffer* (Blocking solution): PBS, 3% BSA (Sigma), 0,5% Tween20 (Merck)
- *Washing buffer:* PBS, 0,5% Tween20 (Merck)
- *primary Ab:* monoclonal anti-$VPAC_1$ (1mg/ml) (Abcam, Cambridge, UK), monoclonal anti-$VPAC_2$ mouse (1mg/ml) (Abcam), polyclonal rabbit anti-actin (1mg/ml) (Sigma Aldrich)
- *secondary Ab:* rabbit polyclonal peroxidase conjugated anti-mouse (Calbiochem Merck), goat polyclonal peroxidase conjugated anti-rabbit (Calbiochem Merck)
- Super Signal West Pico Chemiluminescence Substrate (Pierce)

Nitrocellulose membrane was blocked with blocking buffer for 1h. After blocking both primary antibodies, anti-$VPAC_1$ and anti-$VPAC_2$ were diluted 1:10.000 and anti-actin 1:5000 in blocking buffer and incubated 1h at RT. The membranes were washed 5 times each 5min with washing buffer. Secondary antibody anti-mouse was diluted 1:10.000 and anti-rabbit 1:7500 in blocking buffer and incubated 1h at RT. The membranes were washed 5 times each 5min with washing buffer. The membrane was incubated with Chemiluminescence Substrate mixed 1:1 for 5min and exposed on CL-Xposure film (Pierce) for some minutes.

3.4 Immunocytochemistry (ICC)

An immunocytochemistry staining allows the detection of antigens with specific antibodies. After fixation of cells, a blocking step with FBS and afterwards incubations with primary and secondary antibody conjugated to biotin were performed. Biotin signal was multiplied with streptavidin-peroxidise complex. The enzyme peroxidase converted the substrate DAB into a brown colour precipitation. Schematic drawing of ICC (fig.9) shows the detection of antigen with primary and secondary antibodies. Marker indicates several different visualisation systems.

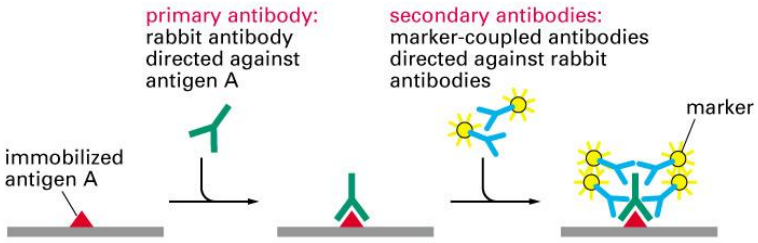

Figure 9–16. Molecular Biology of the Cell, 4th Edition.

Figure 9. **Scheme of immunocytochemistry (ICC) staining**. The primary antibody recognizes the antigen. The secondary antibody covalently linked to a marker molecule, e.g. enzyme, binds to the primary ab. The marker molecule is able to convert a substrate to a visible product. [from (Alberts B 2002)]

ICC Procedure:

10^5 cells/well were grown in 4-well Lab-Tek Chamber Slides (Nunc, Roskilde, Denmark) over night at 37°C with 5%CO_2 in the atmosphere. The cells were washed twice 5min with PBS and fixated with 2% paraformaldehyd (PFA, Sigma) for 30min at 4°C. Cells were washed twice each 5min and air dried for 10min. 30min blocking step with 3%BSA/0,5%Tween20/PBS was performed at RT. Incubation of primary antibodies polyclonal rabbit anti-$VPAC_1$ (1:200, 1mg/ml, Abcam), polyclonal rabbit anti-$VPAC_2$ (1:1000, 1mg/ml, Abcam) and polyclonal rabbit anti-PAC_1 (1:1000, 1mg/ml, Abcam) was done for 1h. As a negative control one well was incubated with PBS without primary antibody. Following three washing steps with PBS were performed and the secondary antibody goat polyclonal anti-rabbit-Ig-biotin (1:500, Dako Cytomation, Glostrup, Denmark) diluted in blocking solution was incubated for 30min. The negative control was treated with secondary antibody under the same conditions. After two washes with 0,3% H_2O_2 in PBS for 10min, the cells were washed with PBS for 5min. The cells were incubated with Streptavidin Peroxidase Ready to Use (Lab Vision, Fremont, USA) for 30min. Additional three washing steps with PBS each 5min were performed. As substrate for peroxidase Liquid DAB+Substrate Chromogen System (Dako Cytomation) was used and it was incubated for 20-40min (brown precipitates), followed by three additional washing steps.

Nuclea staining with Mayer´s Hematoxylin:

Mayer´s Hematoxylin Solution 0,1% (Sigma) was diluted 1:3 and cells were incubated for 10min. The slide was washed with bidest. water and incubated with tap water for 10min (blue staining of cell nuclei).

Mounting:

The slides were incubated with 96% ethanol (Sigma) for 10 min. Slides were further dehydrated with 100% ethanol for 10min. Two incubation steps with xylol (Sigma) were done for 10min each. After dehydration the object slides were mounted in Eukitt (O.Kindler, Freiburg, Germany) and hardened over night. Microscopic analysis was performed with a 60x objective Eclipse 80i microscope (Nikon, Kanawaga, Japan).

3.5 Vitality test

Trypane blue is an acidic dye which cannot penetrate intact living cell membranes. It was used to visualise dead cells. Not coloured cells indicated the survival and vitality of cells. Blue colour in the cells indicate dead cells.

The medium of the cells was aspirated and a staining with 0,4% trypane blue (Sigma Aldrich) diluted 1:20 in PBS was performed for 2min. The solution was aspirated and cells were covered with PBS. Micrographs were taken with an Eclipse TS 100 microscope (Nikon). If cells were cultured after staining, the PBS was aspirated and culture medium was added.

3.6 Proliferation assay (MTT)

A non-radioactive cell proliferation and cytotoxcity assay [MTT test with 3-(4,5-Dimethylthiazol-2-yl)-2,5-diphenyltetrazoliumbromid; EZU4 Kit, Biomedica, Vienna, Austria] was used for studying of peptide analogues behaviour at cells growth conditions. Few cells (10^3-10^5) were grown on 96-well microtiter plates with a defined concentration of peptide analogue and incubated for 72h at 37°C with 5%CO_2 in the atmosphere. Tetrazolium salts (yellow) were used for cell viability; therefore living cells were capable to reduce slightly coloured tretrazolium salt into intensive coloured formazan derivate (deep red). This reduction process requires functional dehydrogenases in mitochondria of living cells, which are inactivated within a few minutes after cell death. This method was an excellent tool to discriminate living from death cells.

Procedure:

10^5 cells/well were grown in medium in a 96-well microtiter plate (Falcon Becton Dickson Labware, Franklin Lakes, USA). Following peptides and analogues were tested

for their proliferation or toxicity: VIP, ($Ala^{11,22,28}$)-VIP, VIP-DOTA, VIP-DOTA-Gd, PACAP. The analogues were analysed in following concentration: 10µM, 10nM and 10pM (table 8). Peptides analogues were diluted in medium and 100µl cell suspension and 100µl peptide dilution of each were mixed and loaded in the microtiter plate. Also a negative control was performed with 100µl cell suspension and 100µ medium. The cells were incubated for 72h at 37°C with 5%CO_2 in the atmosphere. After incubation the medium was aspirated and 200µl RPMI 1640 without phenol red (PAA) was added to each wells. 20µl of premixed dye-solution (2,5ml solution mixed with one bottle of dye) EZU4 Kit (Biomedica) was used to visualise viable cells. The plate was incubated 1-4h, depending on cell line, at 37°C 5%CO_2 to convert dye substrate into a deep red formazan derivate product. The colour reaction was measured at 450nm and 620nm as reference by Synergy HT Microplate Reader (BIO-TEK). For calculation, the reference absorptions (620nm) of each four peptide dilutions and the negative control were subtracted and averaged. The standard deviation for the same values was calculated. The average of the negative control was supposed to 100%, and other data were calculated from this 100%. All calculated data were illustrated in a table, averages and standard deviations are given in the diagram.

Table 8. MTT loading scheme for 96-well plates.

	1	2	3	4	5	6	7	8	9	10	11	12
A	negative control	VIP 10µM	VIP 10nM	VIP 10pM	VIP-DOTA 10µM	VIP-DOTA 10nM	VIP-DOTA 10pM	VIP-PDT 10µM	VIP-PDT 10nM	VIP-PDT 10pM	negative control	medium
B												
C												
D												
E		$Ala^{(11,22,28)}$-VIP 10µM	$Ala^{(11,22,28)}$-VIP 10nM	$Ala^{(11,22,28)}$-VIP 10pM	VIP-DOTA-Gd 10µM	VIP-DOTA-Gd 10µM	VIP-DOTA-Gd 10µM	PACAP 10µM	PACAP 10µM	PACAP 10µM		
F												
G												
H												

3.7 Enzyme Linked Immuno Sorbent Assay (ELISA)

Enzyme linked immuno sorbent assay (ELISA) is a method to detect specific antigens after antibody treatment. The so called “sandwich ELISA” is explained in fig.10. Coated microtiter plate with sera and antigen is recognized by monoclonal primary

antibody. The polyclonal secondary antibody is conjugated to an enzyme which converts a soluble substrate into a precipitate, it detects the primary antibody. A distinct wavelength can be measured by photometry and quantified via a standard curve.

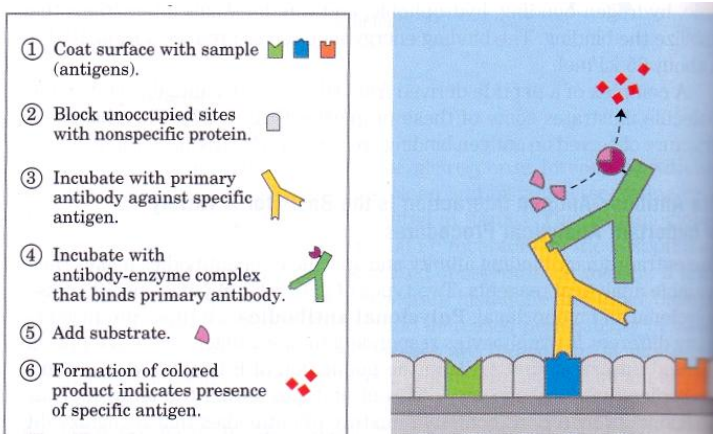

Figure 10. Sandwich ELISA assembly. Unspecific binding sites are blocked with proteins and antigen. Antigen coated surface is detected by primary antibody. Enzyme linked secondary antibody recognizes the primary ab and converts a substrate to a coloured product. [from (Nelson D L 2004)]

The second messenger cAMP is used to detect VIP internalisation and the indirect detection of the VIP signalling pathway. Following chemical substances are influencing VIP signalling pathway (fig.11):

Forskolin is known to activate adenylate cyclase (AC), an enzyme responsible for synthesis of cAMP. It results in an increased amount of available cAMP leading to increased lipolysis and oxidation of fatty acids resulting in increased thermogenesis. Forskolin does not influence or interact with the VIP signalling pathway.

IBMX, 1-methyl-3-(2-methylpropyl)-7H-purine-2,6-dione, is a potent cyclic nucleotide phosphodiesterase inhibitor. Due to this action, the compound increases cAMP and cGMP in tissue and thereby activates cyclic nucleotide-regulated protein kinases. The phosphodiesterase inhibitor IBMX prevents breakdown of cAMP.

SQ22,536; [9-(tetrahydro-2-furanyl)-9H-purin-6-amine], is an adenlyate cyclase inhibitor.

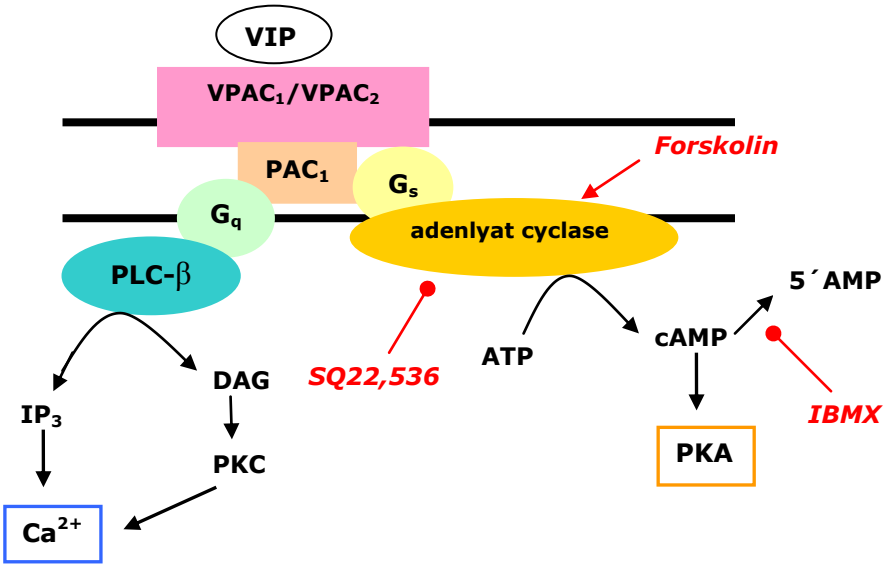

Figure 11. VIP signal transduction pathway and the influence of Forskolin, IBMX and SQ22,536. Red arrows indicate activation and red dots inhibition of proteins. Forskolin actives the adenlyate cyclase directly (VIP independent). SQ22,536 inhibits the adenlyate cyclase. IBMX prevents the degradation of cAMP to 5´AMP by blocking cyclic nuclide phosphodiesterase.
VIP vasoactive intestinal peptide, $VPAC_{1/2}$ VIP receptor subtypes, PAC_1 PACAP-preferring receptor subtype, G_s stimulatory G-protein activates AC, G_q stimulatory G-protein activates PLC-β, PLC-β Phospholiase C, IP_3 Inositol-3-phosphate, DAG Diacylglycerol, PKC Ca^{2+}-depending protein kinase, ATP Adenosintriphosphate, cAMP cyclic adenosinemonophosphate.

3.7.1 ELISA setup

10^5 cells/well of HMEC-1, HT-29 and Capan-1 were grown in medium in a 96-well microtiter plate (Falcon Becton Dickson Labware) at 37°C with 5%CO_2 in the atmosphere over night. The cells were incubated in starvation medium (medium containing only 3% BSA) for 3h at 37°C with 5%CO_2 in the atmosphere.

Following peptide and substance dilutions were used a total concentration/100µl well starvation medium of:

- 10nM of VIP, ($Ala^{11,22,28}$)-VIP, VIP-DOTA-Gd and VIP-PDT
- 500µM 3-isobutyl-1-methyl-xanthine (IBMX, Sigma)
- 20µM Forskolin 20µM (Sigma)
- 100µM SQ22,536 (Sigma)

Table 9. ELISA loading scheme of 96-well plate.

	1	2	3	4	5	6
A	Medium	VIP 1nM	VIP 10nM	VIP 100nM	IMBX 1nM VIP	IMBX 10nM VIP
B	IBMX + 100nM VIP	SQ 1nM VIP	SQ 10nM VIP	SQ 100nM VIP	Forskolin	Forskolin IBMX
C	Medium	VIP 1nM	VIP 10nM	VIP 100nM	IMBX 1nM VIP	IMBX 10nM VIP
D	IBMX 100nM VIP	SQ 1nM VIP	SQ 10nM VIP	SQ 100nM VIP	Forskolin	Forskolin IBMX

5µl of 1µM VIP-conjugates, 25µl of 10mM IBMX stock, 5µl of 1:20 diluted 20mM forskolin stock and 5µl of 20mM SQ22,536 stock were used in the assay. After starvation, peptides and substances were mixed (table 9) and incubated for 20min at 37°C with 5%CO_2 in the atmosphere. Medium was aspirated and cells were lysed using Amersham cAMP Biotrak Enzyme immunoassay (EIA) System (GE Healthcare, Uppsala, Sweden) with 200µl lysis buffer 1B. After 10min shaking, the supernatant was directly used in EIA Kit or stored at -20°C. The complete cell lysis was tested with the vitality test (see chapter 3.5).

ELISA procedure:

EIA cAMP standards were mixed as shown in table 10. Standards were used within 1h.

Table 10. cAMP EIA standard loading scheme.

cAMP [fmol]	µl stock 32 pmol	µl dilution	µl Lyses reagent 1B
1600	500	-	500
800	-	500	500
400	-	500	500
200	-	500	500
100	-	500	500
50	-	500	500
25	-	500	500
12,5	-	500	500

Following amounts were loaded to the microtiter plate (see fig.12):

- 100µl lysis reagent 1B and 100µl lysis reagent 2B were loaded in NSB well.
- 100µl lysis reagent 1B was loaded in Std 0 well.

- 100µl of each standard (0-3200pM) and 100µl sample.

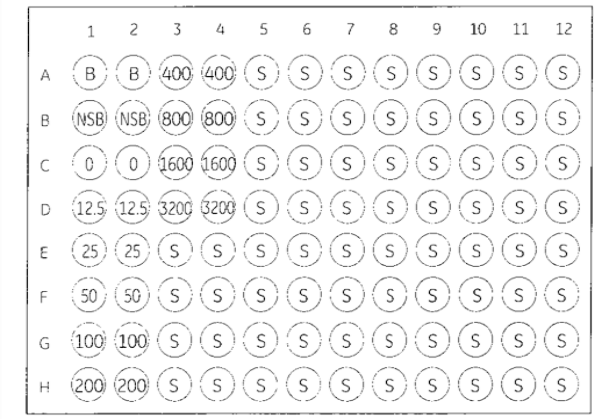

Figure 12. EIA loading scheme of 96-well microtiter plate. B blank, NSB non specific binding, 0-3200 fmol standards, S sample

Samples were run in duplicates. All reagents were warmed up to RT and the plate was put on ice. 100µl antisera were loaded in all wells except NSB und B, and incubated 2h at 4°C. 50µl cAMP-peroxidase conjugate was added to all wells except B and incubated 1h at 4°C. The plate was washed 4 times with 200µl wash buffer. 150µl enzyme substrate was transferred to all wells and incubated 1h at RT with shaking. The blue colour was measured at 630nm (as reference) with Synergy HT Microplate Reader (BIO-TEK). 100µl 1M sulfuric acid (Sigma) was added to stop the reaction. The yellow colour was measured at 450nm within 30min with Synergy HT Microplate Reader (BIO-TEK).
The absorbance data were calculated with a standard calibration curve of cAMP. The averages of the duplicates were built and the standard deviation was calculated. All averages and standard deviations were illustrated in a diagram.

3.7.2 Time course experiment

The cell assay was performed with PASMC (pulmonary artery smooth muscle cells) 10^5cells/well in DMEM medium. Cells were cultured in 24-well plates (Nunc) for 2-3 days at 37°C with 5%CO_2 in the atmosphere. The cells were incubated in starvation medium (medium containing only 3% BSA) for 3h at 37°C with 5%CO_2 in the atmosphere.
Following substances were diluted in starvation medium with a total concentration of (table 11):

- 10nM VIP
- 10nM and 100nM liposomes #L08I
- 10nM and 100nM proticles #G
- 500µM 3-isobutyl-1-methyl-xanthine (IBMX) (Sigma)
- 20µM Forskolin 20µM (Sigma)

Table 11. ELISA loading scheme for lipsome assay in 96-well plate.

	1	2	3	4	5	6
A 5min	Medium	VIP 10nM	Liposome 10nM	Liposome 100nM	Proticle 10nM	Proticle 100nM
B 10min	IBMX	VIP 10nM	Liposome 10nM	Liposome 100nM	Proticle 10nM	Proticle 100nM
C 20min	Forskolin	VIP 10nM	Liposome 10nM	Liposome 100nM	Proticle 10nM	Proticle 100nM
D 60min	IBMX + Forskolin	VIP 10nM	Liposome 10nM	Liposome 100nM	Proticle 10nM	Proticle 100nM

Lane A was incubated for 5min, B for 10min, C for 20min, D for 60min, IBMX, Forskolin and both together each 20min. Cells were washed with PBS and lysated with 150µl 0,1M HCl (Merck) for 10min with shaking. Lysis was repeated twice (each 150µl) and supernatant was stored at -20°C or used directly for cAMP direct EIA Kit (Assay Design, Ann Arbor, USA) .

Also PANC-1 cells passage 4 (P4) were used for time course experiment with proticles #G. The same assay like for liposomes was performed for proticles, but with the cell assay described in chapter 3.7.1. 10^5 cells/well of PANC-1 P4 were cultured in 96-well plates (Falcon Becton Dickson Labware). The agonists were incubated for 5/10/ 20/ 30/ 45/60min. 1µM and 300nM proticles #G and 10nM and 100nM of VIP were used in the assay. Controls were done with forskolin and IBMX. The cAMP level was measured with a ELISA assay (see 3.7.1).

ELISA procedure:

Acetylated assay was used for the cAMP detection. The cAMP standards were mixed as followed (table 12). Standards should be used within 30min.

Table 12. Standard preparation for cAMP assay, Assay Design.

cAMP Standard	c [pmol/ml]	Stock (2000pM/ml)	0,1M HCl	Addition of
1	20	10µl	990µl	-
2	5	-	750µl	250µl of Std 1
3	1,25	-	750µl	250µl of Std 2
4	0,312	-	750µl	250µl of Std 3
5	0,078	-	750µl	250µl of Std 4

10µl acetylating reagent (0,5ml acetic anhydride, 1ml triethylamine) was added to 200µl standards and samples. 50µl acetylating reagent was transferred to NSB and B_0. All standards, samples and controls were run in duplicates (table 13) and measured at 405nm with a Microplate Reader Asys, Expert Plus (Eugendorf, Austria).

Table 13. 96-well plate pipette scheme for cAMP detection assay, Assay Design.

Wells	**Blank A1, B1**	**TA C1, D1**	**NSB E1, F1**	**Std 0 (B_0) G1, H1**	**Std 1-5 A2, B2**	**Samples C3-D3**
Neutralisation Regent	-	-	50 µl	50 µl	50 µl	50 µl
0,1M HCl	-	-	150 µl	100 µl	-	-
Std or sample	-	-	-	-	100 µl	100 µl
Blue Conjugate	-	-	50 µl	50 µl	50 µl	50 µl
Antibody	-	-	-	50 µl	50 µl	50 µl
Incubation 2h RT, shaking						
3x wash each 200µl wash solution (1:20)						
Blue Conjugate	-	5 µl	-	-	-	-
Substrat pNpp	200 µl	200 µl	200 µl	200 µl	200 µl	200 µl
Incubation 2h RT						
Stop Solution	50 µl	50 µl	50 µl	50 µl	50 µl	50 µl

The concentrations of the duplicates were calculated with a standard calibration curve of cAMP. The average and the standard deviation of the duplicates was calculated and illustrated in a diagram.

3.8 Photodynamic therapy assay (PDT)

Photodynamic therapy (PDT) is a method to induce cell growth in healthy cells or induce cell death/apoptosis in tumour cells. PDT is based on a hematoporphyrin ring which produces radicals after irradiation exposure at about 650nm with a laser. Hematoporphyrin is light sensitive and also decays at day light. Free radicals produce oxidative stress and cells go in apoptosis. One method to quantify reacting oxygen species (ROS) uses dichlorofluorescein (DCFDA). DCFDA detects cellular peroxides, accumulates in the cytosol and is cytotoxic in high concentration. An optimal concentration is between 1-10µM. To avoid contaminations with endogenous esterase, serum free medium should be used for the assay. DCFDA´s strong fluorescence is visualised at ex488/em525nm (Halliwell and Whiteman 2004).

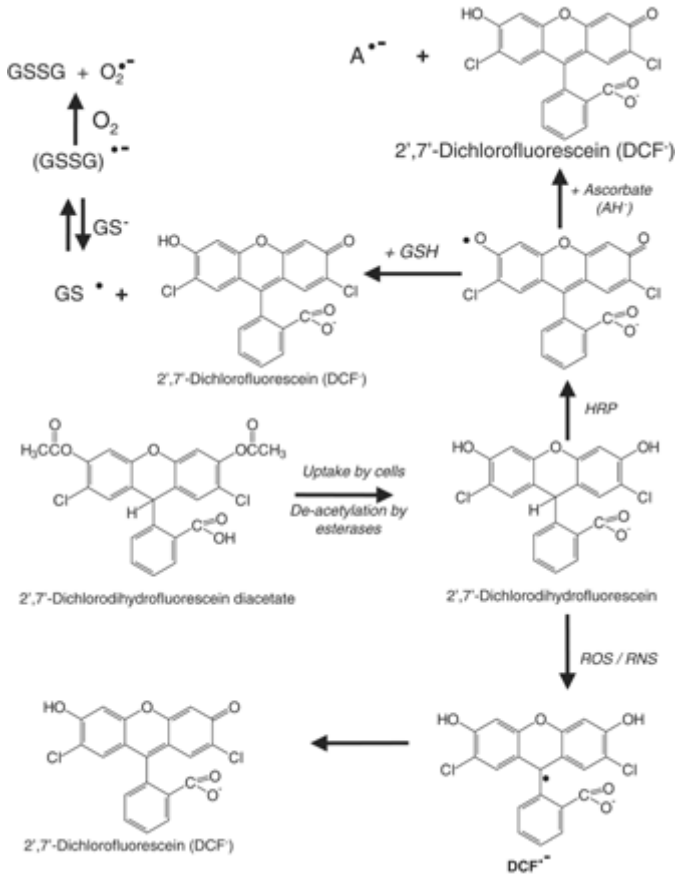

Figure 13. Scheme of redox reaction in PDT. The conversion of DCFDA (2´7´-dichlorofluorescein diacetate) to a fluorescent product.
It is hydrolyzed by cellular esterases to dichlorofluorescin (2´7´-dichlorodihydrofluorescein), whose oxidation by several ROS yields florescent DCF (2´7´-dichlorofluorescein) via an intermediate radial, $DCF^{\bullet-}$. Peroxidases can also convert it into a phenoxyl radical that can interact with antioxidants such as ascorbate (AH^-), reducing the phenoxyl radical and oxidizing ascorbate, or with GSH. $GS^{\bullet}$ resulting from the latter reaction can lead to $O_2^{\bullet-}$generation. The phenoxyl radical can also be recycled by NADH (not shown), producing $NAD^{\bullet}$ radical, which reacts rapidly with O_2 to produce $O_2^{\bullet-}$: $NAD^{\bullet} + O_2 \rightarrow NAD^+ + O_2^{\bullet-}$[from Halliwell and Whiteman, 2004)].

H_2O_2 or $O_2^{\bullet-}$cannot oxidize DCFDA, neither can peroxyl, alcoxyl, $NO_2^{\bullet-}$, carbonate, $OH^{\bullet-}$and peroxynitirte. Also the fluorescence of the medium should be measured. Horseradish peroxidase (HRP) or other heme proteins can also oxidize DCFDA in presents of H_2O_2. This method is a general assay for oxidative stress but not particular for any ROS (fig.13).

3.8.1 Reactive oxygen species (ROS)

Cell assay:

200µl of HCT-15, PC-3, Hep3B, HT-29, HMEC-1 and SW1736 (10^5 cells/well) were grown on 96-well microtiter plate over night at 37°C with 5%CO_2 in the atmosphere in medium containing serum. Two plates were cultured to compare the oxidative stress of radiated and non-radiated cells. Four different cell lines were analysed at one plate (tab.

14). H_2O_2, photosan (PS) and VIP-PDT calibrated an internal standard with following concentrations (200µl/well) in duplicates:

H_2O_2 was diluted 1mM–100pM from 3% stock solution, photosan 10µM-10pM from 1mg/ml stock solution and VIP-PDT 10µM-10pM from 1mM stock solution (table 14). Dilution steps of 10 times each were done. Also a negative control of each cell line was performed in duplicates without a treatment with chemicals.

Table 14. Reactive oxygen species (ROS) assay loading scheme for 96-well plate.

	1	**2**	**3**	**4**	**5**	**6**
	H_2O_2	**PS**	**VIP-PDT**	**cell control**	**cell +PS**	**cell +VIP-PDT**
A	1mM	10µM	10µM	0	1µM	5µM
B	1mM	10µM	10µM	0	1µM	5µM
C	100µM	5µM	5µM	0	100nM	2µM
D	100µM	5µM	5µM	0	100nM	2µM
E	10µM	1µM	1µM	0	1µM	5µM
F	10µM	1µM	1µM	0	1µM	5µM
G	1µM	100nM	100nM	0	100nM	2µM
H	1µM	100nM	100nM	0	100nM	2µM

All dilutions were prepared in RPMI 1640 without phenol red or other supplements, and PBS to compare the autofluorescence and influence of RPMI on DCFDA. 10µM DCFDA (Dichlorofluorescein diacetate, stock 1mM) were transferred to each well and incubated for 30min at 37°C with 5%CO_2 in the atmosphere. One plate was irradiated with 150W 50-60Hz Infratherm Comfort PIL-2200 (Bosch, Stuttgart, Germany) in 20cm distance from plate for 30min at 37°C. The other plate was not radiated but performed with the same conditions. Fluorescence was measured with Synergy HT Microplate Reader (BIO-TEK) at 530nm.

The fluorescence of the values was averaged and the standard deviation was calculated. The averages of the radiated and the non-radiated data were given in a diagram.

3.8.2 PDT experiment

10^5cells/well of CaCo-2, Capan-1, HT-29 and HCT-15 cells were grown in medium on a 96-well microtiter plate (Falcon Becton Dickson Labware) at 37°C with 5%CO_2 in the atmosphere over night. VIP-PDT and Photosan (store in dark!) were added in following

concentration: 0M (control cells), 1µM, 100nM, 10nM, 1nM, and 10pM in RPMI without phenol red supplemented with FCS and 1x Complete protease inhibitor (Roche Diagnostics). Peptide dilutions were incubated at 37°C with 5%CO_2 in the atmosphere for 30min. The light radiation was done with an Infratherm Comfort PIL-2200 (Bosch) 150W/50-60Hz in 20cm distance from plate, for 30min in the incubator. Treated cells were incubated for 5-24h at 37°C with 5%CO_2 in the atmosphere. To compare treated cells also a non-treated cell assay was performed with same conditions but without radiation.

After incubation the medium was aspirated and 200µl RPMI without phenol red (PAA) was added to the wells. 20µl of premixed dye-solution mix (2,5ml solution mixed with 1 bottle of dye) EZU4 Kit (Biomedica) was used to visualise viable cells. The plate was incubated 1-3h, depending on cell line, at 37°C with 5%CO_2 in the atmosphere to convert dye substrate into a deep red formazan derivate product. The colour reaction was measured at 450nm and 620nm as reference by Synergy HT Microplate Reader (BIO-TEK).

The fluorescence values were averaged and the standard deviation was calculated. The survival rate of control cells was calculated and suggested to 100%. The averages of radiated and non-radiated data were given a diagram.

3.9 Fluorescent correlation microscopy (FCS)

FCS is a spectroscopic technique for study molecular interactions in solution. FCS monitors the random motion of fluorescently labelled molecules inside a defined volume element irradiated by a focused laser beam (fig. 14). These fluctuations provide information on the rate of diffusion or diffusion time of a particle and this, in turn, is directly dependent on the particle's mass. As a consequence, any increase in the mass of a molecule, e.g. as a result of an interaction with a second molecule, is readily detected as an increase in the particle's diffusion time. Not least due to its simple underlying principle, FCS is an ideal approach for the study of thermodynamic and kinetic features of molecular interactions in solution (Schwille P 2004).

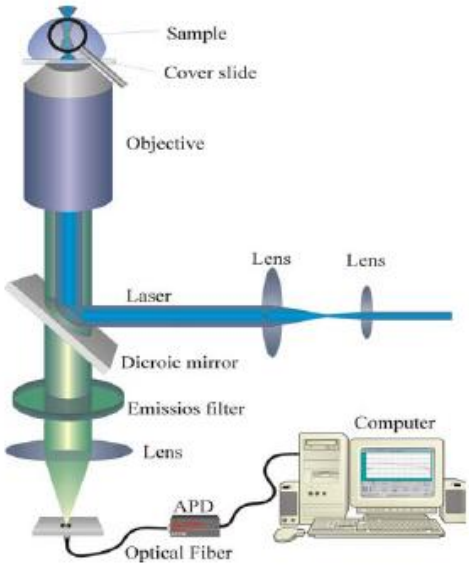

Figure 14. Schematic drawing of FCS setup. The exciting radiation provided by a laser beam is directed into a microscope objective via a dichroic mirror and focused on the sample. Water immersion objectives with a high numerical aperture (ideally > 0.9) are used. The fluorescence light from the sample is collected by the same objective and passed through the dichroic mirror and the emission filter. The pinhole in the image plane (field aperture) blocks any fluorescence light not originating from the focal region, thus providing axial resolution. Afterwards, the light is focused onto the detector, preferably an avalanche photodiode or a photomultiplier. [from (Schwille P 2004)]

FCS was introduced in the early 1970s has become a powerful tool for researchers in life science. Examples of successful FCS applications include studies on molecular diffusion, DNA hybridisation reaction and ultrasensitive pathogen detection. In the last years the first FCS application on living cells has been published. Rigler and co-workers used rhodamine-labelled ligands to demonstrate specific binding sites for C-peptide on human fibroblasts. Schwille et. al (2004) investigated ligand diffusion and specific binding on model membrane, as well as a model receptor system. They obtained typical diffusion constants for ligands freely diffusing in solution, ligands diffusing in the cell membrane, ligands bound to cell membrane receptor and a type of ligand diffusion in the cell which they termed “anomalous subdiffusion”; one possible explanation for the latter being binding to intracellular membranes.

Due to this very high sensitivity and the small measuring volume, FCS is a promising tool investigating low concentrations and confounding factors, e.g. an additional intracellular receptor complicate its detection.

FSC setup:

Ne/He laser 543nm: The measurements were performed with a Confocor (Carl Zeiss-Evotec, Jena, Germany) equipped with an Ne/He-Laser 543nm attenuated with an appropriate density filter, a C-Apochromat 63x/1.2W Korr objective, a dichroic mirror and bandpass filters. The pinhole size was set to 45µm, resulting in a confocal volume element of 0.35m in the xy (lateral) and 2.4µm in the z (axial) dimension as determined

by calibrating using Rhodamine B (Sigma Aldrich). Intensity fluctuations were recovered by an avanche photodiode (SPCM-CD 3017) and autocorrelated with a hardware correlator (ALV 5000, ALV, Langen, Germany)
To calibrate the FCS setup a 1:1000 dilution of Rhodamin B was used and 10 measurements were performed. From the calibration data the structure parameter was calculated and used for all following measurements.

Ar laser 488nm: The measurements were performed with a Confocor (Carl Zeiss-Evotec, Jena, Germany) equipped with an Argon-Laser 5488nm attenuated with an appropriate density filter, a C-Apochromat 63x/1.2W Korr objective, a dichroic mirror and bandpass filters. The pinhole size was set to 45µm, resulting in a confocal volume element of 0.35m in the xy (lateral) and 2.4µm in the z (axial) dimension as determined by calibrating using Rhodamine 6G (Sigma Aldrich). Intensity fluctuations were recovered by an avanche photodiode (SPCM-CD 3017) and autocorrelated with a hardware correlator (ALV 5000, ALV, Langen, Germany).
To calibrate the FCS a 1:100 dilution of Rhodamin 6G was used and 10 measurements were performed. From the calibration data the structure parameter was calculated and used for all following measurements.

Procedure:

PANC-1 cells passage 8 (P8) were used for this study. The cells were grown at 37°C/5%CO_2/95% rel. humidity in 75cm^2 cell culture flasks in RPMI 1640 medium. After one passage, 5x10^4 cells were cultured in a LabTek chambered coverglass (Nagle Nuc, Naperville, IL).
The incubated living cells were taken out of the incubator and the first well was filled with 10µM hepes buffer in PBS, while the other wells remained in medium. The FCS measurements were performed during the first 2h, afterwards a new cell covered Labtek was incubated.
All experiments were performed with 200µl of 1:1000 diluted peptides, VIP-Cy3 and VIP-Fluo in PBS. The negative control, Et-Cy3-OH, was diluted 1:10^5 and Cy3-Scr-VIP 1:1000 in PBS. Labelled proticles #G were diluted 1:100 in PBS.

3.9.1 Freely diffusion in solution

The diluted peptides were transferred to a well and the focus was placed above the glass. The measurement duration of the intensity fluctuations took 30 seconds with 3s delay between each measurement. 10 measurements were performed.

3.9.2 Membrane binding

Measurements were performed by first placing the focus at a cell-free solution volume in order to obtain count rate and autocorrelation function for the ligand diffusing freely in the buffer. A typical measurement series on a cell started several μm above the cell (where count rate and correlation curve were the same as in the pre-measurement lateral of the cell); the focus was then moved in 1μm steps from the top to the bottom of the cell and a 30s measurement was taken at every position. At the end of the scan the unaltered position of the cell was controlled by visual re-evaluation and a second recording of the typical intensity fluctuations at the cell membrane position.

3.9.3 Time course

A method to measure the intensity in the cytoplasm during time is a time course. The focus is placed in the cytoplasm of the cell; this means it is focused on equatorial plate. The focus is fixed and will not be moved anymore. Afterwards intensity fluctuations of peptide were measured during a time periode. Each 30s a measurement of 5s was done over a period of 30 minutes. To calculate the different amounts of intensity in the cytoplasm, a diagram with count rate on y (intensity [kHz]) and time [min] on x was performed.

3.10 Confocal Laser Scanning Microscopy (CLSM)

Confocal laser scanning microscopy (CLSM) is a very good tool to focus distinct regions in a specimen and to illuminate with fluorescence. Fig. 15 shows a simplified diagram which the basic arrangement of optical components is similar to that of the standard fluorescence microscope, except that a laser is used to illuminate a small pinhole whose image is focused at a single point in the specimen (A). Emitted fluorescence from this focal point in the specimen is focused at a second (confocal) pinhole (B). Emitted light from elsewhere in the specimen is not focused here and therefore does not contribute to the final image (C). By scanning the beam of light

across the specimen, a very sharp two-dimensional image of the exact plane of focus is built up that is not significantly degraded by light from other regions of the specimen.

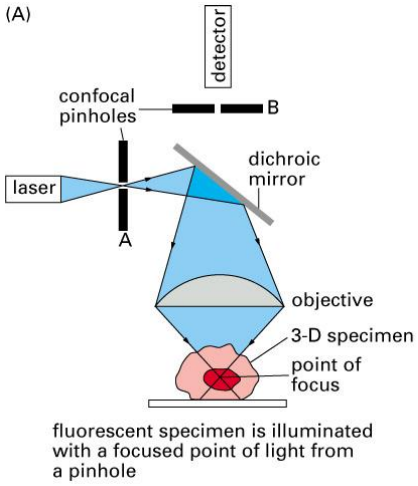

Figure 9–18 part 1 of 2. Molecular Biology of the Cell, 4th Edition.

Figure 15. Scheme of a Confocal Laser Scanning Microscope (CLSM). A laser beam passes a small pinhole and activates the fluorescence in the sample. The emitted fluorescence passes a confocal pinhole, to achieve a z-resolution, and is detected by the detector. After scanning the beam through the specimen a two dimensional image is reconstructed. [from (Alberts B 2002)]

Procedure:

Internalisation studies allow the detection of fluorescent labelled peptides in living cells. 10^4cells/well of LNCaP, Capan-1, PANC-1 passage P14 and P40, A427, Hep3B, SW1736, HT-29, CaCo-2, HCT-116 were grown in medium on coverslips (G. MENZEL, Braunschweig, Germany) over night at 37°C with 5%CO_2 in the atmosphere. The cells were carefully washed twice with PBS. Unspecific binding was blocked with 10% FBS in PBS for 30min. They were incubated for 30min with 1µM VIP-Cy3 or 60min with 3µM ($Ala^{11,22,28}$)-VIP-FITC in PBS. Only HT-29 cells were incubated 15min with ($Ala^{11,22,28}$)-VIP-FITC because of cell apoptosis. Nuclear double staining was performed with 1µM TO-PRO®-3 iodide (Molecular Probes, Leiden, Netherlands). After incubation the cells were washed twice with PBS and mounted with Citifluor (Gröple, Vienna, Austria) and directly analysed with CLSM. Controls were performed with 1µM unlabelled VIP, 3µM ($Ala^{11,22,28}$)-VIP and 1µM TOPRO®-3 and incubated for 30min at 37°C with 5%CO_2 in the atmosphere.

The fluorescence signal of Cy3 (ex/em: 550/570), fluorescein (494/518) and TOPRO®-3 (642/660) were determined with a 63x objective and zoomed by Confocal Laser Scanning Microscope (Leica DM Irbe, Wetzlar, Germany).

4 Results

4.1 VPAC receptor expression by cell line

14 tumour cell lines and one endothelial cell line were analyzed for their receptor expression pattern for VPAC receptors. $VPAC_1$, $VPAC_2$ and PAC_1 receptors were detected with monoclonal and polyclonal specific antibodies for these receptors by immunocytochemistry (ICC) stainings and western blots (WB).

WB analysis was not consulted for determination of VPAC receptors expression pattern, therefore immunocytochemistry staining was performed.

Immunodetections with monoclonal antibodies were performed by ICC stainings. Many tryouts with antibody dilutions did not reveal better signals and the negative control gave often a positive signal. So we decided to stain with polyclonal antibodies. After analysis with polyclonal antibodies the positive control was negative and the signal intensity was increased. ICC stainings from all cell lines were done twice.

Fig.16 shows immunocytochemistry (ICC) stainings with different antibody dilution at different cell lines. PC-3 was used for $VPAC_1$ optimation, because PC-3 cells express $VPAC_1$, which was known previous. HCT-116 cells were detected with $VPAC_2$ ab and LNCaP for PAC_1.

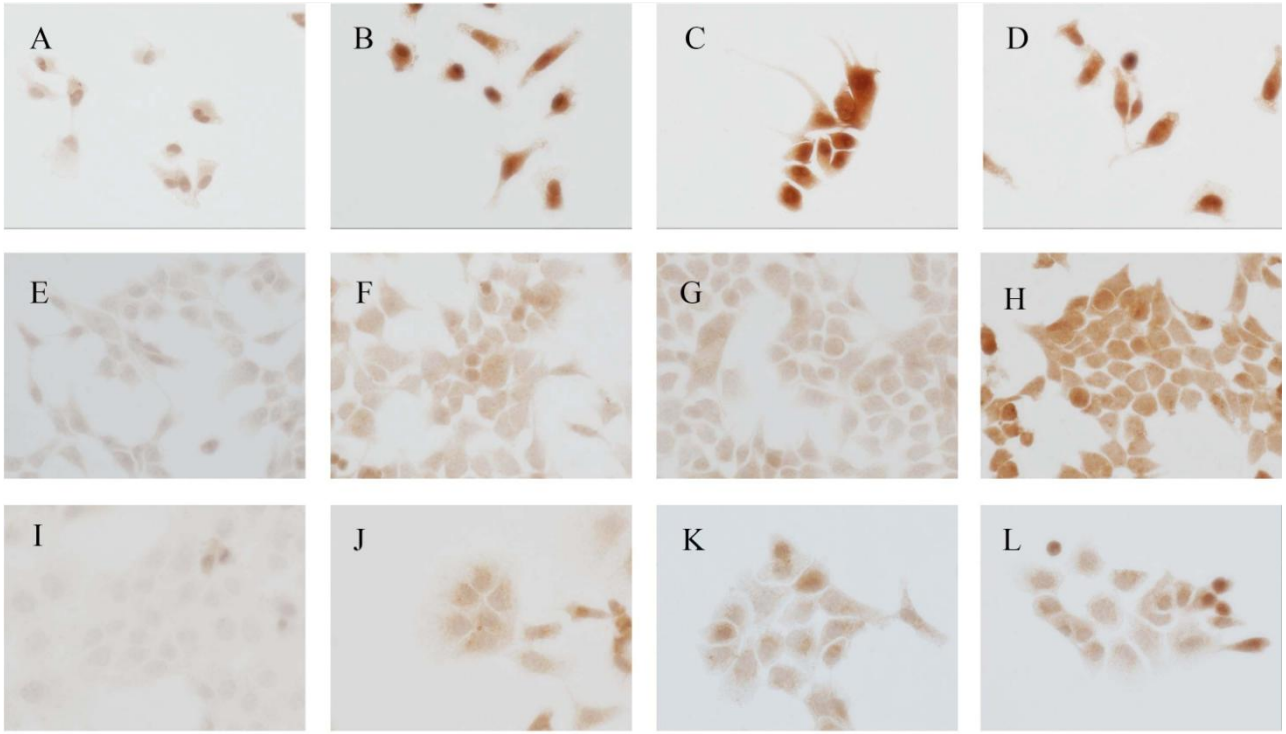

Figure 16. ICC staining with primary antibody dilutions, A-D) PC-3 cells, E-F) HCT-116 cells and I-L) LNCaP cells. Nuclei are stained very light blue with Mayer´s Hematoxylin.
Polyclonal rabbit anti-$VPAC_1$ antibody of PC-3 cells were stained with DAB as a substrate. A) negative control without primary ab, B) 1:200 dilution, C) 1:100 dilution and D) 1:50 dilution of ab. All dilutions show specific signals above negative controls.
Polyclonal rabbit anti-$VPAC_2$ antibody of HCT-116 cells were stained with DAB as a substrate. E) negative control without primary ab, F) 1:3000 dilution of ab, G) 1:2000 dilution and H) 1:1000 dilution of ab. Dilution of 1:1000 gives a specific signal.
Polyclonal rabbit anti-PAC_1 antibody of LNCaP cells were stained with DAB as a substrate. I) negative control without primary ab, J) 1:3000 dilution of ab, K) 1:2000 dilution and L) 1:1000 dilution of ab. Dilution of 1:1000 gives a specific signal.

In the case of $VPAC_1$ antibody, antibody dilutions did not show an effect of specify signal between 1:50-1:200 dilution (fig.16A-D). Further ICCs were done with 1:200 dilution of polyclonal anti-$VAPC_1$ antibody. $VPAC_2$ and PAC_1 indicates a better signal with 1:1000 dilution than 1:2000 and 1:3000 (fig.16E-L), 1:1000 dilution was performed in all other ICC experiments.

Immunocytochemistry of 14 tumour cell lines and one endothelial cell line:

Fig.17 shows ICC of LNCaP cells. Unspecific signal is viewed in the negative control, also $VPAC_1$ staining is unspecific diffuse because only nuclei are visualised. $VPAC_2$ staining indicated a positive brown signal in the cytoplasm. Some nuclei are stained dark brown, which might be a real signal of receptor in the nucleus or a staining/fixing artefact. PAC_1 staining shows a weak punctual brown staining in the cytoplasm; also some nuclei are stained dark brown.

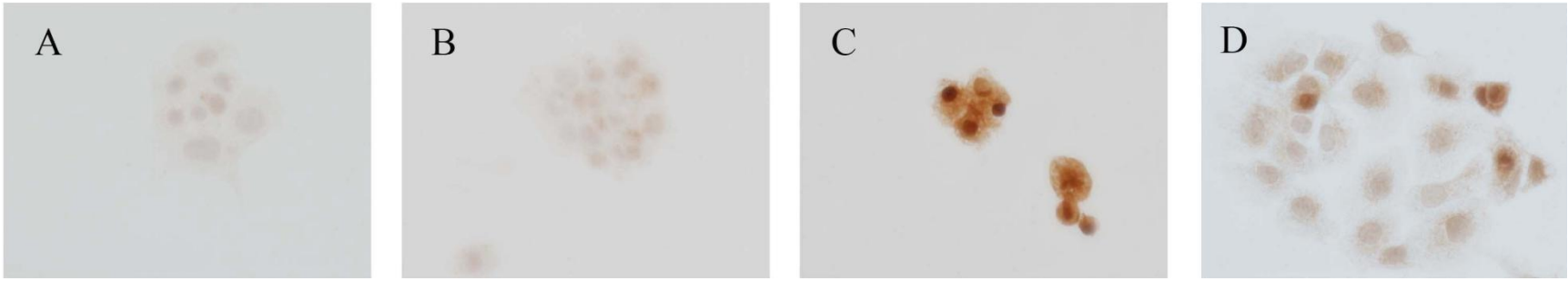

Figure 17. ICC staining of prostate carcinoma LNCaP cells. A) Negative control without prim. ab, B) $VPAC_1$ staining, C) $VPAC_2$ staining and D) PAC_1 staining with DAB as a substrate. Cell nuclei are counter stained with diluted Mayer´s Hematoxylin. $VPAC_1$ staining reveals an unspecific diffuse signal. $VPAC_2$ and PAC_1 show a brown staining which indicates a specific receptor expression.

Fig.18 indicates an ICC staining of PC-3 cells with DAB as a substrate. Negative control gives a diffuse weak signal, all three receptor types, $VPAC_1$, $VPAC_2$ and PAC_1, show a brown signal in the cytoplasm. Also nuclei are stained stronger than cytoplasm.

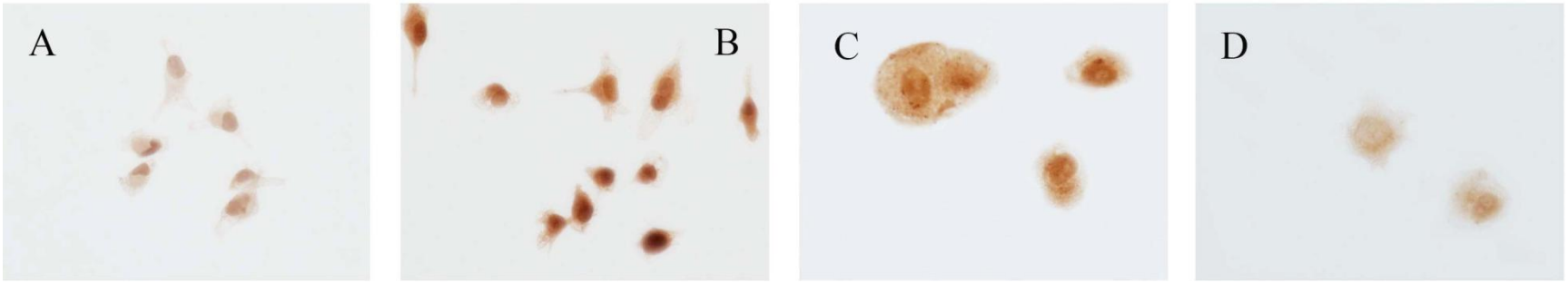

Figure 18. ICC staining of prostate carcinoma PC-3 cells. A) Negative control without prim. ab, B) $VPAC_1$ staining, C) $VPAC_2$ staining and D) PAC_1 staining with DAB as a substrate. Nuclei are stained light blue with Mayer´s Hematoxylin. $VPAC_1$, $VPAC_2$ and PAC_1 show a brown staining which indicates a specific receptor expression.

Fig.19 shows ICC staining of Capan-1 cells. The negative control and $VPAC_1$ receptor displays no specific signal. $VPAC_2$ shows a heterogeneous pattern of DAB staining in the cytoplasm. Some cells are stained strong and other neighbouring cells very weak. Anti-$VPAC_2$ also penetrates the nucleus and gives a signal. PAC_1 receptor is weaker stained than $VPAC_2$ but also indicates a positive signal in the cytoplasm.

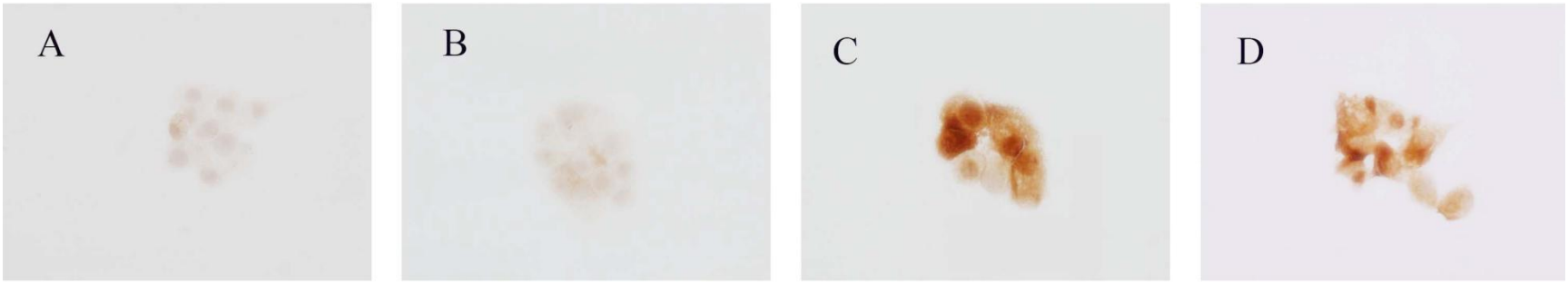

Figure 19. **ICC staining of pancreas carcinoma Capan-1 cells.** A) Negative control without prim. ab, B) $VPAC_1$ staining, C) $VPAC_2$ staining and D) PAC_1 staining with DAB as a substrate. Nuclei are stained light blue with Mayer´s Hematoxylin. No specific $VPAC_1$ signal is visualised. $VPAC_2$ staining shows a heterogeneous distribution of receptor in the same population. Specific staining is also revealed when staining PAC_1receptor.

Fig.20 shows two ICC staining of PANC-1 cells in different passages. A-D) demonstrates PANC-1 cells in passage 6 (P6). Negative control gives a very weak diffuse signal whereas $VPAC_1$ receptor indicates a strong brown signal in the cytoplasm. Note that some cells show a clear blue staining of nuclei with Mayer´s Hematoxylin and other a dark brown staining of DAB. This data might indicate that the brown staining of the nucleus is a fixing or staining artefact. $VPAC_2$ and PAC_1 receptors show a punctual and specific distribution in the cytoplasm and reveals a blue nuclei signal. E-H) visualises PANC-1 cells in passage 20 (P20). Negative control and $VPAC_1$ staining indicates no signal of DAB substrate. $VPAC_2$ and PAC_1 receptors show a weak staining but compared to PANC-1/P6 cells display a much weaker expression of $VPAC_2$ and PAC_1 receptors and no expression of $VPAC_1$ receptor.

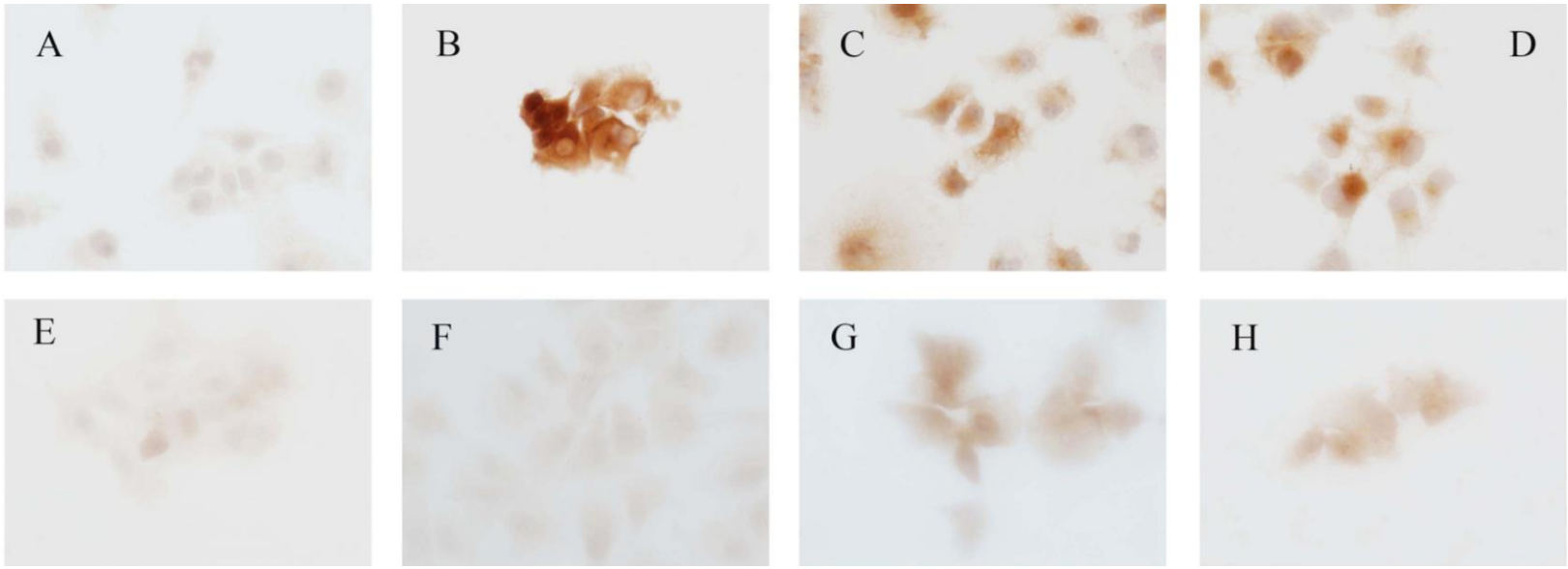

Figure 20. ICC staining of pancreas carcinoma PANC-1 cells. Nuclei are stained light blue with Mayer´s Hematoxylin. A-D) PANC-1 cells in passage 6 (low passage number). E-H) PANC-1 cells in passage 20 (high passage number). A, E) Negative control without prim. Ab; B, F) $VPAC_1$ staining; C, G) $VPAC_2$ staining and H, D) PAC_1 staining with DAB as a substrate. Low passage (P6) shows specific brown staining of $VPAC_1$, $VPAC_2$ and PAC_1 receptor. Whereas high passage (P20) reveals only specific signals of $VPAC_2$ and PAC_1 staining. $VPAC_1$ receptor expression might be downregulated. Note the different VPAC expression pattern in different passages of cell culture.

Fig.21 shows the ICC staining of lung carcinoma A427 cells. $VPAC_1$ demonstrates a very weak signal but a punctual localisation in the cytoplasm which indicates an expression of $VPAC_1$ receptor. A strong brown staining of $VPAC_2$ and PAC_1 receptors staining is shown in the cytoplasm compared to the negative control. Note the brown staining of nuclei in case of $VPAC_2$ and PAC_1. Fig.22 shows ICC stainings of Hep3B liver carcinoma. Also specific signals of $VPAC_1$, $VPAC_2$ and PAC_1 receptors can be seen in this staining.

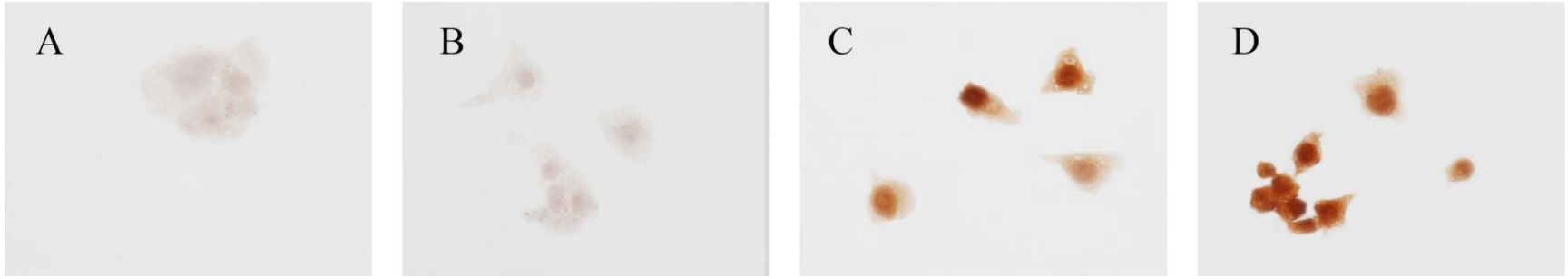

Figure 21. ICC staining of lung carcinoma A427 cells. A) Negative control without prim. ab, B) $VPAC_1$ staining, C) $VPAC_2$ staining and D) PAC_1 staining with DAB as a substrate. Nuclei are stained light blue with Mayer´s Hematoxylin. All three receptor staining showed a specific signal, which indicates a VPAC receptor expression.

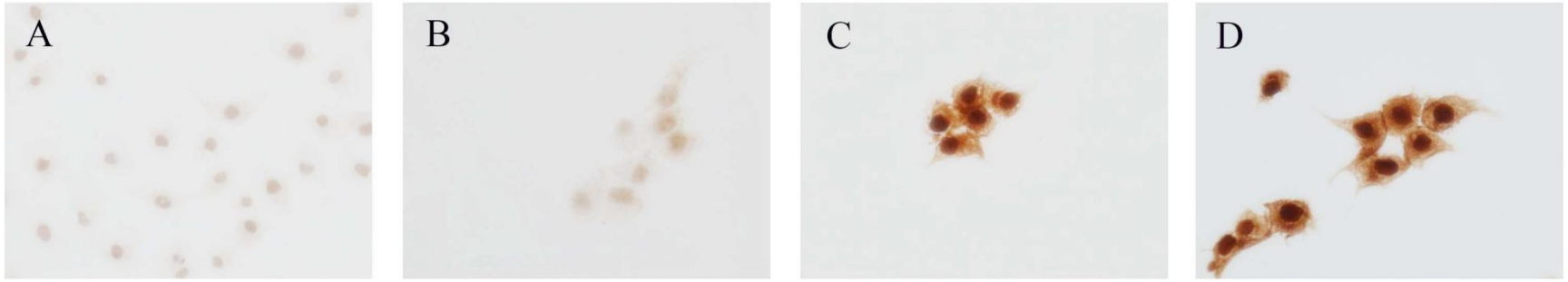

Figure 22. ICC staining of liver carcinoma Hep3B cells. A) Negative control without prim. ab, B) $VPAC_1$ staining, C) $VPAC_2$ staining and D) PAC_1 staining with DAB as a substrate. Nuclei are stained light blue with Mayer´s Hematoxylin. $VPAC_1$, $VPAC_2$ and PAC_1 reveal a specific signal which demonstrates a VPAC receptor expression.

Fig.23 demonstrates an ICC staining of SW1736 cells. $VPAC_1$ receptors don´t show a signal like the negative control. $VPAC_2$ and PAC_1 display a very heterogeneous expression signal in adjacent areas. SW1736 have a large nucleus which is mostly stained brown, it´s difficult to determine between nuclei and cytoplasm. Cells which are stained weak show a light blue nuclei, those who are stained strong have also a dark brown nucleus staining.

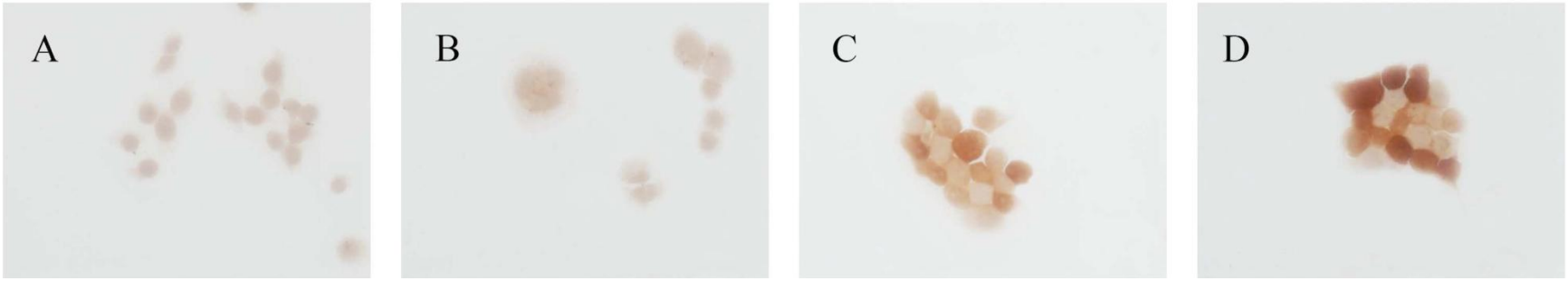

Figure 23. ICC staining of thyroid carcinoma SW1736 cells. A) Negative control without prim. ab, B) $VPAC_1$ staining, C) $VPAC_2$ staining and D) PAC_1 staining with DAB as a substrate. Nuclei are stained light blue with Mayer´s Hematoxylin.$VPAC_1$ does not show a specific signal which indicates no receptor expression. $VPAC_2$ and PAC_1 indicate a heterogeneous receptor expression in the cytoplasm within the same population.

Fig.24 exhibit ICC staining of glioblastoma MGC cells. $VPAC_1$ receptor has a very weak punctual staining in the cytoplasm compared to negative control. $VPAC_2$ shows a strong brown staining in the nucleus and a brighter signal in the cytoplasm whereas brown nuclei can be seen. Also PAC_1 indicates a certain localisation in the cytoplasm furthermore blue staining of nuclei.

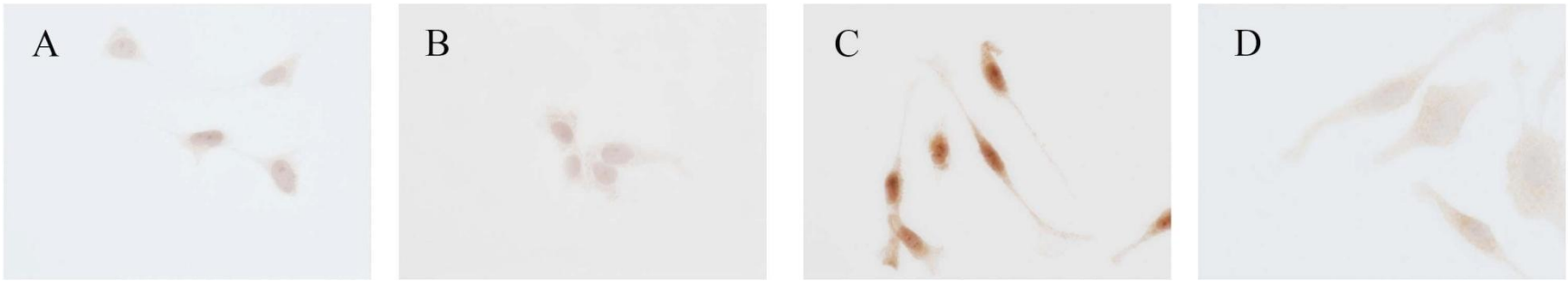

Figure 24. ICC staining of glioblastoma MGC cells. A) Negative control without prim. ab, B) $VPAC_1$ staining, C) $VPAC_2$ staining and D) PAC_1 staining with DAB as a substrate. Nuclei are stained light blue with Mayer´s Hematoxylin. $VPAC_1$and PAC_1 reveal a very weak staining, while $VPAC_2$ is clearly labelled. All three receptor types are expressed in glioblastoma cells at different rates.

Immunocytochemistry staining of HCT-15 cells (fig.25) show a weak diffuse signal in the case of negative control. $VPAC_1$ demonstrates a positive signal, punctual distributed in the cytoplasm and a stronger signal in the nuclei. A non-specific signal in the cytoplasm is shown when staining $VPAC_2$ and PAC_1 receptor.

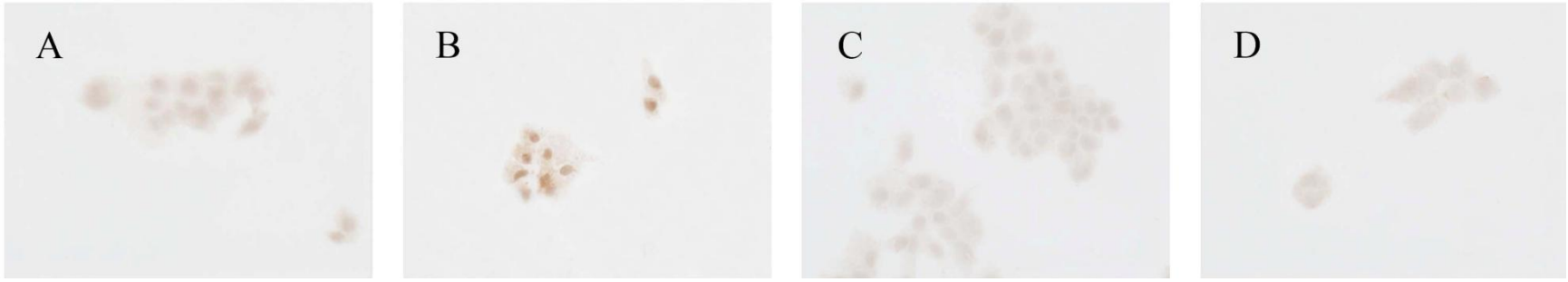

Figure 25. ICC staining of colon carcinoma HCT-15 cells. A) Negative control without prim. ab, B) $VPAC_1$ staining, C) $VPAC_2$ staining and D) PAC_1 staining with DAB as a substrate. Nuclei are stained light blue with Mayer´s Hematoxylin. Note the specific signal of $VPAC_1$, which indicates receptor expression. Whereas $VPAC_2$ and PAC_1 reveal unspecific signals, these indicates no expression of $VPAC_2$ and PAC_1 receptor.

Fig.26 shows ICC staining of HT-29 cells. The negative control shows a weak signal but $VPAC_1$ indicates a stronger staining in the cytoplasm and of the nuclei. $VPAC_2$ and PAC_1 have a heterogeneous signal distribution at adjacent regions. A weak staining of cytoplasm is coupled with a weak staining in the nuclei. Stronger staining occurs in both cytoplasm and nuclei.

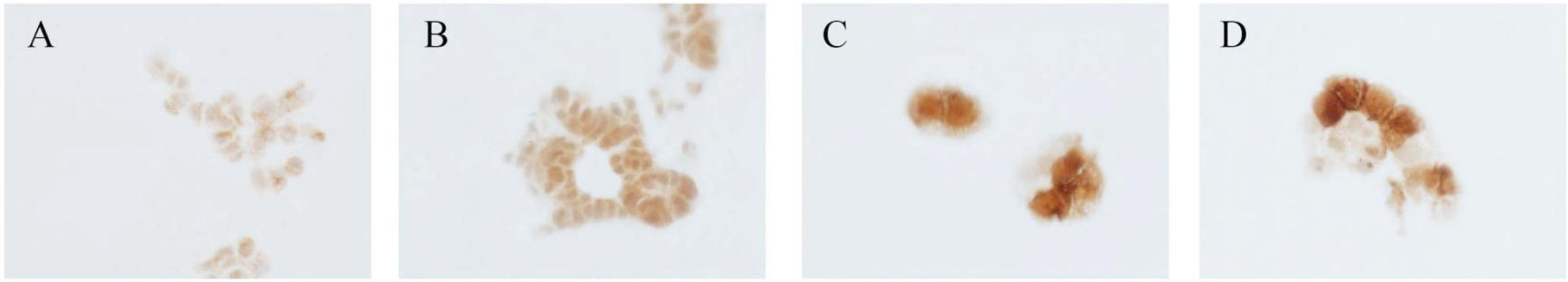

Figure 26. ICC staining of colon carcinoma HT-29 cells. A) Negative control without prim. ab, B) $VPAC_1$ staining, C) $VPAC_2$ staining and D) PAC_1 staining with DAB as a substrate. Nuclei are stained light blue with Mayer´s Hematoxylin. Note the specific signal of $VPAC_1$ and $VPAC_2$ and the heterogeneous distribution of PAC_1 receptor in the same cell culture population.

Fig.27 shows ICC staining of CaCo-2 cells. $VPAC_1$ and PAC_1 receptors are stained in the cytoplasm as well in the nuclei, whereas $VPAC_2$ indicates no signal in the cytoplasm like the control, nuclei are stained blue.

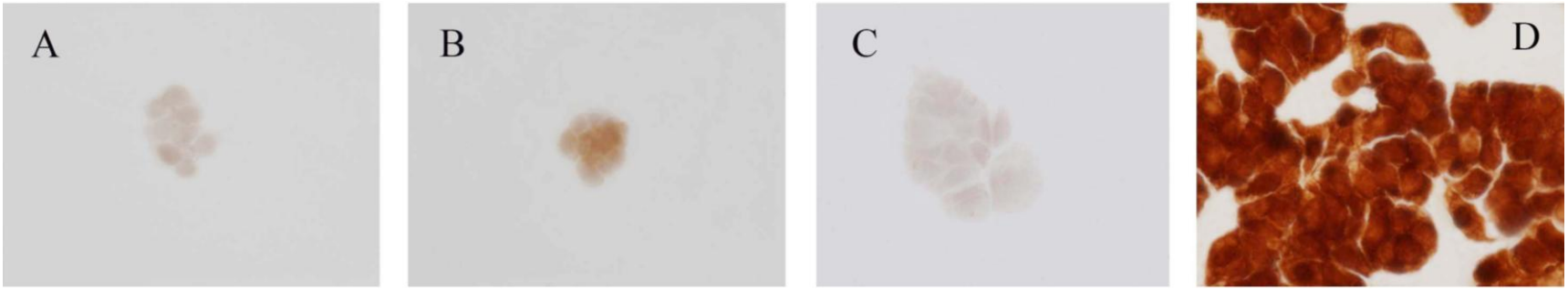

Figure 27. ICC staining of colon carcinoma CaCo-2 cells. A) Negative control without prim. ab, B) $VPAC_1$ staining, C) $VPAC_2$ staining and D) PAC_1 staining with DAB as a substrate. Nuclei are stained light blue with Mayer´s Hematoxylin. $VPAC_1$ and PAC_1 receptor show a specific staining which indicate an expression of these receptors. No specific signal is visible in the case of $VPAC_2$ which demonstrates no $VPAC_2$ receptor expression.

Fig.28 and fig.29 display ICC stainings of colon carcinoma HCT-116 cells and breast carcinoma MCF-7 cells. Both cell lines express the same receptor signal. $VPAC_1$ is punctual and stronger stained than the negative control. Some nuclei show a brown signal, others a blue signal. $VPAC_2$ and PAC_1 have a strong brown staining of DAB substrate with dark brown stained nuclei. The receptor signals are distributed among the whole cytoplasm.

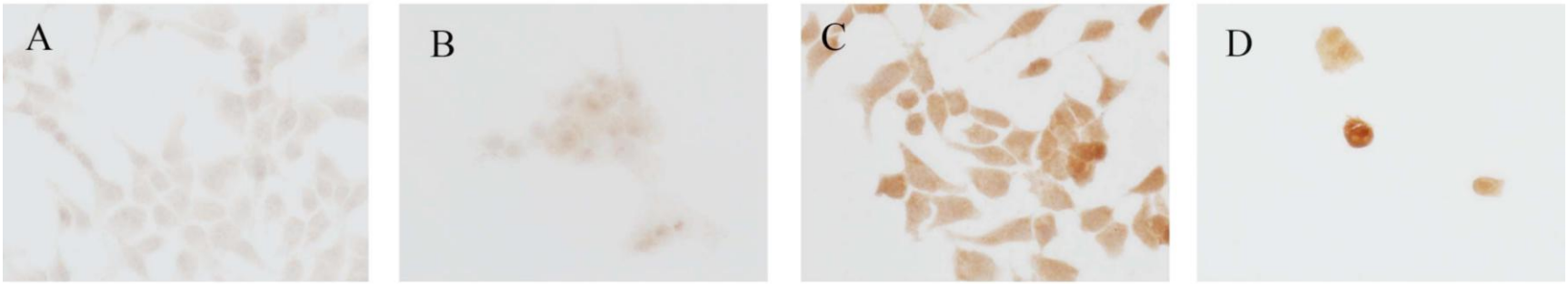

Figure 28. ICC staining of colon carcinoma HCT-116 cells. A) Negative control without prim. ab, B) $VPAC_1$ staining, C) $VPAC_2$ staining and D) PAC_1 staining with DAB as a substrate. Nuclei are stained light blue with Mayer´s Hematoxylin. All three types of VPAC receptors reveal a specific signal. $VPAC_1$ is weaker expressed than $VPAC_2$ and PAC_1.

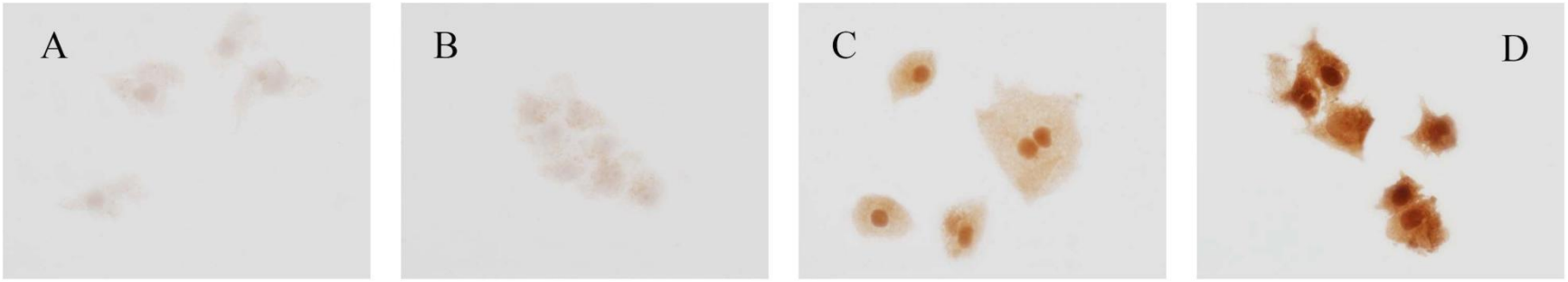

Figure 29. ICC staining of breast carcinoma MCF-7 cells. A) Negative control without prim. ab, B) $VPAC_1$ staining, C) $VPAC_2$ staining and D) PAC_1 staining with DAB as a substrate. Nuclei are stained light blue with Mayer´s Hematoxylin. All three types of VPAC receptors reveal a specific signal. $VPAC_1$ is weaker expressed than $VPAC_2$ and PAC_1.

The microvascular endothelial cells HMEC-1 (fig.30) show an unspecific signal of $VPAC_1$ receptor. A very determined distribution of $VPAC_2$ receptor with a strong brown signal in the cytoplasm and also in the nuclei is visible. Interestingly PAC_1 receptor reveals a non-specific staining like the negative control. The brown dots at the apical or lateral side of the cells might be a specific signal of PAC_1 at the membrane or a staining artefact.

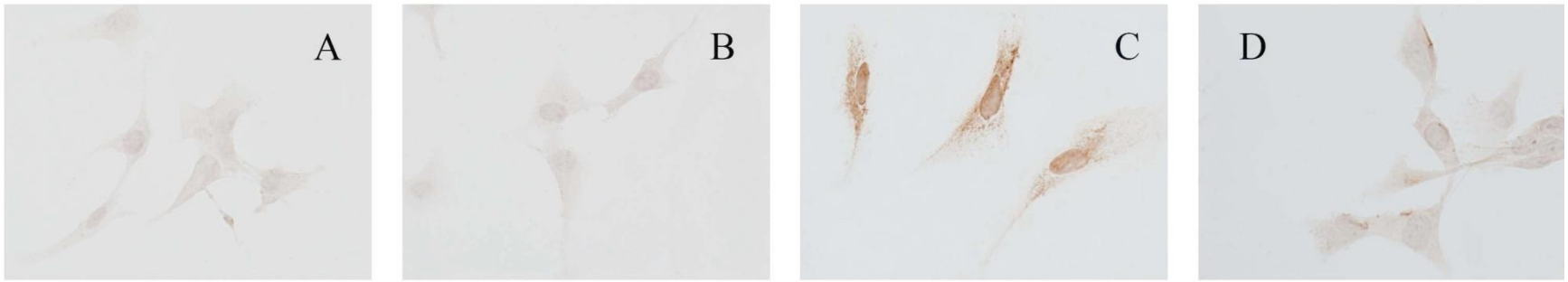

Figure 30. ICC of microvascular endothelial cells HMEC-1. A) Negative control without prim. ab, B) $VPAC_1$ staining, C) $VPAC_2$ staining and D) PAC_1 staining with DAB as a substrate. Nuclei are stained light blue with Mayer´s Hematoxylin. No specific signal of $VPAC_1$ can be seen, which indicates no expression of $VPAC_1$. Note the distribution of $VPAC_2$ and. PAC_1 signal at the membranes. This might indicate a receptor accumulation at the membranes or it simply might be an artefact.

Summary of VPAC receptors ($VPAC_1$, $VPAC_2$ and PAC_1) expression pattern with ICC (table 15):

Table 15. VPAC receptor expression pattern of human cell lines. + expression, -no expression of receptor subtype.

Organ	Tumour cell line	$VPAC_1$	$VPAC_2$	PAC_1
Human prostata carcinoma	LNCaP	-	+	+
Human prostata carcinoma	PC-3	+	+	+
Human pancreas adenocarcinoma	Capan-1	-	+	+
Human pancreas duct epithelioid carcinoma	PANC-1 P6	+	+	+
Human pancreas duct epithelioid carcinoma	PANC-1 P20	-	+	+
Lung carcinoma	A427	+	+	+
Human liver hepatocellular carcinoma	Hep3B	+	+	+
Human thyriod adenocarcinoma	SW1736	-	+	+
Human glioblastoma	MGC	-	+	+
Human colorectal carcinoma	HCT-15	+	-	-
Human colorectal carcinoma	HT-29	+	+	+
Human colorectal carcinoma	CaCo-2	+	-	+
Human colorectal carcinoma	HCT-116	-	+	+
Human mammary gland, breast epithelial adenocarcinoma	MCF-7	+	+	+
Human microvascular endothelial cell	HMEC-1	-	+	-

4.2 Proliferation assays (MTT)

Proliferation studies of all 15 cell lines were performed to test toxicity or proliferative properties of VIP-conjugates. Two experiments with 8 to 12 values of each peptide analogue were averaged and standard deviation was calculated.

Prostate Carcinoma LNCaP data:

Table 16. MTT assay of LNCaP cell line.

peptide analogues	1	2	average n=8	std. deviation n=2
	average n=4	average n=4		
VIP 10µM	103,13	110,21	106,67	5,01
VIP 10nM	93,65	103,43	98,54	6,92
VIP 10pM	108,44	95,89	102,17	8,87
($Ala^{11,22,28}$)-VIP 10µM	101,36	108,49	104,93	5,04
($Ala^{11,22,28}$)-VIP 10nM	97,46	105,38	101,42	5,60
($Ala^{11,22,28}$)-VIP 10pM	101,63	90,83	96,23	7,64
VIP-DOTA 10µM	99,67	96,36	98,02	2,34
VIP-DOTA 10nM	103,26	99,94	101,60	2,35
VIP-DOTA 10pM	101,12	105,81	103,47	3,32
VIP-DOTA-Gd 10µM	117,17	109,95	113,56	5,11
VIP-DOTA-Gd 10nM	118,28	110,06	114,17	5,81
VIP-DOTA-Gd 10pM	109,69	115,36	112,53	4,01
PACAP 10µM	91,94	102,50	97,22	7,47
PACAP 10nM	92,72	100,23	96,48	5,31
PACAP 10pM	94,02	100,44	97,23	4,54
RPMI 1640	3,55	4,09	3,82	0,38

The MTT assays of LNCaP cells show a dose-effect of peptide conjugates. The peptide concentrations don´t indicate a significant difference of proliferation or toxicity of cells because the cell growth is rested at about 100%. No increase or decrease of cell number is observed after treatment with peptides. RPMI 1640 is used as a control of absorption of the medium (fig.31, table 16).

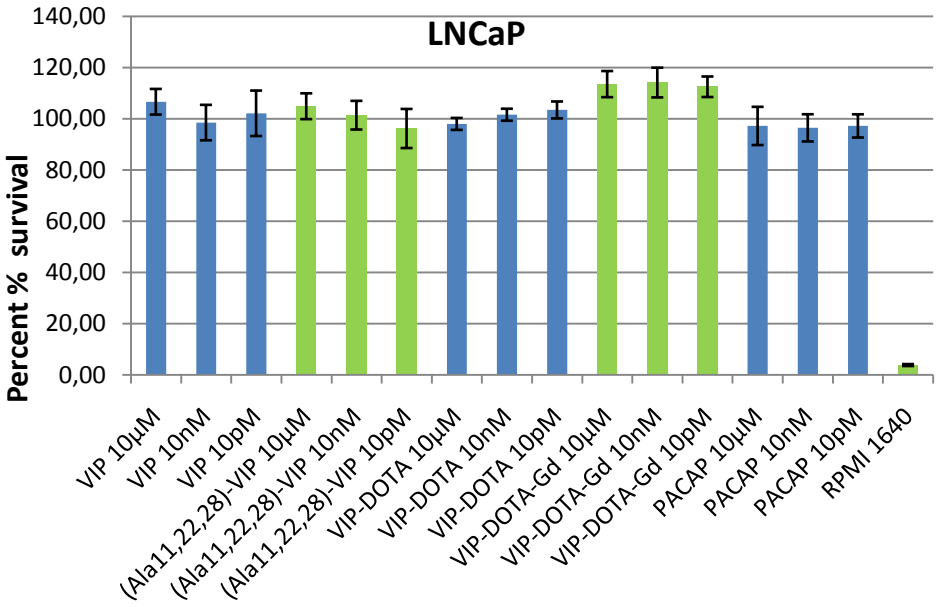

Figure 31. MTT assay of LNCaP cells. No significant proliferation or toxicity of LNCaP cells treated with VIP conjugates can be seen.

Prostate carcinoma PC-3 cells data:

Table 17. MTT assay of PC-3 cells.

peptide analogues	1	2	average n=8	std. deviation n=2
	average n=4	average n=4		
VIP 10µM	116,44	137,08	126,76	14,59
VIP 10nM	117,97	131,25	124,61	9,39
VIP 10pM	111,33	129,44	120,39	12,81
(Ala^{11,22,28})-VIP 10µM	115,02	132,41	123,72	12,30
(Ala^{11,22,28})-VIP 10nM	121,26	128,57	124,92	5,17
(Ala^{11,22,28})-VIP 10pM	122,63	114,74	118,69	5,58
VIP-DOTA 10µM	117,57	133,04	125,31	10,94
VIP-DOTA 10nM	110,46	139,33	124,90	20,41
VIP-DOTA 10pM	109,00	142,19	125,60	23,47
VIP-DOTA-Gd 10µM	94,33	123,17	108,75	20,39
VIP-DOTA-Gd 10nM	95,54	108,01	101,78	8,82
VIP-DOTA-Gd 10pM	98,61	113,46	106,04	10,50
PACAP 10µM	111,37	128,46	119,92	12,08
PACAP 10nM	112,94	134,43	123,69	15,20
PACAP 10pM	108,35	142,07	125,21	23,84
RPMI 1640	4,66	6,11	5,39	1,03

The MTT assays of PC-3 cells reveal an increased cell number of about 20% after incubation with investigated peptides, except VIP-DOTA-Gd. VIP-DOTA-Gd shows no proliferation at different concentrations (fig.32, table 17).

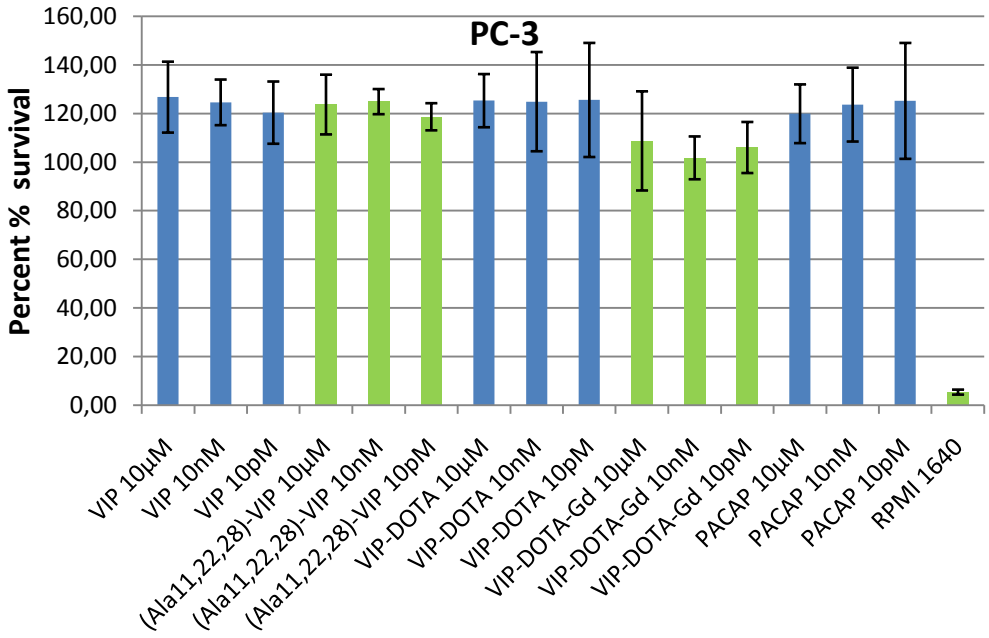

Figure 32. MTT assay of PC-3 cells. All conjugates except VIP-DOTA-Gd show a significant increase of cell number of about 20% cell, indicating increased cell growth by all conjugates except VIP-DOTA-Gd. None of the conjugates reveal any toxicity.

Pancreas carcinoma Capan-1 cells data:

Table 18. MTT assay of Capan-1 cells.

peptide analogues	1	2	average n=8	std. deviation n=2
	average n=4	average n=4		
VIP 10µM	103,51	98,61	101,06	3,465
VIP 10nM	105,86	94,42	100,14	8,089
VIP 10pM	107,90	97,48	102,69	7,368
(Ala^{11,22,28})-VIP 10µM	108,59	102,88	105,74	4,038
(Ala^{11,22,28})-VIP 10nM	99,55	99,74	99,65	0,134
(Ala^{11,22,28})-VIP 10pM	106,60	96,19	101,40	7,361
VIP-DOTA 10µM	101,75	102,85	102,30	0,778
VIP-DOTA 10nM	108,34	104,92	106,63	2,418
VIP-DOTA 10pM	107,42	103,94	105,68	2,461
VIP-DOTA-Gd 10µM	97,79	105,04	101,42	5,127
VIP-DOTA-Gd 10nM	102,36	112,72	107,54	7,326
VIP-DOTA-Gd 10pM	90,48	103,54	97,01	9,235
PACAP 10µM	103,15	99,75	101,45	2,404
PACAP 10nM	106,19	104,65	105,42	1,089
PACAP 10pM	104,95	98,95	101,95	4,243
RPMI 1640	3,52	4,11	3,82	0,417

The diagram of Capan-1 cell shows MTT assays, indicating no proliferative or toxicity properties of peptides. All peptide conjugates reveal no significant increase in cell number cell, the cell growth is rested at about 100% (fig.33, tab.18).

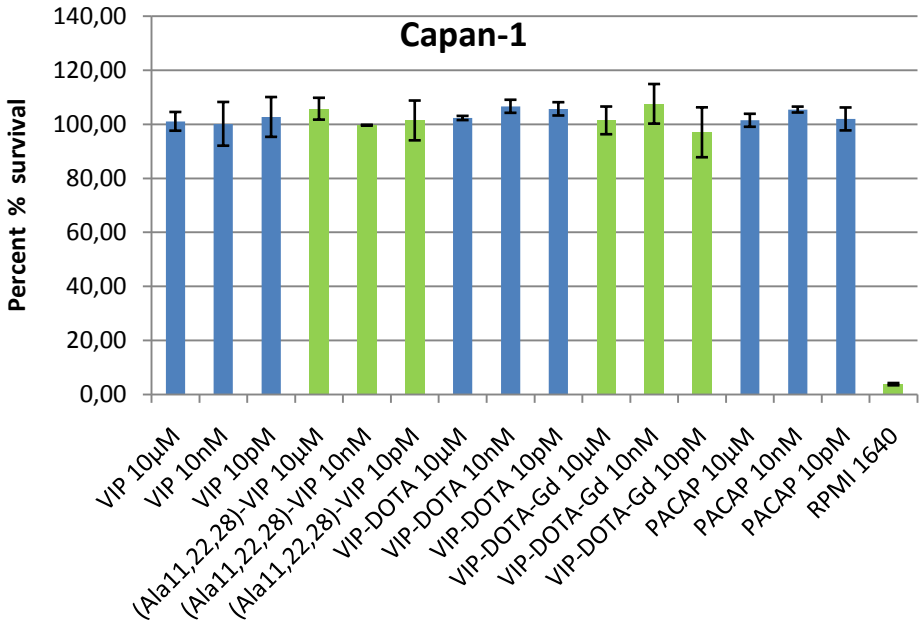

Figure 33. MTT assay of Capan-1 cells. None of the VIP conjugates demonstrate a proliferative or toxic effect.

Pancreas carcinoma PANC-1/P8 cells data:

Table 19. MTT assay of PANC-1 cells passage 8.

peptide analogues	1 average n=4	2 average n=4	average n=8	std. deviation n=2
VIP 10µM	125,11	130,78	127,95	4,01
VIP 10nM	129,40	152,78	141,09	16,53
VIP 10pM	131,77	138,95	135,36	5,08
(Ala^{11,22,28})-VIP 10µM	132,59	114,26	123,43	12,96
(Ala^{11,22,28})-VIP 10nM	130,54	128,14	129,34	1,70
(Ala^{11,22,28})-VIP 10pM	130,61	114,43	122,52	11,44
VIP-DOTA 10µM	131,35	149,09	140,22	12,54
VIP-DOTA 10nM	125,60	168,56	147,08	30,38
VIP-DOTA 10pM	120,08	154,05	137,07	24,02
VIP-DOTA-Gd 10µM	135,22	133,07	134,15	1,52
VIP-DOTA-Gd 10nM	125,11	170,77	147,94	32,29
VIP-DOTA-Gd 10pM	126,57	139,44	133,01	9,10
PACAP 10µM	133,30	128,21	130,76	3,60
PACAP 10nM	132,46	139,54	136,00	5,01
PACAP 10pM	127,33	121,67	124,50	4,00
RPMI 1640	5,73	5,06	5,40	0,47

PANC-1/P8 cells exhibit an increased cell number after incubation with peptide conjugates at about 20-40%. VIP, (Ala^{11,22,28})-VIP and PACAP show the same proliferation properties like the conjugates VIP-DOTA and VIP-DOTA-Gd (fig34, tab.19).

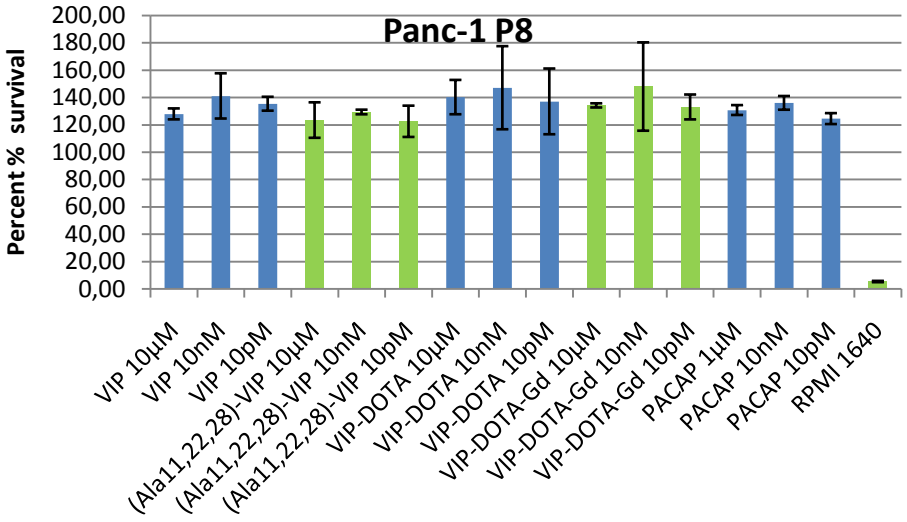

Figure 34. MTT assay of PANC-1 cells, passage 8. At passage 8 PANC-1 cells show a significant increased number of cells of about 40%, indicating a proliferation with all peptide conjugates. None of the conjugates are toxic.

Lung carcinoma A427 cells data:

Table 20. MTT assay of A427 cells.

peptide analogues	1 average n=4	2 average n=4	average n=8	std. deviation n=2
VIP 10µM	67,20	74,70	70,95	5,30
VIP 10nM	132,87	119,32	126,10	9,58
VIP 10pM	128,03	120,22	124,13	5,52
(Ala^{11,22,28})-VIP 10µM	131,67	115,91	123,79	11,14
(Ala^{11,22,28})-VIP 10nM	133,50	112,18	122,84	15,08
(Ala^{11,22,28})-VIP 10pM	123,18	107,43	115,31	11,14
VIP-DOTA 10µM	134,83	125,43	130,13	6,65
VIP-DOTA 10nM	130,69	120,41	125,55	7,27
VIP-DOTA 10pM	128,94	117,07	123,01	8,39
VIP-DOTA-Gd 10µM	111,59	114,82	113,21	2,28
VIP-DOTA-Gd 10nM	125,66	124,70	125,18	0,68
VIP-DOTA-Gd 10pM	121,07	118,53	119,80	1,80
PACAP 10µM	141,63	130,18	135,91	8,10
PACAP 10nM	122,41	101,96	112,19	14,46
PACAP 10pM	123,25	101,96	112,61	15,05
RPMI 1640	27,46	25,72	26,59	1,23

MTT assays of A427 cells indicated an increased cell number increase after treatment with peptides at about 20%. The incubation with 10µM VIP displays a cell viability of about 70%. (fig.35, tab.20). Also the negative control has a higher absorption than in the others MTT assays, because A427 cell metabolise formazan derivate more slowly and the other cell lines. A427 cells need more time to develop red dye product. After 3h incubation of the dye, the absorption rate is not as high as in quick metabolising cells.

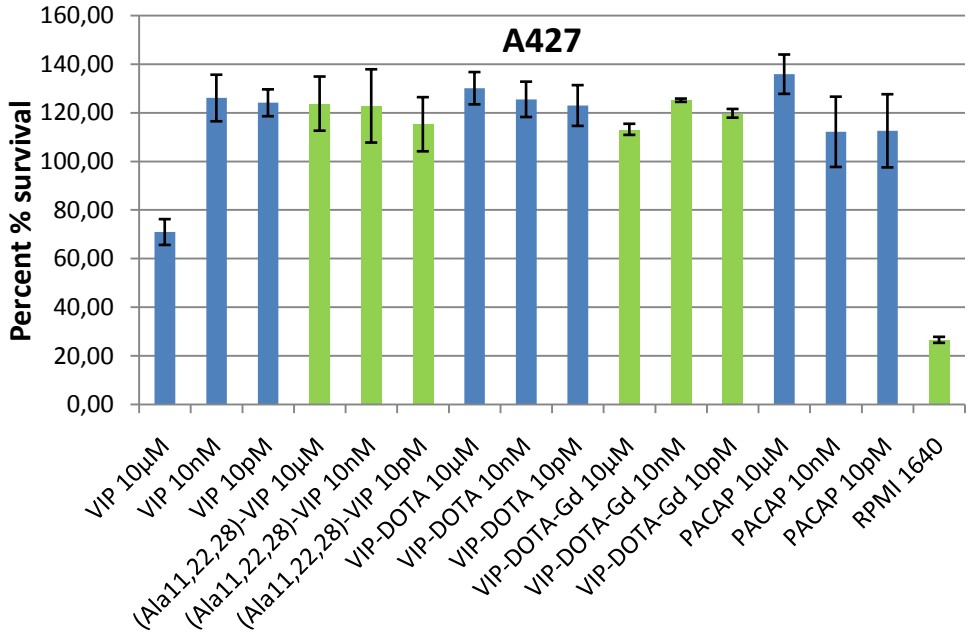

Figure 35. MTT assay of A427 cells. Note the significant lower cell number after incubation with 10µM VIP indicating either a proliferation inhibition or a toxic effect of this concentration on this cell line. The incubation with all other VIP conjugates result in an increase of viable cells of about 20%.

Liver carcinoma Hep3B cells data:

Table 21. MTT assay of Hep3B cells.

peptide analogues	1	2	average n=8	std. deviation n=2
	average n=4	average n=4		
VIP 10µM	105,78	106,60	106,19	0,58
VIP 10nM	101,54	108,18	104,86	4,70
VIP 10pM	108,00	110,46	109,23	1,74
(Ala^{11,22,28})-VIP 10µM	104,93	113,05	108,99	5,74
(Ala^{11,22,28})-VIP 10nM	102,42	110,62	106,52	5,80
(Ala^{11,22,28})-VIP 10pM	98,09	97,34	97,72	0,53
VIP-DOTA 10µM	96,60	106,40	101,50	6,93
VIP-DOTA 10nM	100,82	102,80	101,81	1,40
VIP-DOTA 10pM	101,29	95,99	98,64	3,75
VIP-DOTA-Gd 10µM	98,21	97,11	97,66	0,78
VIP-DOTA-Gd 10nM	99,49	97,41	98,45	1,47
VIP-DOTA-Gd 10pM	93,20	96,03	94,62	2,00
PACAP 10µM	93,50	109,68	101,59	11,44
PACAP 10nM	100,43	104,37	102,40	2,79
PACAP 10pM	96,12	96,24	96,18	0,08
RPMI 1640	3,97	4,52	4,25	0,39

The MTT assays of Hep3B cells indicate no proliferative or toxicity effect of cells after incubation with peptide conjugates. No significant increase in cell number after treatment with peptides is seen at about 100% (fig.36, tab.21).

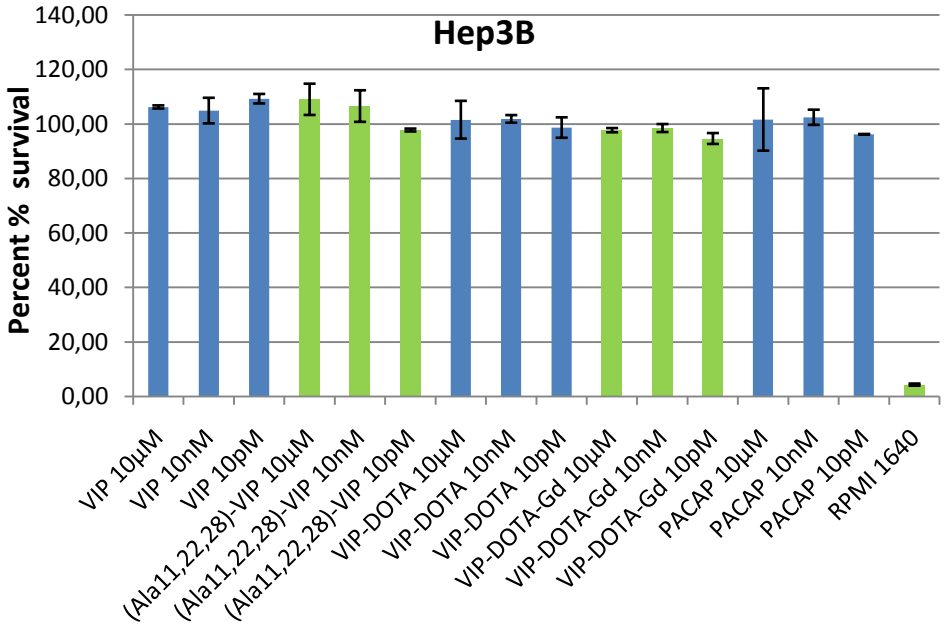

Figure 36. MTT assay of Hep3B cells. No proliferation or toxicity can be seen when cells incubated with VIP conjugates.

Thyroid carcinoma SW1736 cells data:

Table 22. MTT assay of SW1736 cells.

peptide analogues	1	2	3	average n=12	std. deviation n=3
	average n=4	average n=4	average n=4		
VIP 10µM	99,81	99,44	106,43	101,89	3,93
VIP 10nM	92,23	90,30	97,49	93,34	3,72
VIP 10pM	91,54	89,21	111,40	97,38	12,19
(Ala^{11,22,28})-VIP 10µM	99,76	96,62	106,21	100,86	4,89
(Ala^{11,22,28})-VIP 10nM	92,88	97,29	100,06	96,74	3,62
(Ala^{11,22,28})-VIP 10pM	94,56	95,48	105,16	98,40	5,87
VIP-DOTA 10µM	92,25	97,01	106,31	98,52	7,15
VIP-DOTA 10nM	88,73	94,67	106,86	96,75	9,24
VIP-DOTA 10pM	86,68	95,65	110,11	97,48	11,82
VIP-DOTA-Gd 10µM	97,45	101,97	88,22	95,88	7,01
VIP-DOTA-Gd 10nM	94,43	88,08	110,15	97,55	11,36
VIP-DOTA-Gd 10pM	91,26	92,47	118,19	100,64	15,21
PACAP 10µM	97,45	103,06	101,17	100,56	2,85
PACAP 10nM	89,01	95,53	102,53	95,69	6,76
PACAP 10pM	84,71	99,43	101,48	95,21	9,15
RPMI 1640	5,90	5,37	4,99	5,42	0,46

The MTT assays of SW1736 cells reveal no significant proliferative or toxicity of cells after treatment with peptide conjugates (fig.37, tab.22). The cell viability results in about 100%.

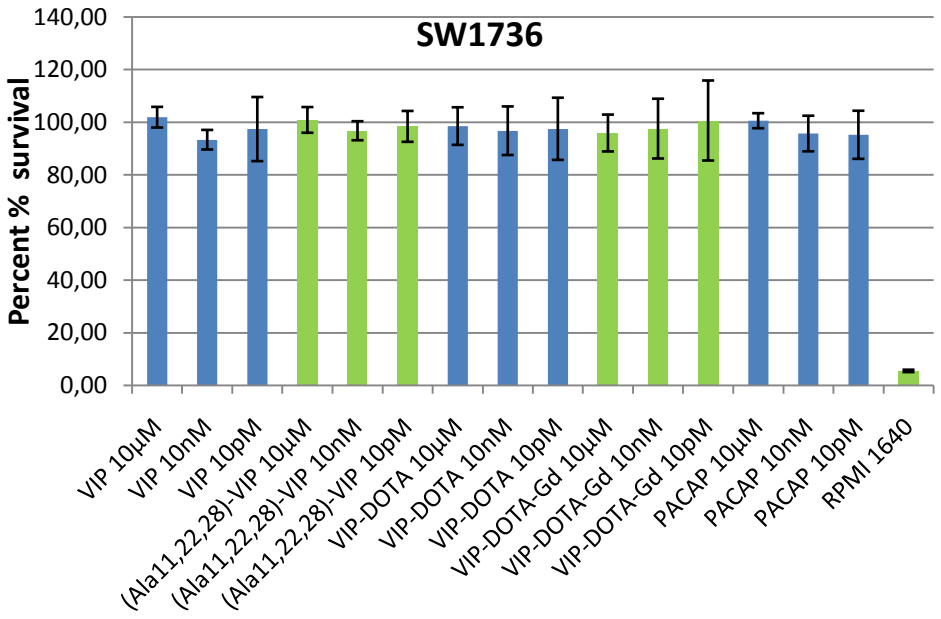

Figure 37. MTT assay of SW1736 cells. No significant proliferation or toxicity can be visualised after treatment with VIP conjugates.

Glioblastoma MGC cells data:

Table 23. MTT assay of glioblastoma MGC cells.

peptide analogues	1	2	average n=8	std. deviation n=2
	average n=4	average n=4		
VIP 10µM	120,54	137,34	128,94	11,88
VIP 10nM	124,47	115,38	119,93	6,43
VIP 10pM	111,71	99,02	105,37	8,97
(Ala^{11,22,28})-VIP 10µM	114,22	97,54	105,88	11,79
(Ala^{11,22,28})-VIP 10nM	116,02	97,24	106,63	13,28
(Ala^{11,22,28})-VIP 10pM	103,18	94,71	98,95	5,99
VIP-DOTA 10µM	106,30	99,12	102,71	5,08
VIP-DOTA 10nM	111,18	97,39	104,29	9,75
VIP-DOTA 10pM	85,27	101,32	93,30	11,35
VIP-DOTA-Gd 10µM	96,73	92,24	94,49	3,17
VIP-DOTA-Gd 10nM	130,02	96,65	113,34	23,60
VIP-DOTA-Gd 10pM	105,01	104,58	104,80	0,30
PACAP 10µM	100,26	98,91	99,59	0,95
PACAP 10nM	99,96	105,71	102,84	4,07
PACAP 10pM	101,42	100,24	100,83	0,83
RPMI 1640	5,98	5,43	5,71	0,39

The MTT assays of MGC cells show a dose-effect of VIP. (Ala^{11,22,28})-VIP and VIP-conjugates like DOTA and DOTA-Gd do not reveal a significant proliferative or toxicity of the cells (fig.38, tab.23).

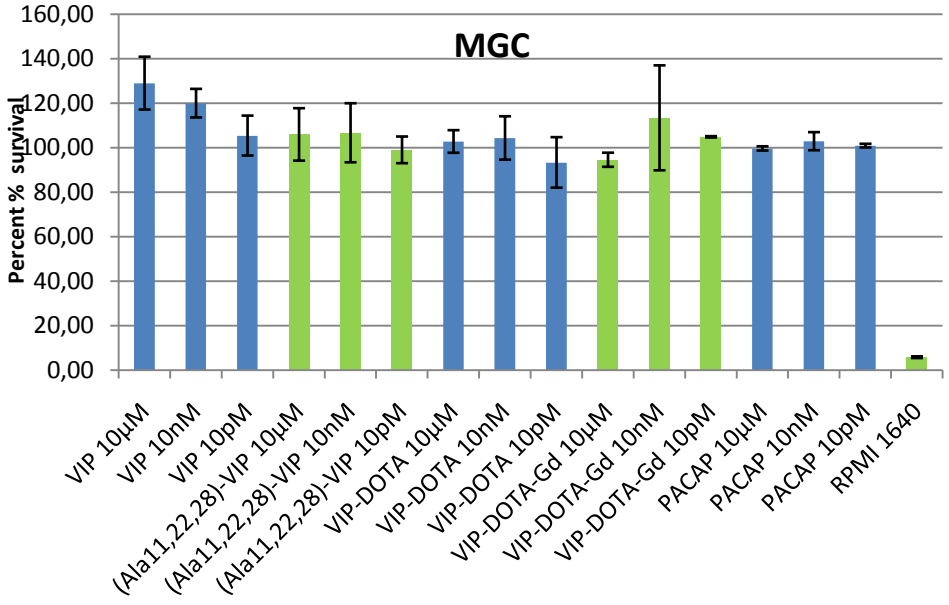

Figure 38. MTT assay of MGC cells. Note the dose-effect of VIP, high concentration of VIP indicates an cell increase to 130%. All conjugates did not show a proliferation or toxicity of treated cells.

Colon carcinoma HCT-15 cells data:

Table 24. MTT assay of HCT-15 cells.

peptide analogues	1	2	average n=8	std. deviation n=2
	average n=4	average n=4		
VIP 10µM	96,29	95,00	95,65	0,91
VIP 10nM	101,13	99,89	100,51	0,88
VIP 10pM	103,18	101,59	102,39	1,12
(Ala^{11,22,28})-VIP 10µM	102,42	95,20	98,81	5,11
(Ala^{11,22,28})-VIP 10nM	108,01	102,52	105,27	3,88
(Ala^{11,22,28})-VIP 10pM	101,46	97,08	99,27	3,10
VIP-DOTA 10µM	103,55	96,75	100,15	4,81
VIP-DOTA 10nM	94,04	97,94	95,99	2,76
VIP-DOTA 10pM	102,39	94,45	98,42	5,61
VIP-DOTA-Gd 10µM	101,20	93,90	97,55	5,16
VIP-DOTA-Gd 10nM	101,38	95,92	98,65	3,86
VIP-DOTA-Gd 10pM	104,05	92,94	98,50	7,86
PACAP 10µM	108,09	101,41	104,75	4,72
PACAP 10nM	98,15	103,40	100,78	3,71
PACAP 10pM	95,56	104,90	100,23	6,60
RPMI 1640	4,14	3,21	3,68	0,66

The MTT assays of HCT-15 cells indicate no proliferative or a toxicity property of the peptide conjugates. The cell growth after treatment with peptides is about 100% (fig.39, tab.24).

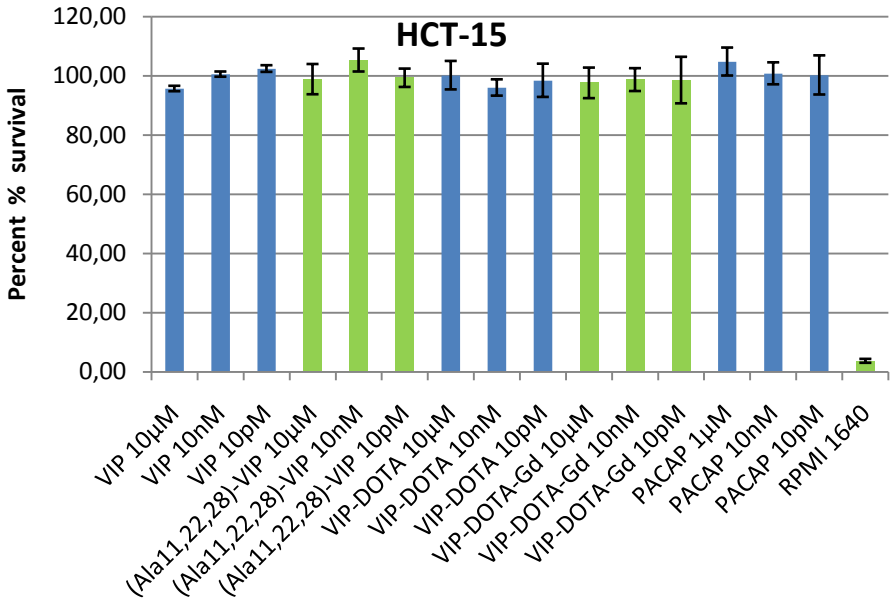

Figure 39. MTT assay of HCT-15. The assay indicates no proliferative or toxic properties of the VIP conjugates.

Colon carcinoma HT-29 cells data:

Table 25. MTT assay of HT-29 cells.

peptide analogues	1	2	average n=8	std. deviation n=2
	average n=4	average n=4		
VIP 10µM	113,30	108,65	110,98	3,29
VIP 10nM	108,00	111,25	109,63	2,30
VIP 10pM	115,03	106,83	110,93	5,80
(Ala^{11,22,28})-VIP 10µM	97,12	108,06	102,59	7,74
(Ala^{11,22,28})-VIP 10nM	96,30	107,22	101,76	7,72
(Ala^{11,22,28})-VIP 10pM	86,74	99,44	93,09	8,98
VIP-DOTA 10µM	93,90	104,89	99,40	7,77
VIP-DOTA 10nM	95,92	106,21	101,07	7,28
VIP-DOTA 10pM	92,94	110,55	101,75	12,45
VIP-DOTA-Gd 10µM	94,23	110,15	102,19	11,26
VIP-DOTA-Gd 10nM	100,61	109,49	105,05	6,28
VIP-DOTA-Gd 10pM	99,02	100,03	99,53	0,71
PACAP 10µM	95,25	96,20	95,73	0,67
PACAP 10nM	96,46	95,81	96,14	0,46
PACAP 10pM	92,70	100,79	96,75	5,72
RPMI 1640	5,95	3,35	4,65	1,84

HT-29 cells show a cell number increase of about 10% after incubation with VIP. The other conjugates like DOTA, DOTA-Gd and $VPAC_1$-specific analogue do not reveal a significant increase of cell number (fig.40, tab.25).

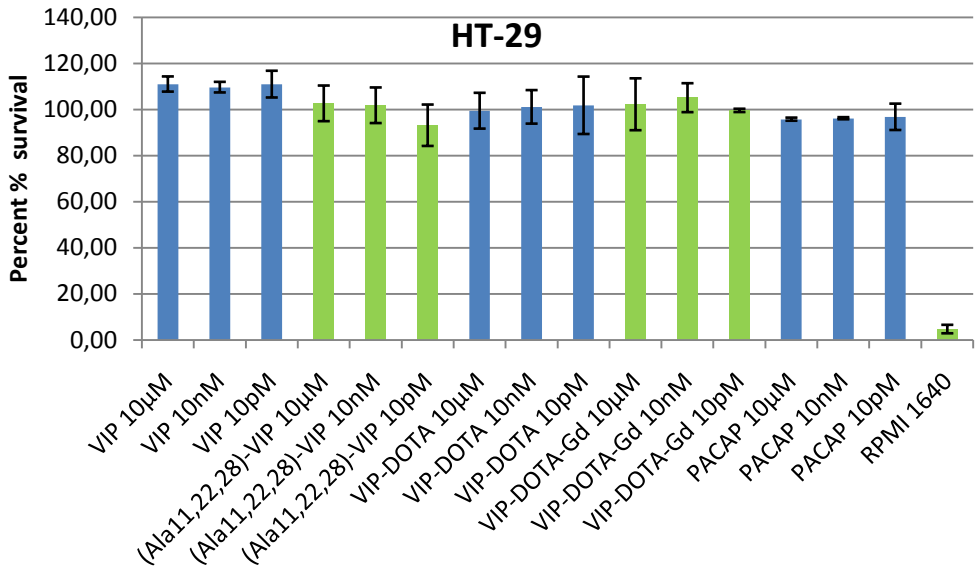

Figure 40. MTT assay with HT-29 cells. Incubation with VIP resulted in a slight proliferation. All other VIP conjugates do not significantly increase the viably cells. None of the substances display cytotoxicity.

Colon carcinoma CaCo-2 cells data:

Table 26. MTT assay of CaCo-2 cells.

peptide analogues	1 average n=4	2 average n=4	3 average n=4	average n=12	std. deviation n=3
VIP 10µM	88,60	100,27	101,66	96,84	7,17
VIP 10nM	87,89	100,88	98,70	95,82	6,96
VIP 10pM	92,43	102,19	96,67	97,10	4,89
(Ala^{11,22,28})-VIP 10µM	92,12	90,72	99,65	94,16	4,80
(Ala^{11,22,28})-VIP 10nM	96,62	93,18	91,87	93,89	2,45
(Ala^{11,22,28})-VIP 10pM	93,59	92,50	89,92	92,00	1,88
VIP-DOTA 10µM	84,45	83,13	97,31	88,30	7,83
VIP-DOTA 10nM	86,14	102,92	94,54	94,53	8,39
VIP-DOTA 10pM	86,14	96,88	101,36	94,79	7,82
VIP-DOTA-Gd 10µM	82,01	94,37	93,87	90,08	7,00
VIP-DOTA-Gd 10nM	85,90	101,59	95,02	94,17	7,88
VIP-DOTA-Gd 10pM	89,19	84,93	104,79	92,97	10,46
PACAP 10µM	106,01	104,51	107,14	105,89	1,32
PACAP 10nM	104,53	96,90	101,22	100,88	3,83
PACAP 10pM	106,06	102,11	102,49	103,55	2,18
RPMI 1640	0,78	6,48	4,05	3,77	2,86

CaCo-2 cells exhibit a slightly reduction of cell number after incubation with peptide conjugates at about 95%. But no significant toxicity of VIP-conjugates is detected (fig.41, tab.26).

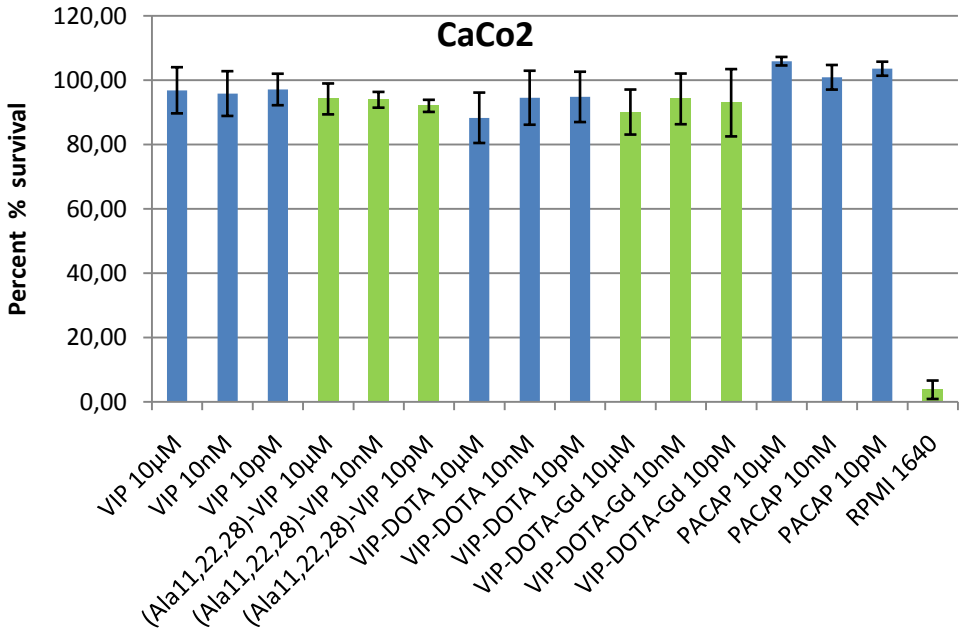

Figure 41. MTT assay with CaCo-2 cells. Incubation with VIP conjugates show a slightly reduction of viable cells, no significant toxicity of the substances is detected.

Colon carcinoma HCT-116 cells data:

Table 27. MTT assay of HCT-116 cells.

peptide analogues	1	2	average n=8	std. deviation n=2
	average n=4	average n=4		
VIP 10µM	93,09	96,40	94,75	2,341
VIP 10nM	98,41	99,58	99,00	0,827
VIP 10pM	96,63	93,49	95,06	2,220
(Ala^{11,22,28})-VIP 10µM	91,22	93,43	92,33	1,563
(Ala^{11,22,28})-VIP 10nM	77,10	82,03	79,57	3,486
(Ala^{11,22,28})-VIP 10pM	96,70	94,29	95,50	1,704
VIP-DOTA 10µM	100,54	96,36	98,45	2,956
VIP-DOTA 10nM	101,46	100,32	100,89	0,806
VIP-DOTA 10pM	106,59	103,46	105,03	2,213
VIP-DOTA-Gd 10µM	100,99	98,08	99,54	2,058
VIP-DOTA-Gd 10nM	106,03	99,11	102,57	4,893
VIP-DOTA-Gd 10pM	100,73	98,45	99,59	1,612
PACAP 10µM	101,50	95,01	98,26	4,589
PACAP 10nM	102,25	93,19	97,72	6,406
PACAP 10pM	105,75	102,10	103,93	2,581
RPMI 1640	3,99	3,80	3,90	0,134

The MTT assays of HCT-116 cells reveal a cytotoxicity of about 20% after incubation with 10nM $VPAC_1$-specific agonist. All other concentrations do not show a significant reduction in cell number (fig.42, tab.27).

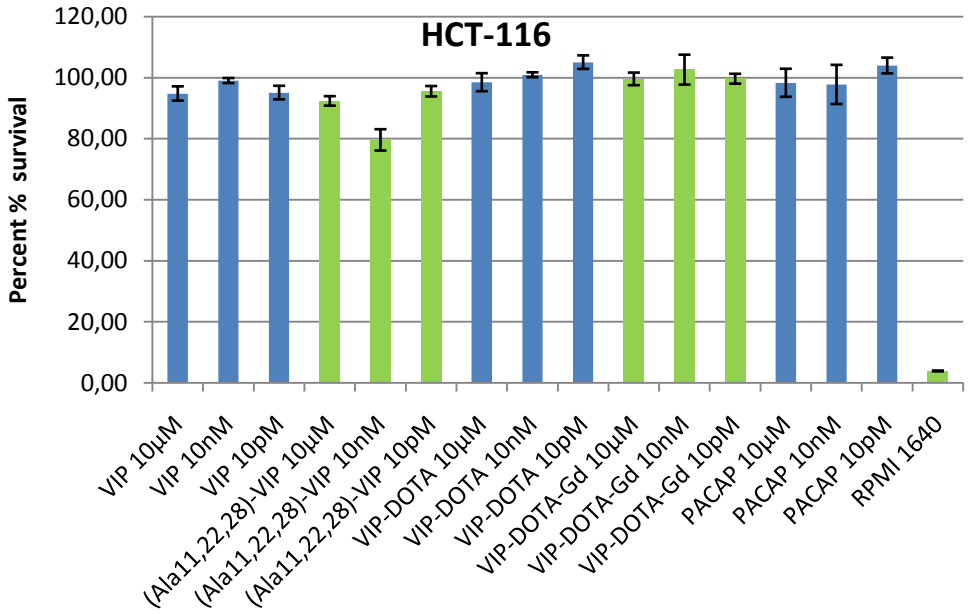

Figure 42. MTT assay HCT-116 cells. VIP conjugates do not show significant proliferation or toxicity. Note the reduction of viable cells when treating cells with 10nM (Ala^{11,22,28})-VIP.

Breast carcinomaMCF-7 cells data:

Table 28. MTT assay of MCF-7 cells.

peptide analogues	1	2	average n=8	std. deviation n=2
	average n=4	average n=4		
VIP 10µM	96,29	105,53	100,91	6,53
VIP 10nM	101,19	94,32	97,76	4,86
VIP 10pM	104,74	92,85	98,80	8,41
(Ala^{11,22,28})-VIP 10µM	98,21	104,74	101,48	4,62
(Ala^{11,22,28})-VIP 10nM	103,32	99,78	101,55	2,50
(Ala^{11,22,28})-VIP 10pM	102,68	97,00	99,84	4,02
VIP-DOTA 10µM	98,28	97,20	97,74	0,76
VIP-DOTA 10nM	100,11	99,36	99,74	0,53
VIP-DOTA 10pM	97,36	99,36	98,36	1,41
VIP-DOTA-Gd 10µM	103,18	104,77	103,98	1,12
VIP-DOTA-Gd 10nM	104,58	106,01	105,30	1,01
VIP-DOTA-Gd 10pM	104,35	104,29	104,32	0,04
PACAP 10µM	103,22	102,47	102,85	0,53
PACAP 10nM	102,20	98,21	100,21	2,82
PACAP 10pM	81,10	101,69	91,40	14,56
RPMI 1640	4,04	3,38	3,71	0,47

The MTT assays with MCF-7 cells indicate no increase in cell number after incubation with peptide conjugates. No significant increase in cell number is observed (fig.43, tab.28).

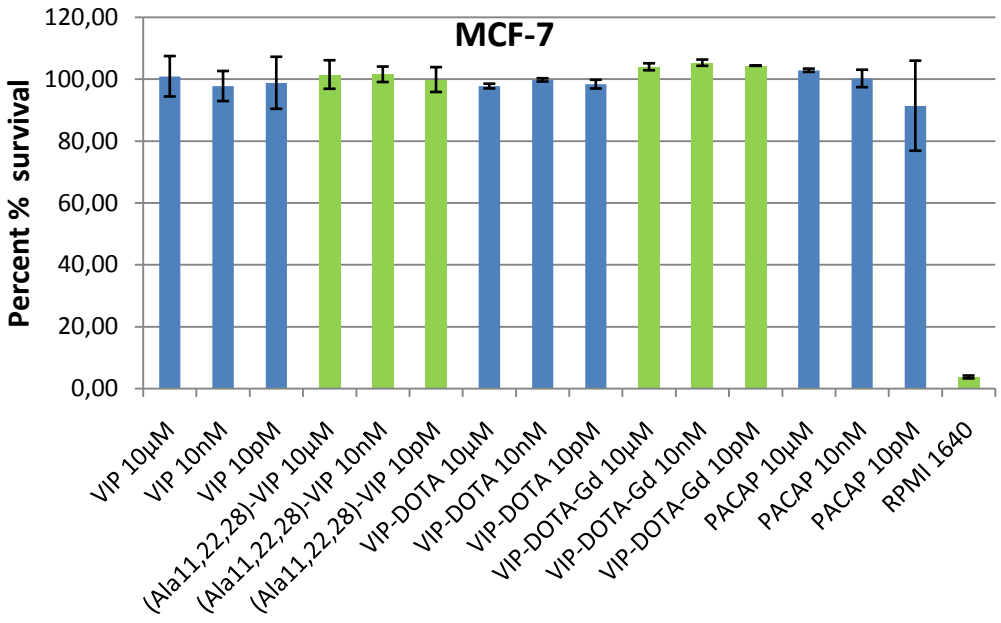

Figure 43. MTT assay of MCF-7 cells. No proliferation or toxicity of peptide conjugates is visualised after treatment of cells.

Microvascular endothelial cells Hmec-1 cells data:

Table 29. MTT assay of HMEC-1 cells.

peptide analogues	1	2	average n=8	std. deviation n=2
	average n=4	average n=4		
VIP 10µM	97,19	111,71	104,45	10,27
VIP 10nM	131,90	127,33	129,62	3,23
VIP 10pM	133,34	142,79	138,07	6,68
$(Ala^{11,22,28})$-VIP 10µM	117,16	106,97	112,07	7,21
$(Ala^{11,22,28})$-VIP 10nM	134,48	134,10	134,29	0,27
$(Ala^{11,22,28})$-VIP 10pM	130,00	135,06	132,53	3,58
VIP-DOTA 10µM	119,56	124,63	122,10	3,59
VIP-DOTA 10nM	118,42	113,96	116,19	3,15
VIP-DOTA 10pM	130,18	141,50	135,84	8,00
VIP-DOTA-Gd 10µM	119,80	136,59	128,20	11,87
VIP-DOTA-Gd 10nM	120,03	131,73	125,88	8,27
VIP-DOTA-Gd 10pM	127,88	139,07	133,48	7,91
PACAP 10µM	104,19	108,83	106,51	3,28
PACAP 10nM	109,26	81,77	95,52	19,44
PACAP 10pM	109,86	94,97	102,42	10,53
RPMI 1640	5,51	7,61	6,56	1,48

The MTT assays of HMEC-1 cells display a dose-effect after incubation with peptide conjugates. Increasing concentration of peptides increased cell number of about 40%. The $VPAC_1$-specific agonist $(Ala^{11,22,28})$-VIP shows more proliferation of cells than PACAP (fig.44, tab.29).

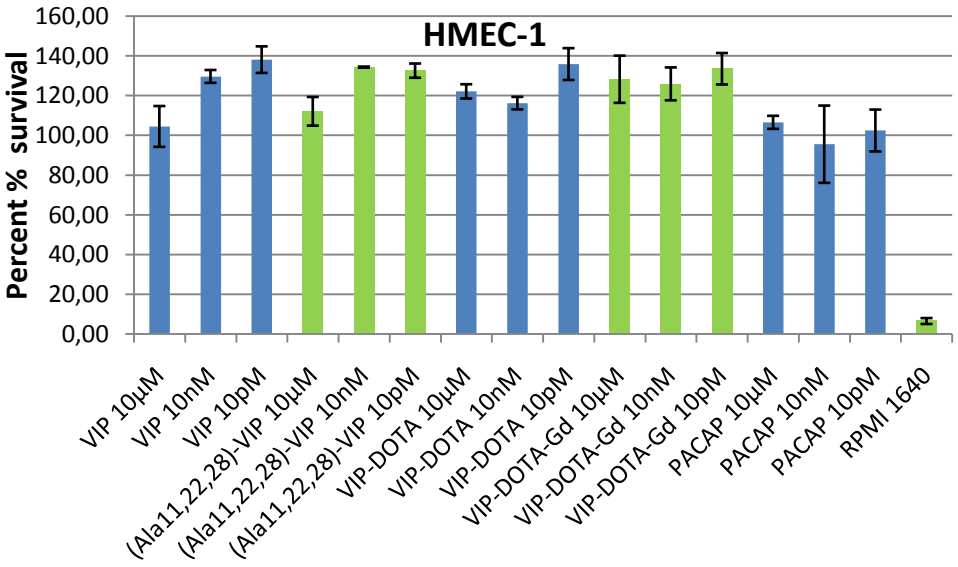

Figure 44. MTT assay of HMEC-1 cells. Note the increased cell number at about 40% of VIP conjugates. $(Ala^{11,22,28})$-VIP shows more cell growth stimulation than PACAP.

4.3 Indirect internalisation by functionality test

The cAMP level of three representative cell lines HMEC-1, HT-29 and MCF-7 were measured with cAMP ELISA. The cells were incubated with VIP, $(Ala^{11,22,28})$-VIP receptor 1 specific agonist and VIP-DOTA-Gd. The cAMP level of cells without treatment was measured as a negative control. Fig.45 indicates the cAMP level of microvascular endothelial cells HMEC-1 cells (black), where the highest amount of cAMP is seen after incubation with VIP. Released cAMP after incubation with the $VPAC_1$-specific agonist is lower than with VIP. VIP-DOTA-Gd is also internalised and released cAMP in the same amount like VIP. Treatment with IBMX reveals higher cAMP level than without IBMX, and lower cAMP level with SQ22,536.

HT-29 cells show the highest cAMP level with VIP, lower with $(Ala^{11,22,28})$-VIP and the lowest with VIP-DOTA-Gd (light gray). Peptides additionally treated with IBMX reveal 10 times higher cAMP level. The treatment with SQ22,536 causes two times less cAMP level than without. The peptide internalisation of Capan-1 cells (dark gray) and cAMP release behave like in HT-29 cells. But Capan-1 cells show low cAMP level after treatment with VIP conjugates, and high cAMP value when additionally treated with IBMX.

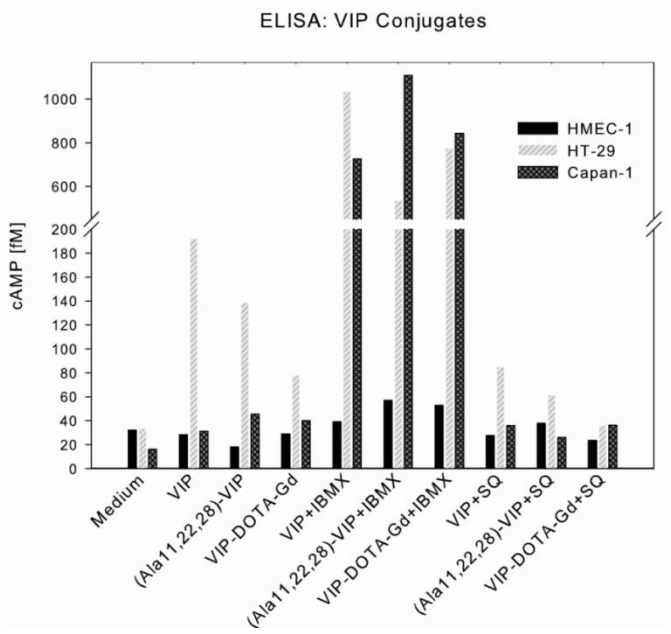

Figure 45. ELISA of VIP conjugates of three cell lines, colon carcinoma HT-29 (light gray) and pancreas carcinoma Capan-1 (dark gray) and endothelial cells HMEC-1 (black). The cAMP level was measured. Treated HMEC-1 cells show no increased cAMP indicating that this cell line may uses another signalling pathway like PLC and Ca^{2+}. HT-29 cells treated with VIP display the highest cAMP increase compared to the other VIP-conjugates. This indicates an internalisation of $(Ala^{11,22,28})$-VIP and VIP-DOTA into the cell which triggers cAMP as second messenger. Capan-1 cells show a cAMP increase after treatment with conjugates and IBMX, indicating that Capan-1 cells may have an increased metabolism rate.

Pulmonary smooth muscle cells PASMC (fig.46) are observed for VIP internalisation via liposomes and proticles. An increase in cAMP level is measured with ELISA. A time depending release of cAMP is seen between liposomes and VIP. Note that 10min incubation with VIP indicates the highest cAMP level, and the incubation with liposomes L08I displays a delayed cAMP release up to 20min. After 60min no increased cAMP is measured. Proticles #G do not show a lagged release of cAMP level because cAMP is lower than cell treated with VIP.

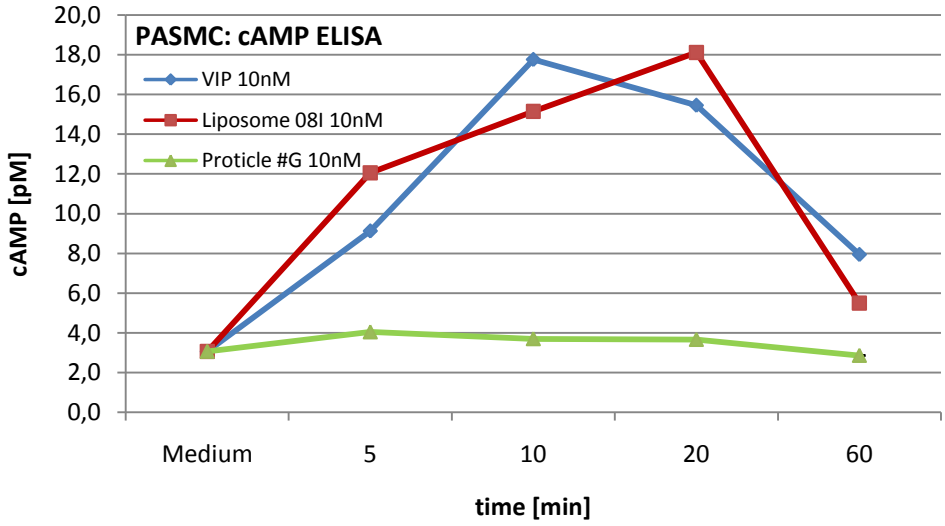

Figure 46. cAMP ELISA of pulmonary smooth muscle cells. PASMC treated with VIP, liposomes L08I and proticles #G in a time course assay 5-60min. VIP treatment displays the highest cAMP increase after 10min incubation. Liposomes 08I show a delayed release effect of cAMP at 20min time point. Proticles #G don´t reveal an increased cAMP at any time point.

Pancreas duct carcinoma PANC-1 P4 cells are used to observe proticles #G internalisation behaviour on carcinoma cells. Fig.47 shows the cAMP level after incubation of VIP and proticles #G at different time points. VIP indicates a time depending increase of cAMP. Proticles #G clearly reveals a delayed release of cAMP compared to free VIP. The highest cAMP release after incubation with proticles #G is reached after 20min. After 30min VIP is not able to induce cAMP, whereas proticles #G do. After 45min and 60min no cAMP respond is observed, neither VIP nor proticles #G induce cAMP.

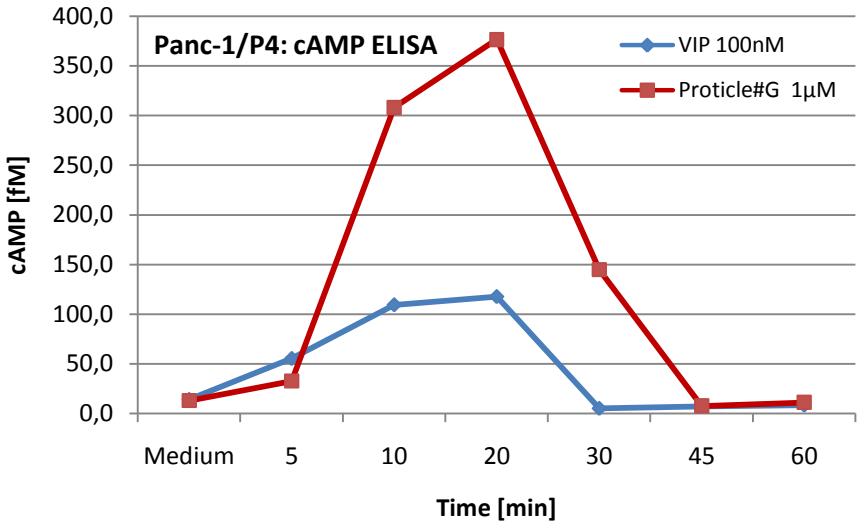

Figure 47. cAMP ELISA of pancreas duct carcinoma PANC-1 P4 treated with VIP and proticles #G in a time course assay (5-60min). VIP induces an increased cAMP release with increasing time. Proticles #G show a delayed increase of cAMP after 30min. After 45min neither VIP nor proticles #G indicate increased cAMP levels, indicating a degradation of cAMP.

4.4 Visualisation by Fluorescence Correlation Spectroscopy

Direct internalisation of VIP and conjugates were measured with Fluorescence correlation spectroscopy. The diffusion time of peptides in buffer is shown in table 30. The size and chemical properties depend on the diffusion time. The bigger the molecular weight the larger the diffusion time.

Table 30. Fluorescent peptide conjugates and their diffusion times measured in PBS.

Peptide	Conc. [µM]	Diffusion time (µs)
VIP-Cy3	0,255	112,5 ± 12,5
VIP-Fluo	0,262	75,3 ± 3,3
Cy3-Scr-VIP	0,256	164,0 ± 43,1
Et-Cy3-OH	0,256	59,8 ± 5,7

Fig.48 shows an intensity scan measured with FCS. Fluorescent signal intensity of a PANC-1 P8 cell is measured in the cytoplasm and at the membrane. VIP-Cy3 shows a high absorption peak on the glass and a second small peak indicating the cell membrane. In buffer solution the intensity goes towards zero, the peptide is enriched in the cell and on the membrane (fig.48).

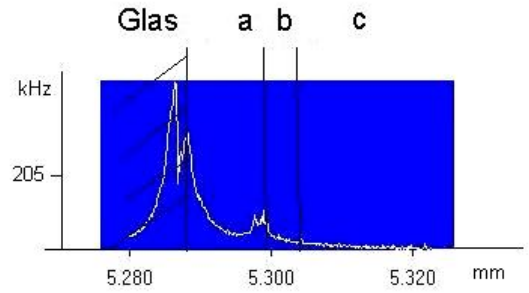

Figure 48. **FCS intensity scan of VIP-Cy3 of a single PANC-1 P8 cell.** a) cytoplasm, b) plasma membrane and c) buffer solution. The highest peak indicates Cy3 glass absorption. The second small peak demonstrates the plasma membrane. Compared to buffer solution, the most Cy3 signal is visible in the cytoplasm, indicating internalisation of VIP-Cy3 into the cell.

Ligand-receptor specifies was tested with Cy3-Src-VIP, which is a VIP sequence in random assembly and covalently linked Cy3 at the N terminus. This peptide should not bind to VPAC receptors because of unfolded interaction site.

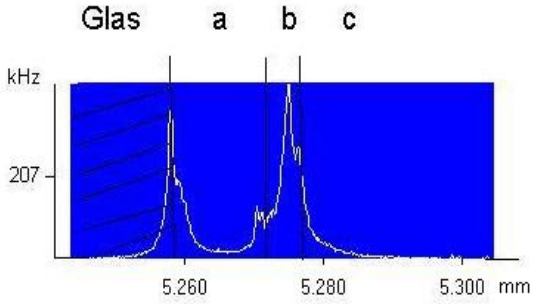

Figure 49. FCS intensity scan of Cy3-Scr-VIP of a PANC-1 P8 cell. a) cytoplasm, b) plasma membrane and c) buffer solution. The first peak at 5,260mm indicates Cy3 glass absorption. The second peak reflects the plasma membrane. Compared to buffer solution, the most Cy3 signal is visible on the membrane, indicating no internalisation of Cy3-Scr-VIP into the cell.

The intensity scan of Cy3-Scr-VIP shows has a very high absorption at the cell membrane (fig.49), more than the glass peak. The time course experiment over 20 minutes reveals a low intensity signal at about 2-3 kHz (fig.52A2) which corresponds with the autofluorescence of PANC-1 cells (fig.52B2). The intensity signal of the autofluorescence is about 2 kHz.

To demonstrate that Cy3 hydrophilic interacts with the membrane, experiments with Cy3 dye were performed. Et-Cy3-OH was used for these analyses. As expected the intensity scan visualises a large membrane peak and lower absorption at the glass (fig.50). Also high intensity signals in the buffer solution and low absorption in the cytoplasm are observed.

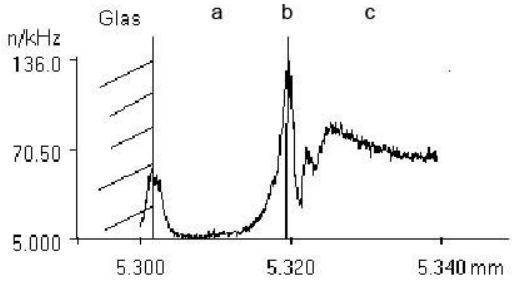

Figure 50. FCS intensity scan of Et-Cy3-OH of a PANC-1 P8 cell. a) cytoplasm, b) plasma membrane and c) buffer solution. The first peak at 5,300mm indicates Cy3 glass absorption. The second peak demonstrates the plasma membrane. Compared to cytoplasm, the most Cy3 signal is visible in the buffer solution, indicating no internalisation of Et-Cy3-OH into the cell.

The time course experiment of Et-Cy3-OH shows the same characteristics like the autofluorescence with PBS. The value of intensity is about 5 kHz. Free diffusion time in solution averages 59,8µs ± 5,7µs. Cy3 is internalised by the cell; it sticks on the membrane by hydrophilic interactions.

These experiments show that VIP-analogues have a specific VIP receptor interaction and is not triggered by Cy3, because Cy3-Scr-VIP and Et-Cy3-OH indicate no signal in the cytoplasm.

The interaction of Cy3 dye with the membrane personates difficulties to calculate the percentage of free/bound receptor, because Cy3 hydrophilic interacts with the membrane without specific peptide-receptor interaction. So VIP was labelled with a fluorescent dye fluorescein, VIP-Fluo, and tested. Fluorescein is not as hydrophilic as Cy3 and does not stick on the membrane. Also glass absorption was seen but not as high as with Cy3 (fig.49). In fig.51 no membrane peak of fluorescein is seen, only an enrichment of peptide in buffer solution is visible.

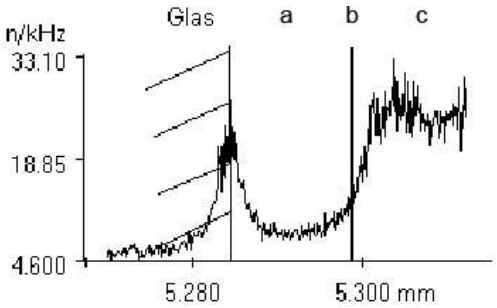

Figure 51. FCS intensity scan of VIP-Fluo of a PANC-1 P8 cell. a) cytoplasm, b) plasma membrane and c) buffer solution. The first peak at 5,300mm indicates fluorescein glass absorption. No membrane absorption is visible. The plateau displays the buffer solution. Also in the cytoplasm the intensity of fluorescein is measured, indicating the internalisation of VIP-Fluo into the cell.

The correlation curve of VIP-Fluo indicates two short components, like the diffusion time of VIP-Fluo in free solution, and one longer component at about 1,5ms. The difference to Cy3 labelled peptides results in the none-hydrophilic interaction of the dyes with the membrane. Fluorescein does not stick to inner membranes and therefore a good correlation is calculated (data not shown).

Time course experiments with both VIP-Cy3 and VIP-Fluo indicate that the fluorescent signal reaches its steady state level after about 5 minutes. Cy3-Scr-VIP does not enter the cell, indicating the importance of the specific ligand receptor reaction for internalisation. No increased fluorescent signal is reached when measuring the autofluorescence. As a conclusion, specific interaction of VIP-conjugates with VPAC

receptors and a following internalisation of the conjugates into the cytoplasm occur (fig.52).

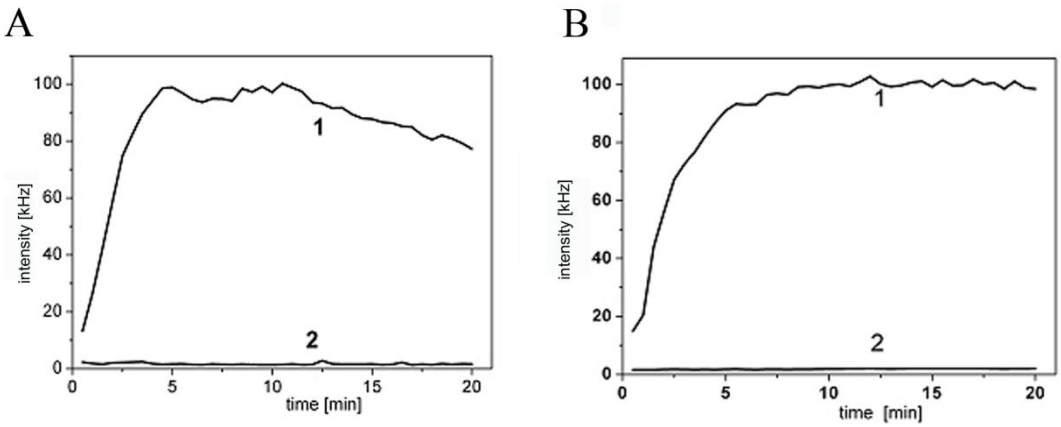

Figure 52. Fluorescence correlation spectroscopy with VIP-conjugates; time course of internalisation in PANC-1 P8 cells of Cy3 (A) VIP-Cy3 (A, line 1) and Cy3-Scr-VIP (A, line 2) and Fluorescein (B) VIP-Fluo (B, line 1) and background due to autofluorescence (B, line 2). With both, VIP-Cy3 and VIP-Fluorescein, the internalisation reaches its steady state level (100%) after about 5 minutes. ScrVIP-Cy3 does not enter the cell, indicating the importance of the specific ligand receptor reaction for the internalisation. The autofluorescence measurement produced no signal.

The intensity scan of VIP-Cy3 labelled proticles #G shows a glass absorption peak of Cy3 and two smaller membrane peaks (fig.53). The fluorescent signal is visible in the cytoplasm, but no signal is seen in the buffer solution. The correlation curve of labelled proticles #G indicate three compnents, one short like free diffusion of VIP-Cy3, and two long components >3000ms (data not shown).

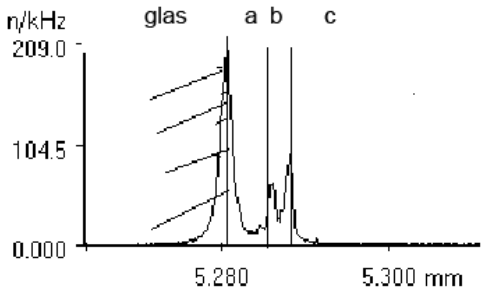

Figure 53. FCS intensity scan of VIP-Cy3 labelled proticles #G of a PANC-1 P8 cell. a) cytoplasm, b) plasma membrane and c) buffer solution. The first peak at 5,280mm indicates Cy3 glass absorption and two membrane peaks are visible. Also in the cytoplasm intensity of Cy3 is measured, indicating internalisation of VIP-Cy3 labelled proticles #G into the cell.

The time course experiment with VIP-Cy3 labelled proticles #G over 30min, reveals a steady state of VIP-Cy3 after about 5min (fig.54). Whereas Cy3 labelled proticles #G continuously increase in the cytoplasm. A steady state is not reached after 30min. Cy3 signal of VIP-Cy3 and labelled proticles #G reach the same intensity after 30min.

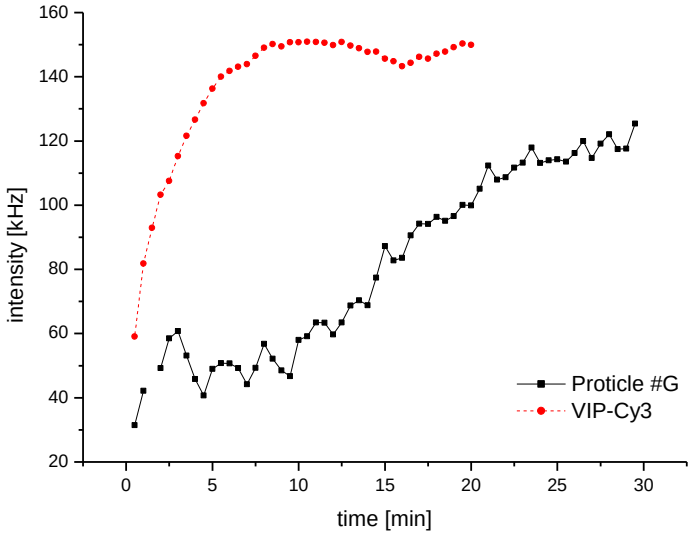

Figure 54. Fluorescence correlation spectroscopy with VIP-Cy3 labelled proticles and VIP-Cy3; time course of internalisation in PANC-1 P8 cells of VIP-Cy3 (red dots) and VIP-Cy3 labelled proticle #G (black line). VIP-Cy3 reaches its steady state level after about 5 minutes. VIP-Cy3 labelled proticles #G showed continuous increase of intensity signal. Steady state is not reached after 30min, this indicates the delayed VIP-Cy3 release from proticles.

4.5 Visualisation by Confocal Laser Scanning Microscopy

In addition to FCS we used Confocal Laser Scanning Microscopy (CLSM) for direct visualisation of VIP conjugates internalisation in living cells. Some cell lines were tested with VIP-Cy3 (red) and (Ala^{11,22,28})-VIP-FITC (green). Cell nuclei were stained with TOPRO-3® (blue).

We observed a relatively high background-signal ratio after incubation with (Ala^{11,22,28})-VIP-FITC, whereas incubation with VIP-Cy3 delivered a very good signal to noise ratio. TOPRO-3® occasionally stained the cytoplasm or the cell membrane which may be an artefact of the experimental system. When testing the autofluorescence for peptides or cells, (negative controls with unlabelled VIP, (Ala^{11,22,28})-VIP and TOPRO-3®) we did not observe specific signal.

Fig.55 shows LNCaP prostate carcinoma cells after incubation with fluorescent labelled peptides. VIP-Cy3 internalises into the cytoplasm, in addition to the marked membrane signal. (Ala^{11,22,28})-VIP-FITC produces a marked membrane signal, without internalisation into the cytoplasm.

Similar signal distributions for the respective peptides are found in the pancreas adenocarcinoma cell line Capan-1 cells (fig.56).

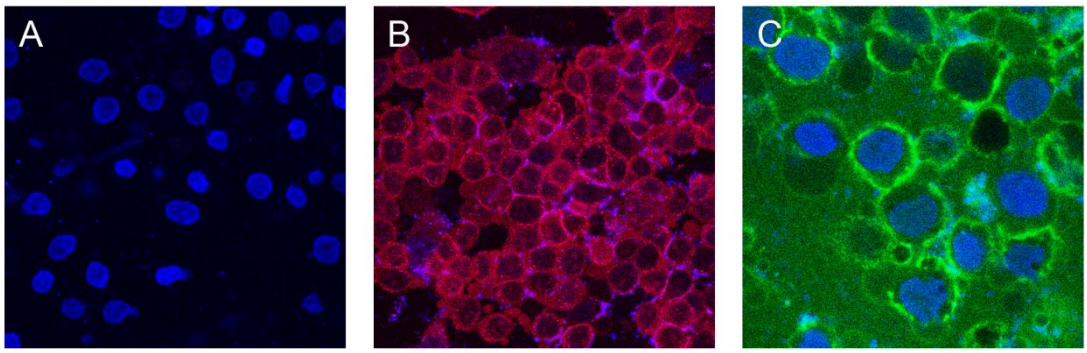

Figure 55. LNCaP cells after incubation with fluorescence-labelled peptides. Cell nuclei are counterstained with TOPRO-3® (blue)**.** A) Control with unlabelled VIP and ($Ala^{11,22,28}$)-VIP. B) Staining with VIP-Cy3 (red) and C) staining with ($Ala^{11,22,28}$)-VIP-FITC (green). Note that VIP-Cy3 reveals a membrane signal and a cytoplasmic signal. $VPAC_1$-specific agonist shows preferentially a membrane signal, indicating that this cell line has no functional $VPAC_1$ receptors.

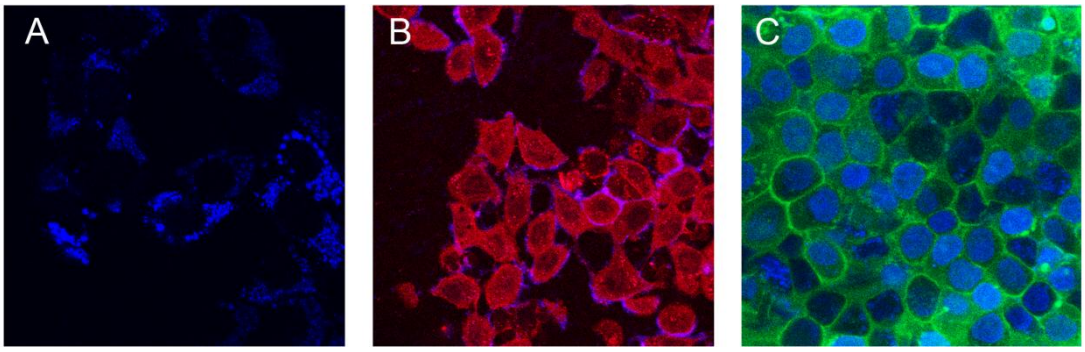

Figure 56. Capan-1 cells after incubation with fluorescence-labelled peptides. Cell nuclei are counterstained with TOPRO-3® (blue)**.** A) Control with unlabelled VIP and ($Ala^{11,22,28}$)-VIP. B) Staining with VIP-Cy3 (red) and C) staining with ($Ala^{11,22,28}$)-VIP-FITC (green). Note that VIP-Cy3 reveals a membrane signal and a cytoplasmic signal. $VPAC_1$-specific agonist shows only a membrane signal, indicating that this cell line has no functional $VPAC_1$ receptors.

Interestingly pancreas duct carcinoma PANC-1 cells in different passages P14 (fig.57A-C) and P40 (fig.57D-F) show differences in internalisation behaviour. Both cell ages indicate VIP-Cy3 signal in the cytoplasm. PANC-1 P14 cells also show a ($Ala^{11,22,28}$)-VIP-FITC signal in the cytoplasm, but PANC-1 cells in P40 reveal much weaker ($Ala^{11,22,28}$)-VIP-FTIC internalisation into the cytoplasm than in P14.

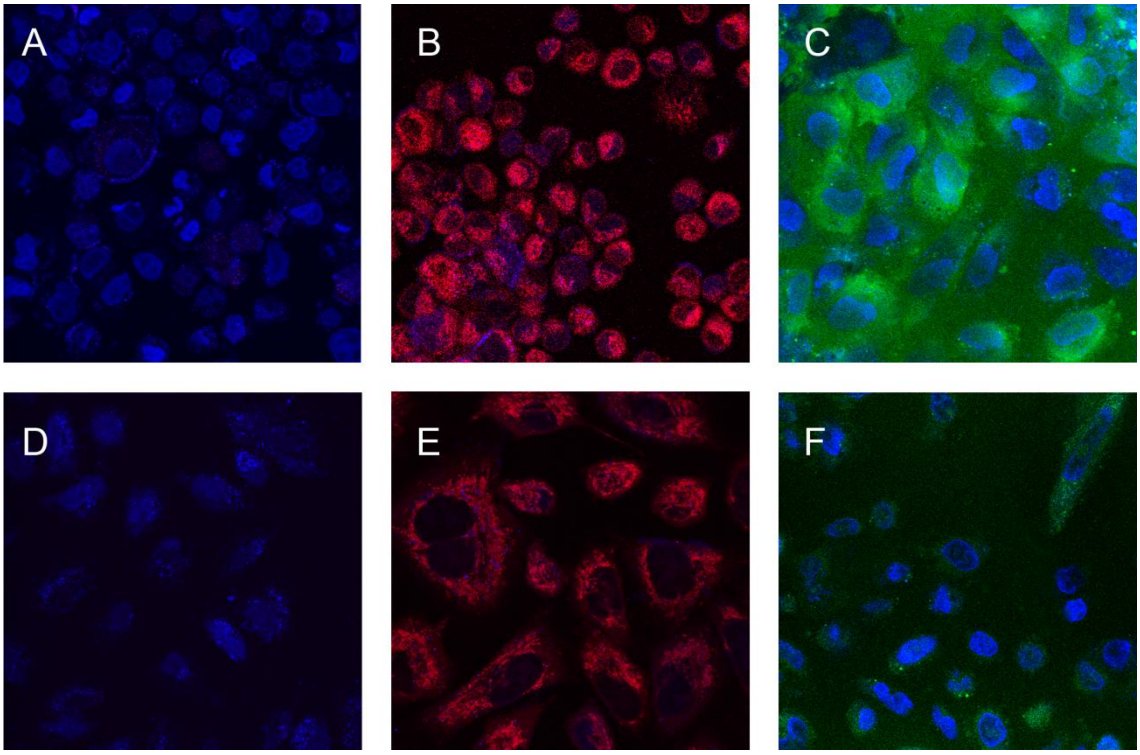

Figure 57. PANC-1 cells, P14 (A-C) and P40 (D-F), after incubation with fluorescence-labelled peptides. Cell nuclei are counterstained with TOPRO-3® (blue)**.** A,D) Control with unlabelled VIP and (Ala^{11,22,28})-VIP. B,E) Staining with VIP-Cy3 (red) and C,F) staining with (Ala^{11,22,28})-VIP-FITC (green). Note that VIP-Cy3 reveals a cytoplasmic signal in both cell ages. $VPAC_1$-specific agonist (Ala^{11,22,28})-VIP-FITC show cytoplasmic signal in PANC-1 P14 cells, whereas PANC-1 P40 cells show a much weaker signal of $VPAC_1$-specific agonist, indicating that P40 cell line looses their functional $VPAC_1$ receptors.

Lung carcinoma A427 cells (fig.58) and hepatocellular carcinoma Hep3B (fig.59) exhibit a strong VIP-Cy3 internalisation into the cytoplasm and a weaker staining with (Ala^{11,22,28})-VIP-FITC but also in the cytoplasm.

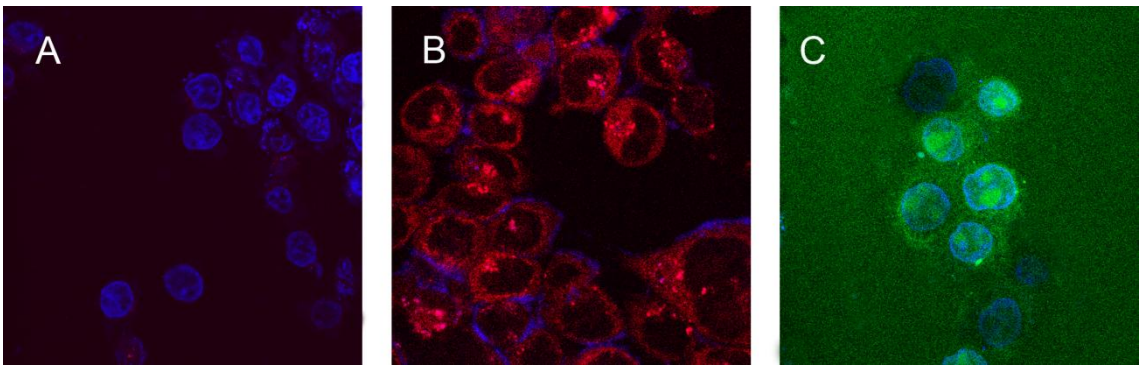

Figure 58. A427 cells after incubation with fluorescence-labelled peptides. Cell nuclei are counterstained with TOPRO-3® (blue)**.** A) Control with unlabelled VIP and (Ala^{11,22,28})-VIP. B) Staining with VIP-Cy3 (red) and C) staining with (Ala^{11,22,28})-VIP-FITC (green). Note that VIP-Cy3 reveals a cytoplasmic signal. $VPAC_1$-specific agonist (Ala^{11,22,28})-VIP-FITC shows a much weaker cytoplasmic signal, indicating that this cell line has less functional $VPAC_1$ receptors.

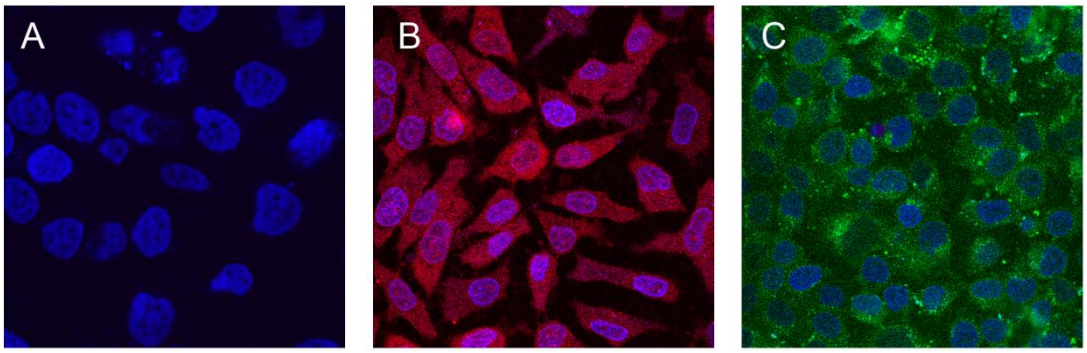

Figure 59. Hep3B cells after incubation with fluorescence-labelled peptides. Cell nuclei are counterstained with TOPRO-3® (blue)**.** A) Control with unlabelled VIP and ($Ala^{11,22,28}$)-VIP. B) Staining with VIP-Cy3 (red) and C) staining with ($Ala^{11,22,28}$)-VIP-FITC (green). Note that VIP-Cy3 reveals a cytoplasmic signal. $VPAC_1$-specific agonist ($Ala^{11,22,28}$)-VIP-FITC displays a much weaker cytoplasmic signal, indicating that this cell line has less functional $VPAC_1$ receptors.

SW1736 cells (thyroid adenocarcinoma) reveal an internalisation of VIP-Cy3 and also display a membrane signal. We observe a green signal on the membrane after incubation with ($Ala^{11,22,28}$)-VIP-FITC, but no signs of internalisation after 1h (Fig.60).

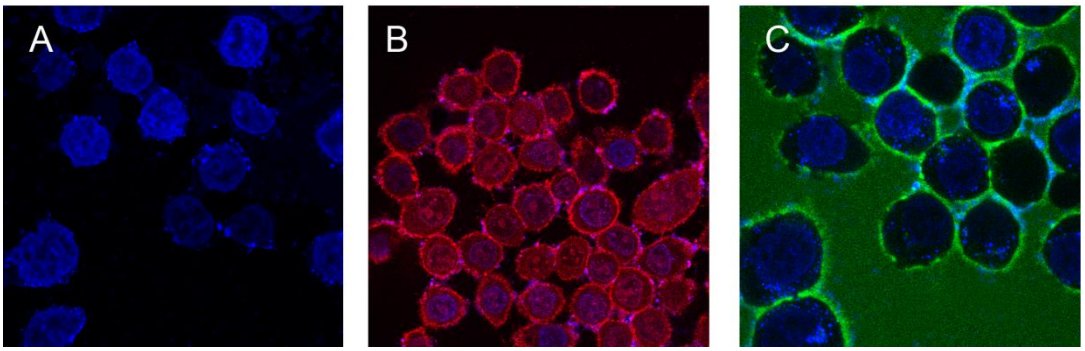

Figure 60. SW1736 cells after incubation with fluorescence-labelled peptides. Cell nuclei are counterstained with TOPRO-3® (blue)**.** A) Control with unlabelled VIP and ($Ala^{11,22,28}$)-VIP. B) Staining with VIP-Cy3 (red) and C) staining with ($Ala^{11,22,28}$)-VIP-FITC (green). Note that VIP-Cy3 reveals a membrane signal and a cytoplasmic signal. $VPAC_1$-specific agonist exhibits only a membrane signal, indicating that this cell line has no functional $VPAC_1$ receptors.

Colorectal carcinoma HT-29 cells (fig.61) display a VIP-Cy3 and ($Ala^{11,22,28}$)-VIP-FITC internalisation into the cytoplasm. Incubation with ($Ala^{11,22,28}$)-VIP-FITC at following time points, 15/ 30/ 45min and 1h, were tried for HT-29 cells. After 30min until 1h, HT-29 cells reveal internalisation signals but show apoptosis. 15min incubation with ($Ala^{11,22,28}$)-VIP-FITC indicate a marked membrane-and internalisation signal (fig.61).

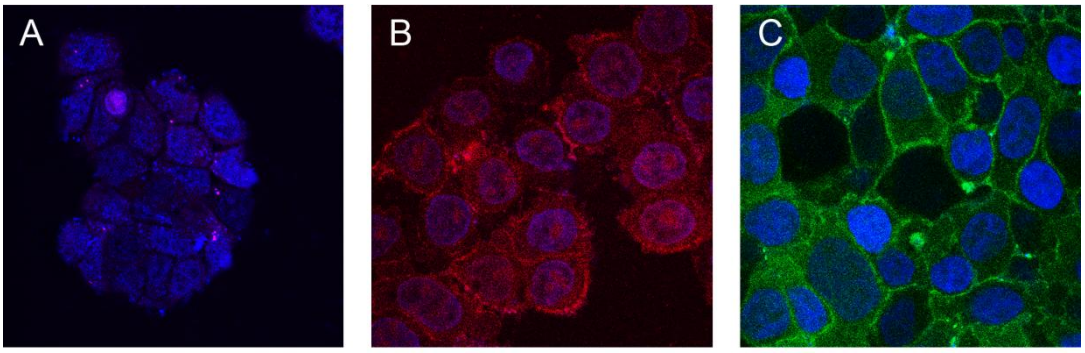

Figure 61. HT-29 cells after incubation with fluorescence-labelled peptides. Cell nuclei are counterstained with TOPRO-3® (blue)**.** A) Control with unlabelled VIP and ($Ala^{11,22,28}$)-VIP. B) Staining with VIP-Cy3 (red) and C) staining with ($Ala^{11,22,28}$)-VIP-FITC (green). Note that both peptides and fluorochromes reveal a membrane signal and a cytoplasmic signal indicating that this cell line has functional $VPAC_1$ receptors which internalise the peptide.

CaCo-2 cells show a VIP-Cy3 signal into the cytoplasm, also ($Ala^{11,22,28}$)-VIP-FITC is seen in the cytoplasm (fig.62). Fig.63 HCT-116 cells exhibit a strong uptake with VIP-Cy3 into the cytoplasm but a weak internalisation of ($Ala^{11,22,28}$)-VIP-FITC.

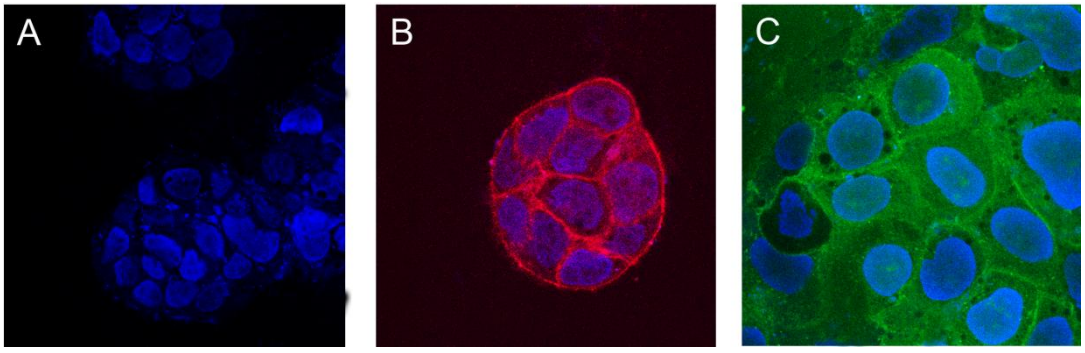

Figure 62. CaCo-2 cells after incubation with fluorescence-labelled peptides. Cell nuclei are counterstained with TOPRO-3® (blue)**.** A) Control with unlabelled VIP and ($Ala^{11,22,28}$)-VIP. B) Staining with VIP-Cy3 (red) and C) staining with ($Ala^{11,22,28}$)-VIP-FITC (green). Note that both peptides and fluorochromes reveal a membrane signal and a cytoplasmic signal indicating that this cell line has functional $VPAC_1$ receptors which internalise the peptide.

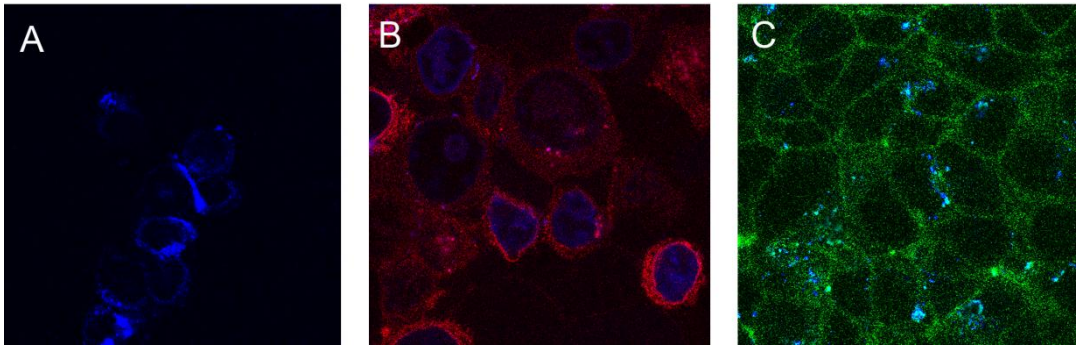

Figure 63. HCT-116 cells after incubation with fluorescence-labelled peptides. Cell nuclei are counterstained with TOPRO-3® (blue)**.** A) Control with unlabelled VIP and ($Ala^{11,22,28}$)-VIP. B) Staining with VIP-Cy3 (red) and C) staining with ($Ala^{11,22,28}$)-VIP-FITC (green). Note that both peptides and fluorochromes reveal a cytoplasmic signal. ($Ala^{11,22,28}$)-VIP-FITC is internalised weaker than VIP-Cy3, indicating that this cell line has less functional $VPAC_1$ receptors which internalise the peptide.

4.6 VIP as carrier for hematoporphyrin (Photodynamic Therapy)

Photodynamic therapy experiments were done to check the potency of VIP-PDT as a pharmacophore. First the oxidative stress level was tested with DCFDA after incubation with H_2O_2 (fig.64) and photosan (fig.65). The readout was fluorescing intensity which correlates with the amout of free oxygen reactive species (ROS). These components are known as standard substances to induce oxidative stress. We were interested in the question whether or not VIP-PDT can increase the celluar oxidative stress level, and investigated incubations with and without light radiation. For control purposes some experiments are performed without cells in PBS (data not shown) and RPMI 1640. The fluoescence in PBS lies between 100-200, which is about three times higher in RPMI 1640 (Fig 64). Fig.64 displays increasing flurescence with increasing concentration of H_2O_2. Radiated assays show a about 1,5 times increased fluorescence signal.

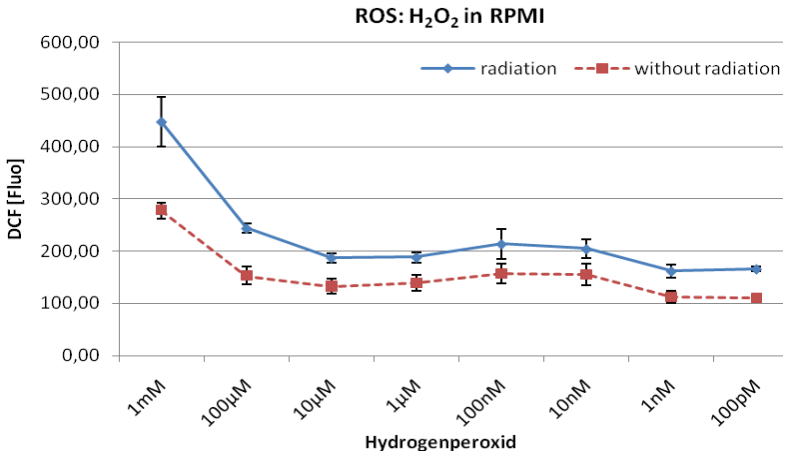

Figure 64. Reactive oxygen species released from H_2O_2 in RPMI measured with DCFDA. Radiated and non-radiated assays is compared (n=8). Note the increase in fluorescent signal after light radiation, 1,5 times more than non-radiated, indicating an increase of ROS after light radiation.

Fig.65 reveals increasing fluorescence with increasing concentration of photosan. Assays treated with radiation shows four times higher fluorescence. The highest fluorescence was observed after incubation with 1µM photosan.

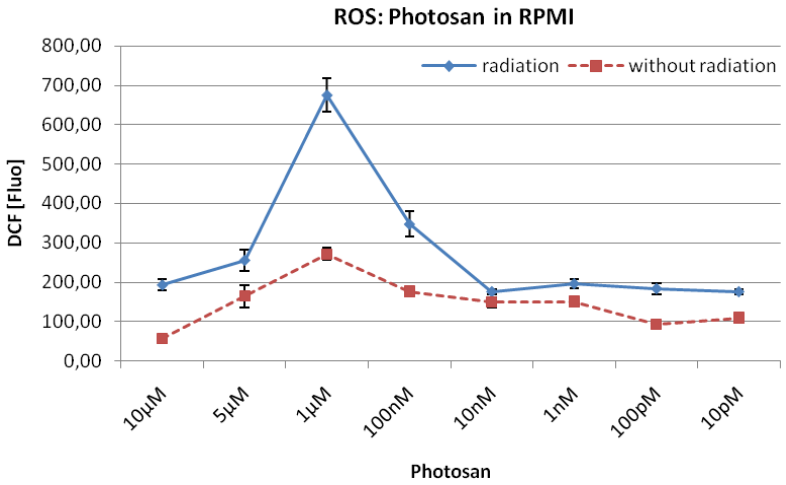

Figure 65. Reactive oxygen species released from photosan in RPMI measured with DCFDA. Radiated and non-radiated assay is compared in the diagram (n=8). Note that 1µM photosan shows the highest fluorescent signal in both assays. Radiated assay shows more signals, indicating an increase of ROS after radiation

Fig.66 shows fluorescence with decreasing concentration of VIP-PDT. Overall the fluorescence release is half as compared with photosan on an equimolar basis, there is little difference between radiated and non-radiated assays. The most effective fluorescence release is with incubation of 1µM VIP-PDT.

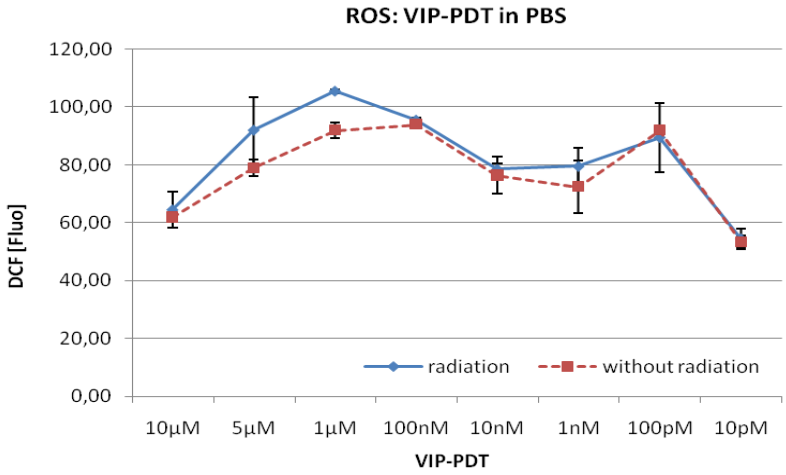

Figure 66. Reactive oxygen species released from VIP-PDT measured with DCFDA. Radiated and non-radiated assay is compared in the diagram (n=4). No difference between radiated or non-radiated assay is visible. 1µM VIP-PDT shows the highest fluorescent signal. Compared to fig. 70, VIP-PDT is not able to release similar amounts of ROS, indicating that VIP-PDT has not the potential of ROS induction than photosan.

The same assay was performed with cells treated with VIP-PDT and photosan. The cell lines PC-3, Hep3B, SW1736, HCT-15, HT-29 and HMEC-1 were analysed for their oxidative stress level and if VIP-PDT or photosan induces ROS in the cell. PC-3 cells

don´t show an increased oxidative stress level compared to the control cells (fig.67). Also without radiation cells produce more fluorescence than radiated once.

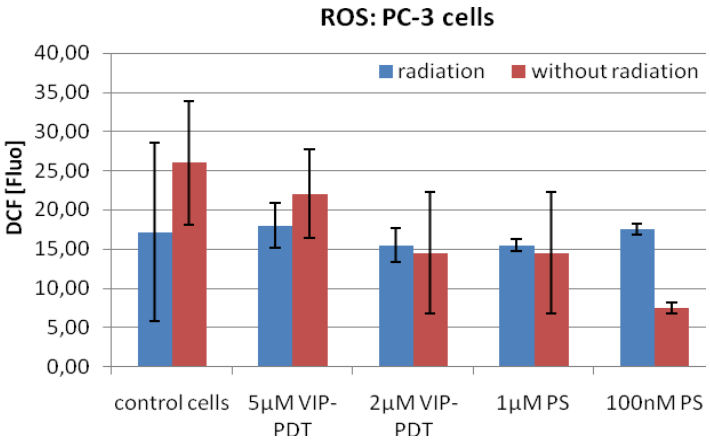

Figure 67. ROS of PC-3 cells measured with DCFDA. VIP-PDT and photosan with different concentrations are tested in radiated and non-radiated assays (n=2). Both peptides are not able to induce ROS level; radiation could not reveal significant increase of ROS, indicating that cells defend against small amounts of ROS.

All analysed cell lines show the same trend as PC-3 cells, where no difference between light radiated and non-radiated assays are observed. This effect might be a defence mechanism of the cell against small amounts of reactive oxygen species (fig.68-72).

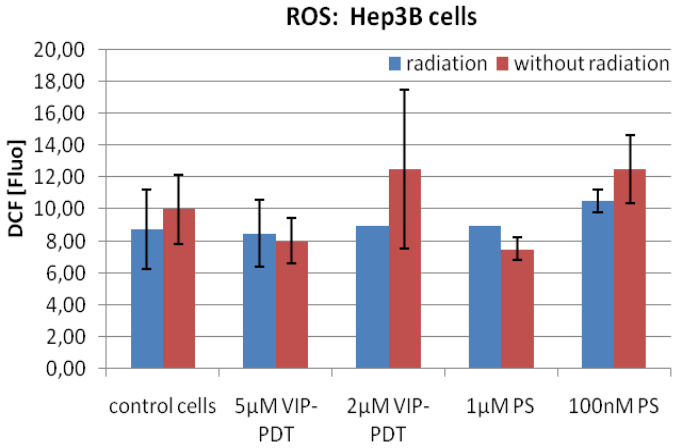

Figure 68. ROS of Hep3B cells measured with DCFDA. VIP-PDT and photosan with different concentrations are tested in radiated and non-radiated assays (n=2). Both peptides are not able to induce ROS level; radiation can not reveal significant increase of ROS, indicating that cells defend against small amounts of ROS.

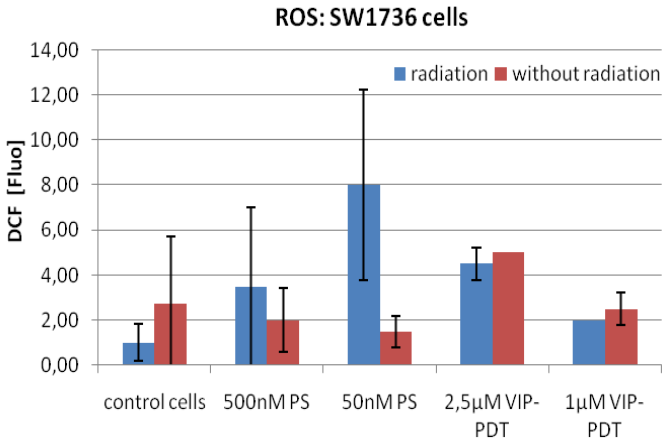

Figure 69. ROS of SW1736 cells measured with DCFDA. VIP-PDT and photosan with different concentrations are tested in radiated and non-radiated assays (n=2). Both peptides are not able to induce ROS level; radiation can not reveal significant increase of ROS, indicating that cells defend against small amounts of ROS.

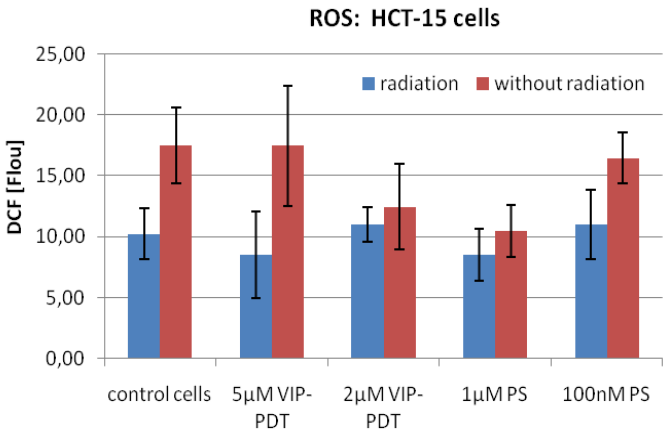

Figure 70. ROS of HCT-15 cells measured with DCFDA. VIP-PDT and photosan with different concentrations are tested in radiated and non-radiated assays (n=2). Both peptides are not able to induce ROS level; radiation can not reveal significant increase of ROS, indicating that cells defend against small amounts of ROS.

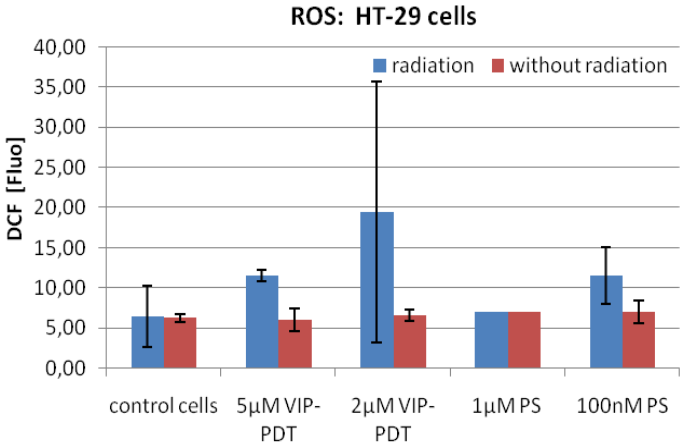

Figure 71. ROS of HT-29 cells measured with DCFDA. VIP-PDT and photosan with different concentrations are tested in radiated and non-radiated assays (n=2). Both peptides are not able to induce ROS level; radiation can not reveal significant increase of ROS, indicating that cells defend against small amounts of ROS.

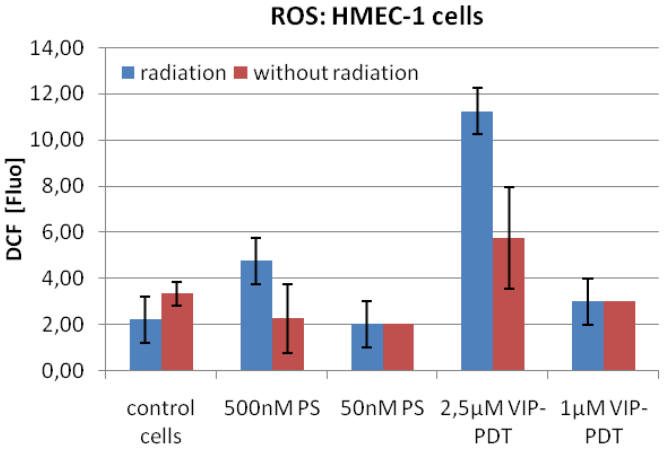

Figure 72. ROS of HMEC-1 cells measured with DCFDA. VIP-PDT and photosan with different concentrations are tested in radiated and non-radiated assays (n=2). Both peptides are not able to induce ROS level; radiation can not reveal significant increase of ROS, indicating that cells defend against small amounts of ROS.

Photodynamic therapy experiments were performed with VIP-PDT and photosan at different concentrations. The concentrations of substances were chosen from the ROS experiment, where 1µM of VIP-PDT and 1µM of photosan showed the most released ROS.

CaCo-2 cells were incubated with VIP-PDT and PS treated with or without radiation. Survival of cells was measured 5h after treatment. Fig 73. reveals an increased cell number after incubation with VIP-PDT or photosan. Non-radiated cells show no significant difference in cell growth stimulation, the cell viability is about 100% compared to control cells.

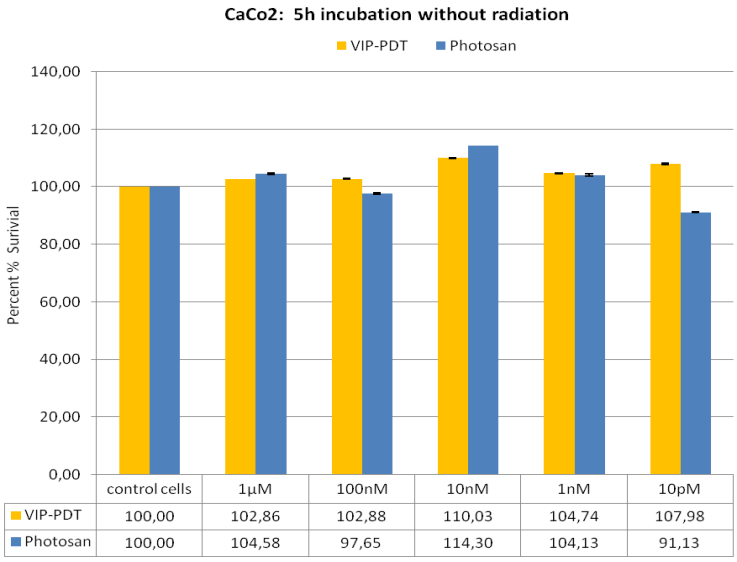

	control cells	1µM	100nM	10nM	1nM	10pM
VIP-PDT	100,00	102,86	102,88	110,03	104,74	107,98
Photosan	100,00	104,58	97,65	114,30	104,13	91,13

Figure 73. Measurement of survival rate of CaCo-2 cells after incubation with VIP-PDT and photosan. Assays were performed without radiation and cell survival was measured 5h after treatment (n=4). Both peptides show no reduction or proliferation in cell growth, indicating that without radiation peptides do not influence cell growth.

Fig.74 shows CaCo-2 cells treated with radiation; a significant decrease in cell survival is seen after treatment with photosan. All concentrations of photosan show the similar effect, 70-80% cell survival of CaCo-2. Whereas cells incubated with VIP-PDT reveal no reduction of cell growth at all concentrations (100%).

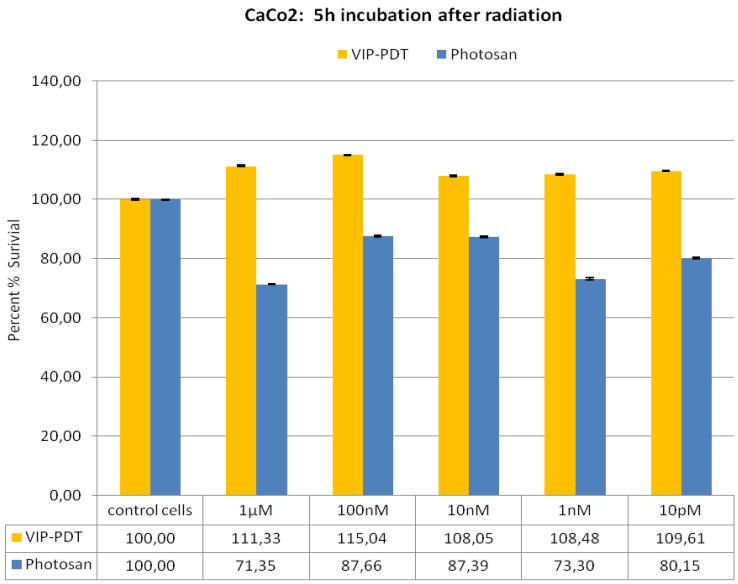

	control cells	1µM	100nM	10nM	1nM	10pM
VIP-PDT	100,00	111,33	115,04	108,05	108,48	109,61
Photosan	100,00	71,35	87,66	87,39	73,30	80,15

Figure 74. Measurement of survival rate of CaCo-2 cells after 5h with radiation of incubated peptides (VIP-PDT and photosan). Assays were performed with radiation and cell survival was measured 5h after treatment (n=4). Photosan shows reduction of cell growth of about 20-30%. VIP-PDT do not reveals a reduction of growth, indicating that only radiation of photosan influence cell growth.

The survival rate of radiated Capan-1 cells after 24h incubation is measured and shows the same trend like CaCo-2 cells. Photosan indicated a significant decrease of viable cells at about 80%, but VIP-PDT has no effect on cell growth behaviour after light radiation (fig.75).

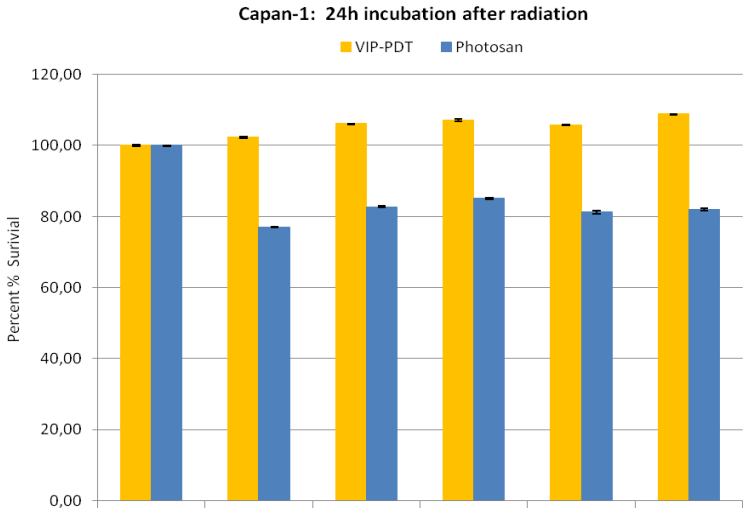

	control cells	1µM	100nM	10nM	1nM	10pM
VIP-PDT	100,00	102,36	106,10	107,13	105,81	108,80
Photosan	100,00	77,03	82,75	85,09	81,30	82,01

Figure 75. Measurement of survival rate of Capan-1 after 24 hours, cells after incubation (VIP-PDT and photosan) and radiation. Assays were performed with radiation and cell survival was measured 24h after treatment (n=4). Photosan shows reduction of cell growth of about 20%. VIP-PDT do not reveals a reduction of growth, indicating that only radiation of photosan reduces the viable cells.

The same experiment was done with HT-29 cells. Non-radiated cells after 5h incubation show no significant difference of cell viability. VIP-PDT and PS incubated cells reveal no significant increase of growth (100%; fig.76). Fig.77 exhibits a reduction of 1µM photosan radiated cells of about 10-20%. Other concentrations of photosan indicate no growth defects. VIP-PDT has no effect on cell growth behaviour after radiation.

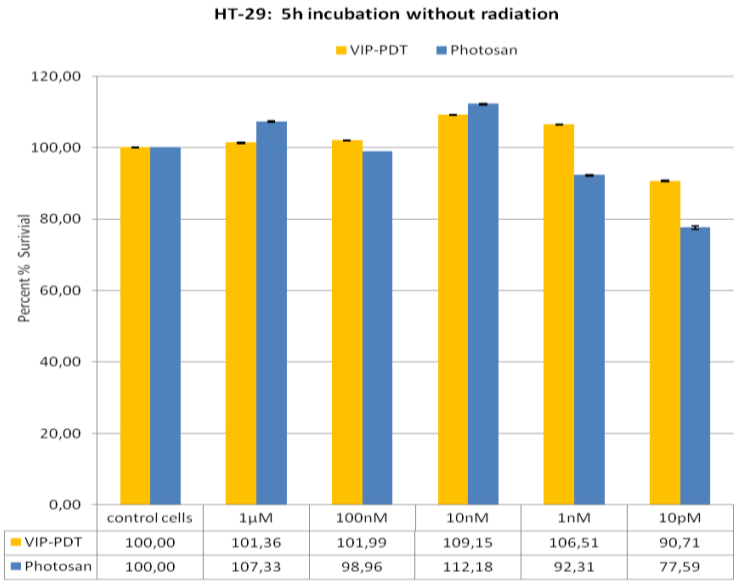

	control cells	1µM	100nM	10nM	1nM	10pM
VIP-PDT	100,00	101,36	101,99	109,15	106,51	90,71
Photosan	100,00	107,33	98,96	112,18	92,31	77,59

Figure 76. Measurement of survival rate of HT-29 cells after 5h incubation with VIP-PDT and photosan. Assays were performed without radiation (n=4). Both peptides show no reduction or proliferation in cell growth, indicating that without radiation peptides do not influence cell numbers.

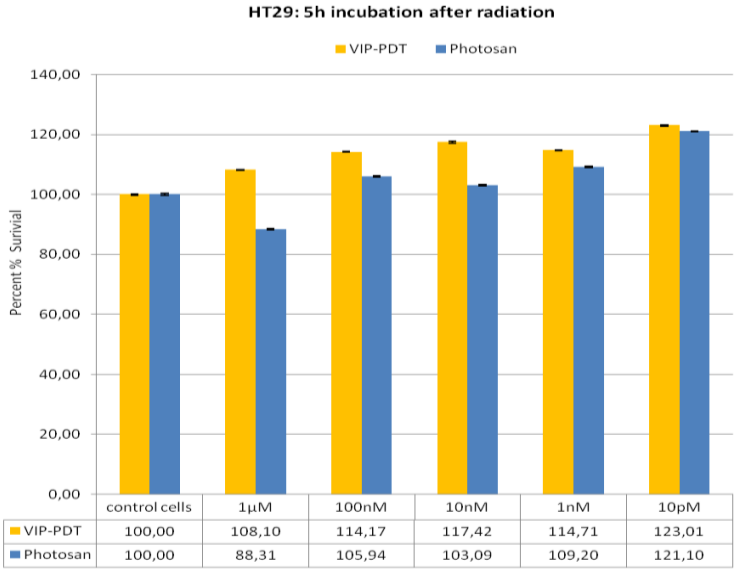

	control cells	1µM	100nM	10nM	1nM	10pM
VIP-PDT	100,00	108,10	114,17	117,42	114,71	123,01
Photosan	100,00	88,31	105,94	103,09	109,20	121,10

Figure 77. Measurement of survival rate of HT-29 cells after after 5 hours, cells after incubation (VIP-PDT and photosan) and radiation. (n=4). 1µM Photosan shows a reduction of cell growth of about 10-20%. Other concentrations of PS or VIP-PDT do not reveal a reduction of growth, indicating that only radiation of 1µM photosan influence cell growth.

Further HT-29 cell survival is measured 24h after cells treated with light radiation (fig.78), because HT-29 do not show similar effect of photosan 5h after treatment like CaCo-2 and Capan-1. Interestingly 24h incubation of radiated photosan reveals the same result like 5h after treatment. 1µM photosan decreases the cell number to 50%, all

other concentrations show an increase of cell growth at about 120%. Cells incubated with VIP-PDT indicate a significant cell survival of about 300%.

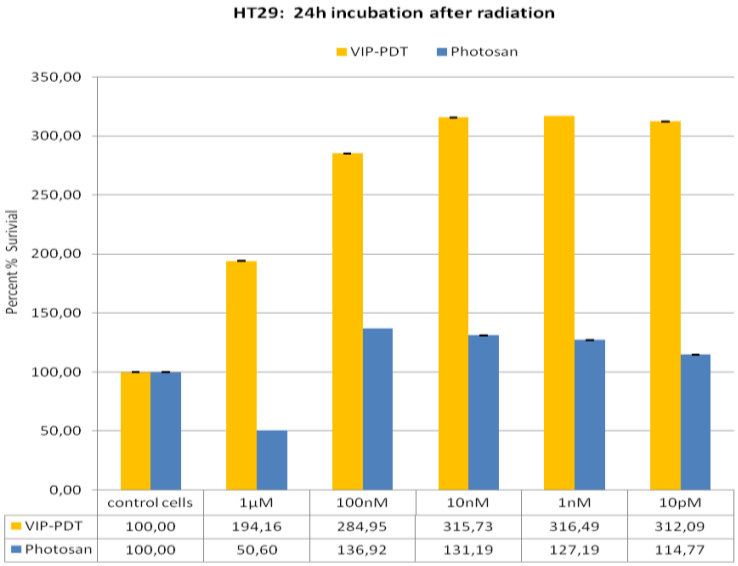

	control cells	1µM	100nM	10nM	1nM	10pM
VIP-PDT	100,00	194,16	284,95	315,73	316,49	312,09
Photosan	100,00	50,60	136,92	131,19	127,19	114,77

Figure 78. Measurement of survival rate of HT-29 after 24 hours, cells after incubation (VIP-PDT and photosan) and radiation (n=4). 1µM Photosan shows reduction of cell growth of about 50%, all other concentrations increase cell growth of about 20%. VIP-PDT reveals an increase of growth of 300%, indicating that only radiation of 1µM photosan reduces cell growth.

5 Discussion

We investigated several aspects of VIP as possible carrier for diagnostic or therapeutic moieties, and revealed some interesting new concepts with potential as anti tumour drug. More specifically the following concepts were investigated:

- VIP-DOTA-Gd revealed some good potential for MRI diagnostics.
- ($Ala^{11,22,28}$)-VIP indicated a good potential to selectively target $VPAC_1$ expressing tumour cells, which is a promising approach to circumvent hypotonic reactions after systemic application.
- VIP-PDT did not release measurable amounts of reactive oxygen species inside the cell, it did not reveal any cytotoxic effect after treatment with red light radiation, whereas photofrin®/photosan with red light radiation raised reactive oxygen species (ROS), which resulted in an cyotoxic effect.
- None of the peptide conjugates or analogue displayed a cytotoxic effect,
- some cell lines were proliferation stimulated by VIP conjugates
- To reveal the potential of VPAC receptors for anti-cancer drug delivery we observed different VIP analogues and conjugates, by FCS, confocal microscopy and ELISA.

5.1 Cell receptor expression

Immunocytochemistry (ICC) stainings of VPAC receptors were performed. We observed unspecific reactions with some of the antibodies; therefore we used a variety of monoclonal and polyclonal antibodies for the ICC staining. The anti-$VPAC_1$ antibodies did not reveal the same signal densities suggesting a lower sensitivity as compared to the anti-$VPAC_2$ and anti-PAC_1 immunoglobulines. Interestingly many cell lines showed very strong nuclear staining with VPAC antibodies which positively correlated with the receptor expression (fig. 17C, 18B, 19C, 20B, 21CD, 22CD, 29CD). It may be an artefact or it may indicate that cells with high receptor expression show receptors within the cell nucleus.

The expression pattern of all cell lines were also performed with Western Blot analysis (n=20). Monoclonal and polyclonal antibodies against VPAC receptors were investigated in WB. Immunodetection with VPAC polyclonal antibodies exhibited a non-specific binding on the blot (data not shown). Also immunodetection with

monoclonal antibody were not as specific as expected also by chancing the nitrocellulose membrane to PVDF membrane, it did not show a better signal. Different buffers with 0,5x TPBS and TTBS were tried but no specification of signal can be visualised. A gently band of protein lysates detected with anti-$VPAC_1$ was seen between 45-55kDa and a stronger band at 55kDa between several unspecific bands. $VPAC_1$ receptor has a molecular weight of 49kDa. A brighter band at 55kDa was made by secondary antibody, which was tested previous (data not shown). The anti-$VPAC_2$ blots displayed many bands, amongst other a band at 55kDa which is the weight of $VPAC_2$. A control blot was detected for actin, where strong specific band could be seen. The WB data was not taken to determine VPAC expression pattern of the cell lines, because of additional unspecific binding of antibodies. Previously experiments performed by DI Dr. Chantal Rodgarkia-Dara indicated the same problems with non-specific binding of these antibodies (personal communication).
In summary the results with ICC and WB indicate that the available immunoglobulines for the receptor expression are prone to produce artefacts next to specific binding.

5.1.1 Cell specificity of receptor expression

However based on negative controls we observed specific staining (signal density beyond negative control) which was indicative for a differential receptor expression of the investigated cell lines.
We observed the expression of $VPAC_1$, $VPAC_2$ and PAC_1 in 14 human tumour cell lines and one human microvascular endothelial cell line (HMEC-1). Many of these cell lines had a preference for $VPAC_1$ receptor expression (for example: PC-3 fig.18; PANC-1 P6 fig.20; A427 fig. 21; Hep3B fig.22; MGC fig.24; HCT-15 fig.25; HT-29 fig.26; CaCo-2 fig.27; HCT-116 fig.28 and MCF-7 fig.29). Others had a preference for $VPAC_2$ receptor expression (LNCaP fig.17; Capan-1 fig.19; SW1736 fig.23 and HMEC-1 fig.30). All cell lines except of HMEC-1 and HCT-15 showed also PAC_1 expression.

Interestingly our data are in agreement with (Reubi 2003) and (Moody et al. 2003), which described dominantly overexpressed $VPAC_1$ receptor in cancer cells compared to healthy tissue. Other colleagues characterized healthy-and tumour tissue and cell lines

for their VPAC expression pattern (table 2 and 3), which are in agreement with our studies.

5.1.2 Variability of receptor expression

We observed that the receptor expression varied within the culture, cells with high expression were found near cells with low expression, For example the PAC_1 receptor expression in SW1736 (fig.23C,D) and in HT-29 (fig.26CD) is heterogeneous. The same situation was observed for $VPAC_2$, heterogenic expression was observed in the same culture of SW1736 (fig.23CD). These results indicate that within the same cell population the receptor expression of individual cells can vary from high to low.

We have seen that in PANC-1 cells the receptor expression is variable and depends on culture age. PANC-1 cells in passage about 1-15 express $VPAC_1$, $VPAC_2$ and PAC_1 receptors, whereas PANC-1 cells in passage about 20 loose $VPAC_1$ receptor completely and downregulate the expression of $VPAC_2$ and PAC_1 receptor (fig.20). This might indicate a technical artefact and differences in sensitivity of signal, or a gradual receptor downregulation under experimental *in vitro* conditions.

Based on my work I conclude the receptor expression in culture is variable to each individual cell and possibly depends on the age of the culture.

5.2 Internalisation behaviour of VIP-conjugates

Fluorescence correlation spectroscopy (FCS) and Confocal Laser Scanning Microscopy (CLSM) was used to observe the direct internalisation of VIP-conjugates in living cells via the specific VIP signalling pathway.

5.2.1 Indirect visualisation of internalisation by cAMP measurement

Indirect visualisation of internalisation was shown with cAMP ELISA of HT-29, Capan-1 and HMEC-1 cells. Fig.45 clearly displayed the one signalling pathway of HT-29 and Capan-1 tumour cell lines. cAMP was released after stimulation with VIP, ($Ala^{11,22,28}$)-VIP and VIP-DOTA-Gd. VIP revealed the highest cAMP release compared with the other conjugates, because VIP-conjugates increase in molecular size, differ in chemical properties and may have other interaction behaviour. All these causes contributed to less cAMP release. Capan-1 cells showed less cAMP response compared to HT-29 cells, this might be explained by individual degradation velocities of cAMP of each cell line. Also the functionality of the peptide conjugates and biological activity of

VIP-conjugates are proven by cAMP signalling response. My data also indicate that VPAC receptor recycling is not interfering and disabled with conjugates. HMEC-1 cells did not exhibit a cAMP signalling when stimulation with VIP and conjugates, this could have several reasons. Endothelial cells are cultured on collagen basis, either cells were not grown or lysated properly, the most important reason might be that endothelial-and smooth muscle cells dominantly expressing $VPAC_2$ receptor (Adamou et al. 1995; Reubi 2000; 2003; Schulz et al. 2004), $VPAC_2$ signalling prefers phospholipase C pathway (Yamada et al. 2004) and not adenlyate cyclase with second messenger cAMP. This phenomenon is described for PAC_1 signalling. In this case HMEC-1 could not be visualised via cAMP, therefore increased Ca^{2+} should be measured.

As known before (Rubinstein 2005; Sejourne et al. 1997; Sethi et al. 2005; Stark et al. 2007) enclosed VIP in liposomes are used for systemic application and peptide protection of proteases. We tested whether or not liposomes and proticles release VIP with a delay and were functional active. Our data indicated that liposomes were a good tool for VIP delayed release. We observed lower cAMP level at low proticle #G concentration at different time points. This might be because of too less concentration of proticles. Liposomes 08I indicated a delay in the first 20 minutes compared to free VIP in equal concentrations of PASMCs (fig.46). Also proticles #G revealed an increased cAMP response and a delay effect in PANC-1 P8 cells through the first 30min compared to free VIP. After 45min no cAMP release was triggered with 1µM proticle #G and 10nM VIP (fig.47).

Both liposomes and proticles indicated a delay of cAMP release after stimulation, indicating an advantage for VIP application in patients.

5.2.2 Fluorescence correlation spectroscopy (FCS)

FCS of PANC-1 P8 cells revealed a long diffusion component in the membrane area and in the cytoplasm for VIP-Cy3 (data not shown), which indicates a strong binding to the plasma membrane and inside the cell (fig.48). This phenomenon might be explained by hydrophilic properties of Cy3, which immobilize with the molecules on the membranes especially at the plasma membrane, endoplasmatic reticulum (ER) or other membranes in the cell. To test this theory we changed the conjugate to fluorescein which is not as hydrophilic as Cy3. VIP-Fluo revealed much better correlation of diffusion (data not shown), we found no long component indicating a membrane

association (fig.51). In addition there was less photobleaching with VIP-Fluo (fig.52B1) than with VIP-Cy3 (fig.52A1). Controls with Et-Cy3-OH and Cy3-Scr-VIP, with random VIP sequence, showed high membrane peaks (Fig.49b, 50b) indicating strong membrane binding. No signal in the cytoplasm indicated sequence specific peptide internalisation. Haberl et al. (2006) showed the relevance of Cy3 conjugation with a ethyl group or a lysine as linker to VIP at N-or C-terminus. Amino terminal and ethyl conjugated VIP resulted in less internalisation than the carboxy terminal with lysine conjugated VIP. But both conjugates were still active and biological functional.

My results indicated that VIP conjugates internalised via VPAC receptors because controls Et-Cy3-OH, Cy3-Scr-VIP and autofluorescence did not show an internalisation into the cell. Et-Cy3-OH and Cy3-Scr-VIP showed fluorescence intensities between 2-5kHz, which correlated with the autofluorescence of the cell (fig.52A2,B2). Whereas VIP-Cy3 and VIP-Fluo showed a rapid internalisation within the first 5 minutes and revealed a steady state after VIP-conjugate uptake. An decreasing fluorescence over 20 minutes of VIP-Cy3, and less of VIP-Fluo was observed because of photobleaching induced by the laser (fig.52A1,B1). Therefore we assumed that VIP had a specific interaction with $VPAC_{1/2}$ and $PAC_{1,}$ and Cy3 interacted with the membranes. Cy3 is a high hydrophilic molecule which intercalates in hydrophilic structures at the membrane.

Additionally we tested VIP-Cy3 labelled proticles #G (fig.53), which showed a continuously increase of Cy3 signal in the cytoplasm. After 30min no saturation effect could be reached, whereas free VIP-Cy3 reached a steady state after 5min (fig.54). As seen in fig.47 PANC-1 P8 cells displayed a delay of cAMP release after incubation with proticles #G, which was in agreement with FCS data, indicating a delayed release of VIP-Cy3 from proticles in the time period of 30min.

5.2.3 Confocal Laser Scanning Microscopy (CLSM)

A non-radioactive technique with confocal laser scanning microscopy (CLSM) was described by Haberl et al. (2006) and used as a direct method for internalisation in living cells. Technical difficulties were observed with nuclear staining with TOPRO-3®. Partly staining of the cytoplasm or the whole cell was observed in some cell lines (fig.56A, 58AC, 62A, 63AC). Others showed only nuclear staining. The staining of the dye might work cell line depended or oblique on cell vitality, indicating that TOPRO-3® might not be the best tool for *in vivo* staining.

We showed that the fluorescently labelled conjugates VIP-Cy3 and ($Ala^{11,22,28}$)-VIP-FITC internalised in carcinoma cells from different tissue origin (LNCaP fig.55; Capan-1 fig.56; PANC-1 fig.57; A427 fig.58; Hep3B fig.59; SW1736 fig.60; HT-29 fig.61; CaCo-2 fig.62 and HCT-116 fig,63). A high background-signal ratio was seen in with ($Ala^{11,22,28}$)-VIP-FITC staining. In spite of blocking with more percent of FBS, FITC showed a very high background signal. Because we frequently observed a membrane signal when using $VPAC_1$ selective agonists ($Ala^{11,22,28}$)-VIP-FITC even after 1 hour of incubation, might indicate that the $VPAC_1$ receptor needed more time for internalisation. HT-29 cells were incubated only 15min with ($Ala^{11,22,28}$)-VIP-FITC (fig.61C) because of apoptosis of cells with increasing time.

Ala(^{11,22,28})-VIP internalisation into the cytoplasm indicated a functional $VPAC_1$ receptor.

5.3 VIP receptor expression and internalisation function

Interestingly my confocal data were in agreement with the immunocytochemistry (ICC) data. Those cells which did not express $VPAC_1$ receptor (LNCaP fig. 17B, Capan-1 fig.19B, PANC-1 P8 fig.20F, SW1736 fig.23B and HMEC-1 fig.28B) showed only weak or no internalisation of the $VPAC_1$-selective agonist into the cytoplasm (LNCaP fig. 55C, Capan-1 fig.56C, PANC-1 P40 fig.57F, SW1735 fig.60C and HCT-116 fig.63C).

PANC-1 cells at different age P14 and P40 indicated differences of their internalisation pattern. Interestingly ICC staining showed clearly different expression patterns of aged PANC-1 cells (fig.34). Some internalisation was observed, possibly the ICC staining was less sensitive than the internalisation of fluorescent peptides, alternatively we would have to assume that the receptor specific ($Ala^{11,22,28}$)-VIP-FITC is using alternative receptors.

5.4 Peptide conjugates and their cellular effects

We used three types of ligands with a potential for clinical use. VIP-DOTA-Gd which might be applied in MRI diagnostics, $VPAC_1$ selective agonist ($Ala^{11,22,28}$)-VIP for specific tumour targeting and VIP-PDT as an application for photodynamic therapy (PDT).

5.4.1 VIP-DOTA-Gd

^{123}I-VIP is known as a chelator for tumour targeting (Virgolini et al. 1994a; 1996; 1994b) which has been successfully used in tumour search and therapy (Krenning et al. 2004; Virgolini et al. 1998). Based on this knowledge we designed a DOTA-Gd conjugated to VIP for selective VPAC tumour targeting for MRI diagnostics. The advantage of DOTA chelated with Gd^{3+} is the loss of cytotoxicity of free Gd^{3+} as described by Idee et. al (2006). As shown in fig.45 VIP-DOTA-Gd exposed to tumour cells increase the cAMP level. We concluded that the VIP conjugate entered the cell to receive this reaction; this implies that the conjugated DOTA with the gadolinium entered the cell via the VIP signalling pathway. MTT tests were performed to characterise the cell growth behaviour of incubated VIP-conjugates. The MTT assays showed no toxicity after incubation with VIP-DOTA or VIP-DOTA-Gd. Both peptide conjugates were similar in growth behaviour. LNCaP (fig.31), Capan-1 (fig.33), Hep3B (fig.36), SW1736 (fig.37), MGC (fig.38), HCT-15 (fig.39), HT-29 (fig.40), CaCo-2 (fig.41), HCT-116 (fig.42) and MCF-7 (fig.43) showed no proliferation after treatment. Increased cell number of about 20% was observed in PC-3 (fig.32), PANC-1 P8 (fig.34), A427 (fig.35) and HMEC-1 (fig.44) cells. These cell lines also indicated increased proliferation when treated with VIP as a control.

Free Gd^{3+} is cytotoxic, but chelated to DOTA and linked to VIP, none of all cell lines demonstrated cytotoxic effects of VIP-DOTA-Gd in the MTT assays; therefore they could be useful for MRI diagnostics as a non-radioactive tool in clinical applied studies.

5.4.2 (Ala^{11,22,28})-VIP

(Ala^{11,22,28})-VIP selective agonist (Nicole et al. 2000) was investigated to for $VPAC_1$ tumour trageting while blood vessels and smooth muscle cells express dominantly $VPAC_2$. Fluorescent labelled and unlabelled (Ala^{11,22,28})-VIP internalisation was shown by confocal microscopy, MTT assays were performed to test the proliferative or cytotoxic behaviuor of tghe peptide. Following cell lines exhibited no significant inrease or decrease in cell growth after treatment with conjugate: LNCaP (fig.31), Capan-1 (fig.33), Hep3B (fig.36), SW1736 (fig.37), MGC (fig.38), HCT-15 (fig.39), HT-29 (fig.40), CaCo-2 (fig.41), HCT-116 (fig.42) and MCF-7 (fig.43). An increased cell number of about 20% was observed in PC-3 (fig.32), PANC-1 P8 (fig.34), A427 (fig.35) and HMEC-1 (fig.44) cells. Interestingly HMEC-1 were growth stimulated by

VIP and ($Ala^{11,22,28}$)-VIP compared to PACAP, even though HMEC-1 cells predominantly express $VPAC_2$ receptor.

5.4.3 VIP-PDT

VIP-PDT has the potential to increase the selectivity of photodynamic therapy (PDT), because VIP may be a carrier for PDT which targets the PDT to specific VPAC receptor expressing cells. First we were interested in the potency of VIP-PDT and photosan releasing free radicals and inducing programmed cell death. Different concentrations of H_2O_2, VIP-PDT and photosan in PBS or RPMI 1640 were measured with and without radiation. Data showed increased fluorescence in the case of RPMI 1,5 times more than with PBS (fig.64-66). A saturation of DCFDA system is possible, because 1µM of photosan and VIP-PDT showed less fluorescence than all other concentrations (fig.64,65). Photosan induced more reactive oxygen species (ROS) than VIP-PDT. Also the oxidative stress level of investigated cell lines was measured (fig.67-72), these results revealed no measurable amounts of ROS with DCFDA.

We did not observe a cytotoxic effect after incubation of 1µM-10pM VIP-PDT with or without radiation (fig.73-78). We expect that the VIP-PDT oligomer polymerisation during internalisation was destroyed; which means that single hematoporphyrin groups has entered the cell. Photofrin®/photosan is an oligomer of hematoporphyrin groups, which has been more efficient in producing ROS after radiation. May be a defence reaction of the cell is activated after exposure to radiation.

CaCo-2 and HT-29 cells treated with photosan without radiation showed no increased or decreased cell viability (fig.73,76), whereas cells treated with 1µM-10pM photosan and radiation revealed a significant reduction in growth of about 20% in CaCo-2 (fig.74), Capan-1 (fig.75), HT-29 (fig.77,78). Interestingly HT-29 cells displayed massive increase in cell number after radiation, only 1µM photosan stops proliferation and reduced cell growth of about 20% (fig.77). HT-29 cells needed a high concentration (1µM) of photosan to reach a cytotoxic effect with radiation. Capan-1 and HT-29 were measured 24 hours after treatment (fig.75,78). These data indicated that programmed cell death of 20% was visible after 5h and 20-50% after 24h. Photofrin can induce oxidative stress which has been shown by Gomer et al. (1996), and reduces in cell growth in colon carcinoma (Yang et al. 2007) and in HT-29 cells (Marchal et al. 2005).

Experiments with ROS and cell growth stimulation or cytotoxicity of VIP-PDT and photosan after radiation, were not in agreement. ROS induced by photosan showed the highest signal at 1µM concentration, whereas cell survival after radiation depended not on photosan concentration. An explanation for this phenomenon might be that small amount of ROS are enough to activate programmed cell death. Less ROS induction could lead to a defence mechanism of the cell, which converts ROS to non-cytotoxic products.

Finaly we conclude that VIP-PDT has not the potential to induce cell death of tumour cells, because of missing accumulation of hematoporphyin groups, whereas photosan revealed a reduction of cell number of about 20% which depended among the cell lines.

.

6 Abstract

In this work we were interested in the potency of VPAC receptors as target for anti-cancer drug delivery. There are three subtypes of VPAC receptors, $VPAC_1$, $VPAC_2$ and PAC_1. They belong to the large superfamily of G-protein coupled receptors (GPCR) which play an important role in cell signalling. The two most major specific VPAC receptor ligands are neuropeptides, vasoactive intestinal peptide (VIP) and pituitary adenlyate cyclase activating polypeptide (PACAP). These small peptides function as trophic factor in neurodevelopment, stimulate hormone release, have anti-inflammatory effects and benefit tumour proliferation. VIP is an important vasodilator and relaxant of smooth muscle cells. Previously VIP´s action for tumour targeting and use in tumour diagnostics has been well studied by many groups. Lot of specific agonists and antagonists have been developed to target VPAC expressing tumour cells. VIP is widely distributed in the most tissue (pancreas, prostate, stomach, thyroid, lung, breast, brain, skeletal and smooth muscles and vessels) and VPAC expression pattern showed that most endocrine tumours express dominantly $VPAC_1$ receptor and vessels and smooth muscles $VPAC_2$, PAC_1 is mostly present in the brain.

We investigated three ideas in this work, on the one hand selective tumour targeting with a $VPAC_1$ specific peptide ($Ala^{11,22,28}$)-VIP, because of the $VPAC_2$ expressing vessels and muscles cells. This receptor pattern helps use to circumvent the hypotonic shock after systemic application and can be used for patients without adverse effects. ($Ala^{11,22,28}$)-VIP engulfed in liposomes and loaded with anti-sense RNA or other downregulating or destroying drugs could be used as pharmacophor. On the other hand we designed a peptide conjugate, VIP-DOTA-Gd, for non-radioactive tumour targeting for magnet resonance imaging (MRI) diagnosis. At last a VIP-hematoporphyrin conjugate, VIP-PDT, was developed to increase selective photodynamic therapy (PDT) for VPAC expressing cancer cells.

First we characterized 14 human tumour cell lines from different organs and one microvascular endothelial cell line for their VPAC receptor expression pattern performed with immunocytochemistry (ICC) stainings with specific antibodies. Cell culture showed heterogenic expression of VPAC receptors and different expression pattern with cell age (PANC-1), therefore living surgically removed human tumour tissue should be analysed. Specific interaction of ligand and receptor and the following

internalisation into the cytoplasm of VIP conjugates, (Ala^{11,22,28})-VIP, VIP-DOTA-Gd and VIP-PDT, were visualised by fluorescence correlation spectroscopy (FCS), confocal laser scanning microscopy (CLSM) and cAMP ELISA. Also VIP engulfed in liposomes or proticles was tried for delayed VIP release, because VIP is proteolytic cleaved in extracellular fluid and therefore its half life time is about 1-2 min. These assays performed with cAMP ELISA indicated a 20min to 30min delay of cAMP release compared to free VIP. Proliferation properties of VIP-conjugates were obtained with MTT assays and analysed for their cytotoxic behaviour. None of the tested peptides, VIP, VIP-DOTA-Gd, (Ala^{11,22,28})-VIP and PACAP showed cytotoxic effects, some cell lines used VIP or conjugates as proliferative factor. VIP-hematoporphyrin conjugate was tested for its potential as selective light sensible chemical substance, photo-sensitiser, for PDT. Experiments performed with DCFDA as detection system revealed a release of reactive oxygen species (ROS) after incubation of VIP-PDT treated with radiation. Cells treated with VIP-PDT and radiation did not increase ROS and no reduction of cell growth was observed. As control we used a classical PDT substance, Photofrin® (hematoporphyrin oligomer), which indicated apoptosis of tumour cells of about 20%-50% after treatment with radiation. So we conclude that VIP-PDT with a single hematoporphyrin group is not able to induce enough ROS inside the cell, which might depend on defence mechanisms of the cell.

Finally we can say that the development of a selective $VPAC_1$ tumour targeting system with (Ala^{11,22,28})-VIP could be useful for anti-cancer drug delivery. Further VIP-DOTA-Gd can be used to target VPAC positive tumours to increase the sensitivity of tumour screenings by MRI. Because we observed inhomogeneous receptor expression in the very same cell line and receptor loss in the *in vitro* models when cells grow over time future investigations should employ surgically removed human material and mouse models.

7 Zusammenfassung

Diese Arbeit beschäftigt sich mit dem Thema, ob VPAC-Rezeptoren als Schlüssel zur Krebsbekämpfung benützt werden können. Es gibt drei Subtypen von VPAC-Rezeptoren, $VPAC_1$, $VPAC_2$ und PAC_1, welche alle zur großen Familie der G-Protein gekoppelten Rezeptoren (GPCR) gehören und eine wichtige Rolle in der Zellsignaltransduktion spielen. Die zwei wesentlichsten VPAC-Rezeptor Liganden sind Neuropeptide, wie das Vasoaktive Intestinale Peptide (VIP) und das Hypophysen-Adenlyatzyklase-aktivierendes Polypeptid (PACAP). Diese kleinen Peptide üben ihre Funktion als Wachstumsfaktor in der Neurogenese und Entwicklung aus, stimulieren Hormonausschüttung, vermindern Entzündungen und unterstützen den Tumorwachstum. VIP wirkt auch als Vasodilator und relaxiert glatte Muskulatur. Frühere Studien vieler Arbeitsgruppen haben sich mit VPAC-Rezeptor Tumorerkennung und Diagnostik beschäftigt, wobei viele spezifische Agonisten und Antagonisten wurden dabei entwickelt. VIP ist in vielen Geweben weit verbreitet, wie zum Beispiel im Pankreas, Prostata, Thyroidea, Lunge, Brust, Skelett-und glatte Muskulatur und Gefäßen. Die VPAC Expression in endokrinen Tumorzellen zeigt eine Dominanz des $VPAC_1$ Rezeptors, in Gefäßen und Muskelzellen des $VPAC_2$ Rezeptors. PAC_1 ist hauptsächlich im Hirngewebe zu finden.

In dieser Arbeit haben wir uns mit drei Fragestellungen beschäftigt. Der selektive Agonist $(Ala^{11,22,28})$-VIP wird für die spezifische $VPAC_1$ Tumorerkennung eingesetzt. Mit diesem System können wir den durch Applikation ausgelösten hypotonen Schock umgehen und schaffen eine im Patienten angewandte spezifische $VPAC_1$ Tumorerkennung ohne Nebenwirkungen. $(Ala^{11,22,28})$-VIP verpackt in Liposome oder Proticle ermöglicht die spezifische Eintrittsstelle über den $VPAC_1$ Rezeptor, um Chemotherapeutika oder anti-sense RNS oder andere Pharmakophore einzuschleusen. Das zweite Thema behandelt sich mit dem Einsatz von VIP-DOTA-Gd in der Tumordiagnostik. Ein neuer nicht-radioaktiver Ansatz mit VIP-DOTA-Gd ermöglicht die Anwendung des Peptidkonjugates für Tumorscreens in der Magnetresonanz (MRI). Der dritte Gedanke beschäftigt sich mit einer selektiveren Anwendung von photodynamischer Therapie (PDT) über VPAC-Rezeptoren. Ein VIP-Hematoporphyrin Konjugat erkennt spezifisch VPAC positive Tumore und ermöglicht eine selektive Bestrahlung von erkranken Gewebe.

Am Beginn dieser Arbeit stand die Charakterisierung von 14 humanen Tumorzelllinien verschiedener Organe und einer mikrovaskulären endothelialen Zelllinie, welche mittels Immunozytochemie (ICC) mit spezifischen Antikörpern durchgeführt wurde. In der Zellkultur wurde eine heterogene Expression der VPAC-Rezeptoren gefunden, zB. bei PANC-1 Zellen, deshalb sollte eine Charakterisierung auch in lebenden Tumorgewebe, dass nach der Operation erhalten wird, durchgeführt werden. Die spezifische Interaktion zwischen Ligand und Rezeptor und die anschließende Internalisierung von VIP-Konjugaten, (Ala^{11,22,28})-VIP, VIP-DOTA-Gd und VIP-PDT, wurde mittels Fluoreszenz Korrelationsspektroskopie (FCS), Konfokale Laserscan Mikroskopie (CLSM) und cAMP ELISA durchgeführt. VIP eingeschlossen in Liposomen oder Proticle wurden als Beförderungsmittel zur Tumorzelle getestet, da VIP im Blut proteolytisch abgebaut wird und daher eine sehr geringe Halbwertszeit von 1-2 Minuten hat. Dieser Ansatz wurde mit cAMP ELISA nachgewiesen und zeigten Liposome und Protcles eine 20-30 minütige verzögerte cAMP-Ausschüttung gegenüber freiem VIP. Proliferations-und Zytotoxizitätsstudien (MTT-Test) wurden mit allen VIP-Konjugaten durchgeführt. Keines der VIP-Konjugate, VIP, VIP-DOTA-Gd, (Ala^{11,22,28})-VIP und PACAP zeigte eine zytotoxische Wirkung, manche Zelllinien nützen VIP und Konjugate sogar als Wachstumsfaktor. Das VIP-Hematoporphyrin Konjugat wurde auf seine Potenz als lichtempfindlicher chemischer Stoff, Photosensibilisator, getestet. Als Detektionssystem wurde DCFDA verwendet um die Freisetzung von Sauerstoff-reaktiven Spezies (ROS) durch VIP-PDT nach Bestrahlung nachzuweisen. Behandelte Tumorzellen mit VIP-PDT nach Bestrahlung zeigten keinen Anstieg von Sauerstoff-reaktiven Spezies und keine Reduktion des Zellwachstums. Die Apoptose oder Proliferation der Zellen wurde mit dem MTT-Test ermittelt. Als Kontrolle wurden die Tumorzellen mit einem bekannten Photosenibilisator, Photofrin® (Hematoporphyrin Oligomer), getestet. Ungefähr 20% der Zellen gingen nach Bestrahlung in Apoptose, daraus schließen wir, dass VIP-PDT mit einer einzelnen Hematoporphyrin Gruppe nicht in der Lage ist Sauerstoff-reaktive Spezies in der Zelle zu induzieren. Möglicherweise verhindert ein durch Strahlen ausgelöster Abwehrmechanismus der Zelle eine vermehrte Produktion von Sauerstoff-reaktiven Spezies.

Abschließend möchte ich die Wirksamkeit von (Ala^{11,22,28})-VIP, einem selektiven $VPAC_1$ Agonisten, hervorheben, welcher zukünftig der Schlüssel zur Einschleusung

von Chemotherapeutika oder anderen zellschädigenden Substanzen von VPAC-Rezeptor expremierenden Krebszellen sein könnte. Weiters hat VIP-DOTA-Gd das Potential als nicht-radioaktives Peptidkonjugat VPAC positive Tumore in einem Tumorscan mit MRI zu erkennen. Da wir inhomogene VPAC-Rezeptorexpression in der Zellkultur gezeigt haben, sollten die zukünftigen Arbeiten zu diesem Thema mit postoperativen Lebendtumorgewebe und Mausmodellen durchgeführt werden.

8 References

Adamou JE, Aiyar N, Van Horn S, Elshourbagy NA (1995) Cloning and functional characterization of the human vasoactive intestinal peptide (VIP)-2 receptor. Biochem Biophys Res Commun 209: 385-92

Ades EW, Candal FJ, Swerlick RA, George VG, Summers S, Bosse DC, Lawley TJ (1992) HMEC-1: establishment of an immortalized human microvascular endothelial cell line. J Invest Dermatol 99: 683-90

Alberts B JA, Lewis J, Raff M, Roberts K, Walter P (2002) Molecular Biology of the Cell. vol fourth edition. Garland Science, New York

Bachem (2005) Product Monograph VIP/PACAP. Bubendorf, Switzerland

Bellan C, Fabre C, Secchi J, Marvaldi J, Pichon J, Luis J (1992) Modulation of the expression of the VIP receptor by serum factors on the human melanoma cell line IGR39. Exp Cell Res 200: 34-40

Bhargava S, Licha K, Knaute T, Ebert B, Becker A, Grotzinger C, Hessenius C, Wiedenmann B, Schneider-Mergener J, Volkmer-Engert R (2002) A complete substitutional analysis of VIP for better tumor imaging properties. J Mol Recognit 15: 145-53

Bokaei PB, Ma XZ, Byczynski B, Keller J, Sakac D, Fahim S, Branch DR (2006) Identification and characterization of five-transmembrane isoforms of human vasoactive intestinal peptide and pituitary adenylate cyclase-activating polypeptide receptors. Genomics 88: 791-800

Busto R, Prieto JC, Bodega G, Zapatero J, Fogue L, Carrero I (2003) VIP and PACAP receptors coupled to adenylyl cyclase in human lung cancer: a study in biopsy specimens. Peptides 24: 429-36

Buytaert E, Dewaele M, Agostinis P (2007) Molecular effectors of multiple cell death pathways initiated by photodynamic therapy. Biochim Biophys Acta 1776: 86-107

Christophe J, Svoboda M, Waelbroeck M, Winand J, Robberecht P (1988) Vasoactive intestinal peptide receptors in pancreas and liver. Structure-function relationship. Ann N Y Acad Sci 527: 238-56

Dagar S, Sekosan M, Lee BS, Rubinstein I, Onyuksel H (2001) VIP receptors as molecular targets of breast cancer: implications for targeted imaging and drug delivery. J Control Release 74: 129-34

Delgado M (2002) Vasoactive intestinal peptide and pituitary adenylate cyclase-activating polypeptide inhibit CBP-NF-kappaB interaction in activated microglia. Biochem Biophys Res Commun 297: 1181-5

Delgado M, Leceta J, Ganea D (2003) Vasoactive intestinal peptide and pituitary adenylate cyclase-activating polypeptide inhibit the production of inflammatory mediators by activated microglia. J Leukoc Biol 73: 155-64

Delgado M, Martinez C, Johnson MC, Gomariz RP, Ganea D (1996) Differential expression of vasoactive intestinal peptide receptors 1 and 2 (VIP-R1 and VIP-R2) mRNA in murine lymphocytes. J Neuroimmunol 68: 27-38

Dickinson T, Fleetwood-Walker SM, Mitchell R, Lutz EM (1997) Evidence for roles of vasoactive intestinal polypeptide (VIP) and pituitary adenylate cyclase activating polypeptide (PACAP) receptors in modulating the responses of rat dorsal horn neurons to sensory inputs. Neuropeptides 31: 175-85

Domschke S, Domschke W, Bloom SR, Mitznegg P, Mitchell SJ, Lux G, Strunz U (1978) Vasoactive intestinal peptide in man: pharmacokinetics, metabolic and circulatory effects. Gut 19: 1049-53

Dong M, Pinon DI, Asmann YW, Miller LJ (2006) Possible endogenous agonist mechanism for the activation of secretin family G protein-coupled receptors. Mol Pharmacol 70: 206-13

Estival A, Mounielou P, Trocheris V, Scemama JL, Clemente F, Hollande E, Ribet A (1983) Presence of VIP receptors in a human pancreatic adenocarcinoma cell line. Modulation of the cAMP response during cell proliferation. Biochem Biophys Res Commun 111: 958-63

Goetzl EJ, Kodama KT, Turck CW, Schiogolev SA, Sreedharan SP (1989) Unique pattern of cleavage of vasoactive intestinal peptide by human lymphocytes. Immunology 66: 554-8

Gomer CJ, Ryter SW, Ferrario A, Rucker N, Wong S, Fisher AM (1996) Photodynamic therapy-mediated oxidative stress can induce expression of heat shock proteins. Cancer Res 56: 2355-60

Gourlet P, De Neef P, Cnudde J, Waelbroeck M, Robberecht P (1997a) In vitro properties of a high affinity selective antagonist of the VIP1 receptor. Peptides 18: 1555-60

Gourlet P, Vandermeers A, Vertongen P, Rathe J, De Neef P, Cnudde J, Waelbroeck M, Robberecht P (1997b) Development of high affinity selective VIP1 receptor agonists. Peptides 18: 1539-45

Gourlet P, Vertongen P, Vandermeers A, Vandermeers-Piret MC, Rathe J, De Neef P, Waelbroeck M, Robberecht P (1997c) The long-acting vasoactive intestinal polypeptide agonist RO 25-1553 is highly selective of the VIP2 receptor subclass. Peptides 18: 403-8

Gozes I, Bardea A, Reshef A, Zamostiano R, Zhukovsky S, Rubinraut S, Fridkin M, Brenneman DE (1996) Neuroprotective strategy for Alzheimer disease: intranasal administration of a fatty neuropeptide. Proc Natl Acad Sci U S A 93: 427-32

Gozes I, Brenneman DE (1989) VIP: molecular biology and neurobiological function. Mol Neurobiol 3: 201-36

Gozes I, Brenneman DE (2000) A new concept in the pharmacology of neuroprotection. J Mol Neurosci 14: 61-8

Gozes I, Meltzer E, Rubinrout S, Brenneman DE, Fridkin M (1989) Vasoactive intestinal peptide potentiates sexual behavior: inhibition by novel antagonist. Endocrinology 125: 2945-9

Gozes I, Reshef A, Salah D, Rubinraut S, Fridkin M (1994) Stearyl-norleucine-vasoactive intestinal peptide (VIP): a novel VIP analog for noninvasive impotence treatment. Endocrinology 134: 2121-5

Gozes Y, Brenneman DE, Fridkin M, Asofsky R, Gozes I (1991) A VIP antagonist distinguishes VIP receptors on spinal cord cells and lymphocytes. Brain Res 540: 319-21

Grant S, Lutz EM, McPhaden AR, Wadsworth RM (2006) Location and function of VPAC1, VPAC2 and NPR-C receptors in VIP-induced vasodilation of porcine basilar arteries. J Cereb Blood Flow Metab 26: 58-67

Gressens P, Hill JM, Gozes I, Fridkin M, Brenneman DE (1993) Growth factor function of vasoactive intestinal peptide in whole cultured mouse embryos. Nature 362: 155-8

Haberl I, Habringer DS, Andreae F, Artl A, Mosgoeller W (2006) New nonradioactive technique for vasoactive intestinal peptide-receptor-ligand-binding studies. Ann N Y Acad Sci 1070: 313-6

Hajos F SB, Hensler S, Prassl R, Mosgoeller W (2008) Inhalable liposomal formulation for vasoactive intestinal peptide. International Journal of Pharmaceutics in press

Halliwell B, Whiteman M (2004) Measuring reactive species and oxidative damage in vivo and in cell culture: how should you do it and what do the results mean? Br J Pharmacol 142: 231-55

Harmar AJ, Arimura A, Gozes I, Journot L, Laburthe M, Pisegna JR, Rawlings SR, Robberecht P, Said SI, Sreedharan SP, Wank SA, Waschek JA (1998) International Union of Pharmacology. XVIII. Nomenclature of receptors for vasoactive intestinal peptide and pituitary adenylate cyclase-activating polypeptide. Pharmacol Rev 50: 265-70

Hashimoto H, Nogi H, Mori K, Ohishi H, Shigemoto R, Yamamoto K, Matsuda T, Mizuno N, Nagata S, Baba A (1996) Distribution of the mRNA for a pituitary adenylate cyclase-activating polypeptide receptor in the rat brain: an in situ hybridization study. J Comp Neurol 371: 567-77

Henderson BW, Waldow SM, Mang TS, Potter WR, Malone PB, Dougherty TJ (1985) Tumor destruction and kinetics of tumor cell death in two experimental mouse tumors following photodynamic therapy. Cancer Res 45: 572-6

Heppeler A, Froidevaux S, Eberle AN, Maecke HR (2000) Receptor targeting for tumor localisation and therapy with radiopeptides. Curr Med Chem 7: 971-94

Hill JM, Gozes I, Hill JL, Fridkin M, Brenneman DE (1991) Vasoactive intestinal peptide antagonist retards the development of neonatal behaviors in the rat. Peptides 12: 187-92

Ichikawa Y, Nishida M, Miyazaki Y, Satoh T, Oki A, Nishide K, Kohno K, Tsunoda H, Kubo T (1996) [Incidence of synchronous or metachronous multiple primary cancers and aggregation of cancers in families of patients with endometrial cancer]. Nippon Sanka Fujinka Gakkai Zasshi 48: 835-40

Idee JM, Port M, Raynal I, Schaefer M, Le Greneur S, Corot C (2006) Clinical and biological consequences of transmetallation induced by contrast agents for magnetic resonance imaging: a review. Fundam Clin Pharmacol 20: 563-76

Igarashi H, Ito T, Hou W, Mantey SA, Pradhan TK, Ulrich CD, 2nd, Hocart SJ, Coy DH, Jensen RT (2002) Elucidation of vasoactive intestinal peptide pharmacophore for VPAC(1) receptors in human, rat, and guinea pig. J Pharmacol Exp Ther 301: 37-50

Ishihara T, Shigemoto R, Mori K, Takahashi K, Nagata S (1992) Functional expression and tissue distribution of a novel receptor for vasoactive intestinal polypeptide. Neuron 8: 811-9

Ito T, Igarashi H, Pradhan TK, Hou W, Mantey SA, Taylor JE, Murphy WA, Coy DH, Jensen RT (2001) GI side-effects of a possible therapeutic GRF analogue in monkeys are likely due to VIP receptor agonist activity. Peptides 22: 1139-51

Jiang S, Kopras E, McMichael M, Bell RH, Jr., Ulrich CD, 2nd (1997) Vasoactive intestinal peptide (VIP) stimulates in vitro growth of VIP-1 receptor-bearing human pancreatic adenocarcinoma-derived cells. Cancer Res 57: 1475-80

Juarranz MG, Bodega G, Prieto JC, Guijarro LG (2001) Vasoactive intestinal peptide (VIP) stimulates rat prostatic epithelial cell proliferation. Prostate 47: 285-92

Juarranz MG, Van Rampelbergh J, Gourlet P, De Neef P, Cnudde J, Robberecht P, Waelbroeck M (1999) Different vasoactive intestinal polypeptide receptor domains are involved in the selective recognition of two VPAC(2)-selective ligands. Mol Pharmacol 56: 1280-7

Kim WK, Kan Y, Ganea D, Hart RP, Gozes I, Jonakait GM (2000) Vasoactive intestinal peptide and pituitary adenylyl cyclase-activating polypeptide inhibit tumor necrosis factor-alpha production in injured spinal cord and in activated microglia via a cAMP-dependent pathway. J Neurosci 20: 3622-30

Koenig JA, Edwardson JM (1997) Endocytosis and recycling of G protein-coupled receptors. Trends Pharmacol Sci 18: 276-87

Kojima M, Ito T, Oono T, Hisano T, Igarashi H, Arita Y, Kawabe K, Coy DH, Jensen RT, Nawata H (2005) VIP attenuation of the severity of experimental pancreatitis is due to VPAC1 receptor-mediated inhibition of cytokine production. Pancreas 30: 62-70

Krempels K, Usdin TB, Harta G, Mezey E (1995) PACAP acts through VIP type 2 receptors in the rat testis. Neuropeptides 29: 315-20

Krenning EP, Kwekkeboom DJ, Valkema R, Pauwels S, Kvols LK, De Jong M (2004) Peptide receptor radionuclide therapy. Ann N Y Acad Sci 1014: 234-45

Laburthe M, Boissard C, Chevalier G, Zweibaum A, Rosselin G (1981) Peptide receptors in human lung tumor cells in culture: vasoactive intestinal peptide (VIP) and secretin interaction with the Calu-1 and SW-900 cell lines. Regul Pept 2: 219-30

Laburthe M, Couvineau A (2002) Molecular pharmacology and structure of VPAC Receptors for VIP and PACAP. Regul Pept 108: 165-73

Laburthe M, Couvineau A, Marie JC (2002) VPAC receptors for VIP and PACAP. Receptors Channels 8: 137-53

Laburthe M, Couvineau A, Tan V (2007) Class II G protein-coupled receptors for VIP and PACAP: Structure, models of activation and pharmacology. Peptides 28: 1631-9

Lelievre V, Meunier AC, Caigneaux E, Falcon J, Muller JM (1998) Differential expression and function of PACAP and VIP receptors in four human colonic adenocarcinoma cell lines. Cell Signal 10: 13-26

Levy A, Gal R, Granoth R, Dreznik Z, Fridkin M, Gozes I (2002) In vitro and in vivo treatment of colon cancer by VIP antagonists. Regul Pept 109: 127-33

Lilling G, Wollman Y, Goldstein MN, Rubinraut S, Fridkin M, Brenneman DE, Gozes I (1994) Inhibition of human neuroblastoma growth by a specific VIP antagonist. J Mol Neurosci 5: 231-9

Lutz EM, Sheward WJ, West KM, Morrow JA, Fink G, Harmar AJ (1993) The VIP2 receptor: molecular characterisation of a cDNA encoding a novel receptor for vasoactive intestinal peptide. FEBS Lett 334: 3-8

Marchal S, Fadloun A, Maugain E, D'Hallewin MA, Guillemin F, Bezdetnaya L (2005) Necrotic and apoptotic features of cell death in response to Foscan photosensitization of HT29 monolayer and multicell spheroids. Biochem Pharmacol 69: 1167-76

Maruno K, Absood A, Said SI (1998) Vasoactive intestinal peptide inhibits human small-cell lung cancer proliferation in vitro and in vivo. Proc Natl Acad Sci U S A 95: 14373-8

Miyata A, Arimura A, Dahl RR, Minamino N, Uehara A, Jiang L, Culler MD, Coy DH (1989) Isolation of a novel 38 residue-hypothalamic polypeptide which stimulates adenylate cyclase in pituitary cells. Biochem Biophys Res Commun 164: 567-74

Moody TW (1996) Peptides and growth factors in non-small cell lung cancer. Peptides 17: 545-55

Moody TW, Czerwinski G, Tarasova NI, Moody DL, Michejda CJ (2004) The development of VIP-ellipticine conjugates. Regul Pept 123: 187-92

Moody TW, Hill JM, Jensen RT (2003) VIP as a trophic factor in the CNS and cancer cells. Peptides 24: 163-77

Moody TW, Leyton J, Chan D, Brenneman DC, Fridkin M, Gelber E, Levy A, Gozes I (2001) VIP receptor antagonists and chemotherapeutic drugs inhibit the growth of breast cancer cells. Breast Cancer Res Treat 68: 55-64

Moody TW, Leyton J, Gozes I, Lang L, Eckelman WC (1998) VIP and breast cancer. Ann N Y Acad Sci 865: 290-6

Moody TW, Walters J, Casibang M, Zia F, Gozes Y (2000) VPAC1 receptors and lung cancer. Ann N Y Acad Sci 921: 26-32

Moro O, Lerner EA (1997) Maxadilan, the vasodilator from sand flies, is a specific pituitary adenylate cyclase activating peptide type I receptor agonist. J Biol Chem 272: 966-70

Moro O, Wakita K, Ohnuma M, Denda S, Lerner EA, Tajima M (1999) Functional characterization of structural alterations in the sequence of the vasodilatory peptide maxadilan yields a pituitary adenylate cyclase-activating peptide type 1 receptor-specific antagonist. J Biol Chem 274: 23103-10

Muller JM, Lelievre V, Becq-Giraudon L, Meunier AC (1995) VIP as a cell-growth and differentiation neuromodulator role in neurodevelopment. Mol Neurobiol 10: 115-34

Nelson D L CMM (2004) Lehninger Principles of Biochemistry. vol fourth edition. Palgrave Macmillan

Nicole P, Lins L, Rouyer-Fessard C, Drouot C, Fulcrand P, Thomas A, Couvineau A, Martinez J, Brasseur R, Laburthe M (2000) Identification of key residues for interaction of vasoactive intestinal peptide with human VPAC1 and VPAC2 receptors and development of a highly selective VPAC1 receptor agonist. Alanine scanning and molecular modeling of the peptide. J Biol Chem 275: 24003-12

Ou X, Tan T, He L, Li Y, Li J, Kuang A (2005) Antitumor effects of radioiodinated antisense oligonuclide mediated by VIP receptor. Cancer Gene Ther 12: 313-20

Pilzer I, Gozes I (2006) VIP provides cellular protection through a specific splice variant of the PACAP receptor: a new neuroprotection target. Peptides 27: 2867-76

Pisegna JR, Wank SA (1993) Molecular cloning and functional expression of the pituitary adenylate cyclase-activating polypeptide type I receptor. Proc Natl Acad Sci U S A 90: 6345-9

Reubi C, Gugger M, Waser B (2002) Co-expressed peptide receptors in breast cancer as a molecular basis for in vivo multireceptor tumour targeting. Eur J Nucl Med Mol Imaging 29: 855-62

Reubi JC (2000) In vitro evaluation of VIP/PACAP receptors in healthy and diseased human tissues. Clinical implications. Ann N Y Acad Sci 921: 1-25

Reubi JC (2003) Peptide receptors as molecular targets for cancer diagnosis and therapy. Endocr Rev 24: 389-427

Reubi JC, Laderach U, Waser B, Gebbers JO, Robberecht P, Laissue JA (2000) Vasoactive intestinal peptide/pituitary adenylate cyclase-activating peptide receptor subtypes in human tumors and their tissues of origin. Cancer Res 60: 3105-12

Reubi JC, Waser B, Schmassmann A, Laissue JA (1999) Receptor autoradiographic evaluation of cholecystokinin, neurotensin, somatostatin and vasoactive intestinal peptide receptors in gastro-intestinal adenocarcinoma samples: where are they really located? Int J Cancer 81: 376-86

Rosselin G, Anteunis A, Astesano A, Boissard C, Gali P, Hejblum G, Marie JC (1988) Regulation of the vasoactive intestinal peptide receptor. Ann N Y Acad Sci 527: 220-37

Rubinstein I (2005) Human VIP-alpha: an emerging biologic response modifier to treat primary pulmonary hypertension. Expert Rev Cardiovasc Ther 3: 565-9

Saczko J, Mazurkiewicz M, Chwilkowska A, Kulbacka J, Kramer G, Lugowski M, Snietura M, Banas T (2007) Intracellular distribution of Photofrin in malignant and normal endothelial cell lines. Folia Biol (Praha) 53: 7-12

Said SI MV (1970) Potent peripheral and splanchnic vasodilator peptide from normal gut. Nature 225: 863-864

Said SI MV (1972) Isolation from porcine-intestinal wall of a vasoactive octacosapeptide related to secretin and to glucagon. Eur J Biochem. 28: 199-204

Schmidt DT, Ruhlmann E, Waldeck B, Branscheid D, Luts A, Sundler F, Rabe KF (2001) The effect of the vasoactive intestinal polypeptide agonist Ro 25-1553 on induced tone in isolated human airways and pulmonary artery. Naunyn Schmiedebergs Arch Pharmacol 364: 314-20

Schulz S, Rocken C, Mawrin C, Weise W, Hollt V, Schulz S (2004) Immunocytochemical identification of VPAC1, VPAC2, and PAC1 receptors in normal and neoplastic human tissues with subtype-specific antibodies. Clin Cancer Res 10: 8235-42

Schwille P HE (2004) Fluorescence Correlation Spectroscopy, An Introduction to its Concepts and Applications. Biophysics Textbook Online

Sejourne F, Rubinstein I, Suzuki H, Alkan-Onyuksel H (1997) Development of a novel bioactive formulation of vasoactive intestinal peptide in sterically stabilized liposomes. Pharm Res 14: 362-5

Sethi V, Onyuksel H, Rubinstein I (2005) Liposomal vasoactive intestinal peptide. Methods Enzymol 391: 377-95

Sherwood NM, Krueckl SL, McRory JE (2000) The origin and function of the pituitary adenylate cyclase-activating polypeptide (PACAP)/glucagon superfamily. Endocr Rev 21: 619-70

Shetzline MA, Walker JK, Valenzano KJ, Premont RT (2002) Vasoactive intestinal polypeptide type-1 receptor regulation. Desensitization, phosphorylation, and sequestration. J Biol Chem 277: 25519-26

Sheward WJ, Lutz EM, Harmar AJ (1995) The distribution of vasoactive intestinal peptide2 receptor messenger RNA in the rat brain and pituitary gland as assessed by in situ hybridization. Neuroscience 67: 409-18

Sosabowski JK, Mather SJ (2006) Conjugation of DOTA-like chelating agents to peptides and radiolabeling with trivalent metallic isotopes. Nat Protoc 1: 972-6

Spengler D, Waeber C, Pantaloni C, Holsboer F, Bockaert J, Seeburg PH, Journot L (1993) Differential signal transduction by five splice variants of the PACAP receptor. Nature 365: 170-5

Stark B, Debbage P, Andreae F, Mosgoeller W, Prassl R (2007) Association of vasoactive intestinal peptide with polymer-grafted liposomes: structural aspects for pulmonary delivery. Biochim Biophys Acta 1768: 705-14

Sundler F, Ekblad E, Hannibal J, Moller K, Zhang YZ, Mulder H, Elsas T, Grunditz T, Danielsen N, Fahrenkrug J, Uddman R (1996) Pituitary adenylate cyclase-activating peptide in sensory and autonomic ganglia: localization and regulation. Ann N Y Acad Sci 805: 410-26; discussion 427-8

Uchida D, Tatsuno I, Tanaka T, Hirai A, Saito Y, Moro O, Tajima M (1998) Maxadilan is a specific agonist and its deleted peptide (M65) is a specific antagonist for PACAP type 1 receptor. Ann N Y Acad Sci 865: 253-8

Usdin TB, Bonner TI, Mezey E (1994) Two receptors for vasoactive intestinal polypeptide with similar specificity and complementary distributions. Endocrinology 135: 2662-80

Vanneste G, Robberecht P, Lefebvre RA (2004) Inhibitory pathways in the circular muscle of rat jejunum. Br J Pharmacol 143: 107-18

Vaudry D, Gonzalez BJ, Basille M, Yon L, Fournier A, Vaudry H (2000) Pituitary adenylate cyclase-activating polypeptide and its receptors: from structure to functions. Pharmacol Rev 52: 269-324

Virgolini I, Kurtaran A, Leimer M, Kaserer K, Peck-Radosavljevic M, Angelberger P, Hubsch P, Dvorak M, Valent P, Niederle B (1998) Location of a VIPoma by iodine-123-vasoactive intestinal peptide scintigraphy. J Nucl Med 39: 1575-9

Virgolini I, Raderer M, Kurtaran A, Angelberger P, Banyai S, Yang Q, Li S, Banyai M, Pidlich J, Niederle B, Scheithauer W, Valent P (1994a) Vasoactive intestinal peptide-receptor imaging for the localization of intestinal adenocarcinomas and endocrine tumors. N Engl J Med 331: 1116-21

Virgolini I, Raderer M, Kurtaran A, Angelberger P, Yang Q, Radosavljevic M, Leimer M, Kaserer K, Li SR, Kornek G, Hubsch P, Niederle B, Pidlich J, Scheithauer W, Valent P (1996) 123I-vasoactive intestinal peptide (VIP) receptor scanning: update of imaging results in patients with adenocarcinomas and endocrine tumors of the gastrointestinal tract. Nucl Med Biol 23: 685-92

Virgolini I, Yang Q, Li S, Angelberger P, Neuhold N, Niederle B, Scheithauer W, Valent P (1994b) Cross-competition between vasoactive intestinal peptide and somatostatin for binding to tumor cell membrane receptors. Cancer Res 54: 690-700

Warner RR, O'Dorisio T M (2002) Radiolabeled peptides in diagnosis and tumor imaging: clinical overview. Semin Nucl Med 32: 79-83

Wei Y, Mojsov S (1996) Tissue specific expression of different human receptor types for pituitary adenylate cyclase activating polypeptide and vasoactive intestinal polypeptide: implications for their role in human physiology. J Neuroendocrinol 8: 811-7

Williams C (2004) cAMP detection methods in HTS: selecting the best from the rest. Nat Rev Drug Discov 3: 125-35

Wollman Y, Lilling G, Goldstein MN, Fridkin M, Gozes I (1993) Vasoactive intestinal peptide: a growth promoter in neuroblastoma cells. Brain Res 624: 339-41

Xia M, Sreedharan SP, Bolin DR, Gaufo GO, Goetzl EJ (1997) Novel cyclic peptide agonist of high potency and selectivity for the type II vasoactive intestinal peptide receptor. J Pharmacol Exp Ther 281: 629-33

Yamada H, Watanabe M, Yada T (2004) Cytosolic Ca2+ responses to sub-picomolar and nanomolar PACAP in pancreatic beta-cells are mediated by VPAC2 and PAC1 receptors. Regul Pept 123: 147-53

Yang XM, Ma HJ, Geng XZ, Zhang XR (2007) [Hematoporphyrin derivative-mediated photodynamic therapy for human colon carcinoma: a comparative study with LoVo and CoLo205 cells in vitro]. Nan Fang Yi Ke Da Xue Xue Bao 27: 1251-3, 1256

Zia H, Hida T, Jakowlew S, Birrer M, Gozes Y, Reubi JC, Fridkin M, Gozes I, Moody TW (1996) Breast cancer growth is inhibited by vasoactive intestinal peptide (VIP) hybrid, a synthetic VIP receptor antagonist. Cancer Res 56: 3486-9

9 Abbreviations used

$^1O_2$	Singlet oxygen
$^3O_2$	Triplet oxygen
aa	Amino acid
Ab	Antibody
AC	Adenlyate cyclase
Approx.	Approximate
ATCC	American Type Culture Collection
ATP	Adenosinetriphosphate
BBB	Blood-brain barrier
Bidest.	Bidestillated
bp	Base pair
cAMP	cyclic Adenosinemonophosphate
CLSM	Confocal laser scanning microscope
CNS	Central nerve system
conc.	Concentration
CRE	cAMP response element
CREB	CRE binding protein
C-terminus	Carboxy terminus
Cy3	Indocarbocanin 3
Cy3-Scr-VIP	Cy3-scrambled-vasoactive intestinal peptide
DAG	Diacylglycerol
DCF	2´7´-dichlorofluorescein
DCFDA	Dichlorofluorescin diacetate
DMEM	Dulbecco´s Modified Eagle´s Medium
DNA	Desoxyribonuclein acid
DOTA	1,4,7,10-tetraazacyclododecane-1,4,7,10-tetraacetic acid
DOTA-Gd	DOTA-Gadolinium, Gadoteratemeglumine
DTPA	dietyhlenetriaminopentaacetic acid
EC	Extracellular
EGF	Endothelial growth factor
ELISA	Enzyme linked immune sorbent assay

ER	endoplasmatic reticulum
Et-Cy3-OH	Ethyl-Cy3-hydroxy
FBS	fetal bovine serum
FCS	Fluorescence correlation spectroscopy
Fig.	Figure
Fluo	Fluorescein
FMOC-SPPS	FMOC solid-phase peptide synthesis
GALT	Gut associated lymphoid tissue
Gd-DPTA	Gadopentetatedimeglumine
Gd-DTPA-BMA	Gadodiamide
Gd-HP-DO3A	Gadoteridol
GDT	Guanine diphosphate
GH	Growth hormone
GLP-1/2	Glucagon like peptide-1/2
GPCR	G-protein coupled receptors
G_q	Stimulating G protein (activtes PLC-β)
GRF	Growth releasing factor
GRK	G-protein kinases
G_s	stimulatory G protein
GTP	Guanine triphosphate
h	hour
HRP	Horseradish peroxidase
IBMX	1-methyl-3-(2-methylpropyl)-7H-purine-2,6-dione
IC	Intracellular
IC_{50}	Half maximum inhibitory concentration
ICC	Immunocytochemistry
IP_3	Inositol-1,4,5-triphosphate
kDa	Kilo Dalton
LH	Luteinizing hormone
max.	Maximum
MEME	Egale´s Minimum Essential with Egale´s Salt
min	Minutes

MRI	Magnet resonance imaging
MTT	3-(4,5-Dimethylthiazol-2-yl)-2,5-diphenyltetrazoliumbromid test
NEAA	Non-essential amino acids
NFAT-RE	Nuclear factor of activated T-cells response element
Nle	Norleucine
N-ted	Ectodomain
N-terminus	Amino-terminus
OCT	Octreatide
PAC_1	PACAP-preferring receptor subtype
PACAP	Pituitary adenlyate cyclase activating polypeptide
PAGE	Polyacrylamide gel electrophoresis
PALS	Periateriolar lymphocyte sheath
PBS	Phosphate buffer saline
PCD	Programmed cell death
PDT	Photodynamic therapy
PET	Photon emission tomography
PFA	Paraformaldehyd
PIP_2	Phosphatidylinositol biphosphate
PKA	cAMP-depending protein kinase
PKC	Ca^{2+}-depending protein kinase
PLC/PI	Inositol phospholipid signalling pathway
PP_i	Pyrophosphate
PRL	Prolactin
PRP	PACAP released peptide
PS	Photosan
RNS	Ribonukleinsäure
ROS	Reactive oxygen species
RP-HPLC	Reverse phase- high pressure liquid chromatographie
RT	Room temperature
s	Seconds
SCLC	Small cell lung cancer
SCN	Suprachiasmatic nucleus

SCR	Short consensus repeats
SDS	Sodium dodecyl sulphate
SP	signal peptide
SQ22,536	[9-(tetrahydro-2-furanyl)-9H-purin-6-amine]
Std	Standard
$T_{1/2}$	Half life time
Tab.	Table
TFA	Trifluoracetat salt
TM	Transmembrane domain
TPBS	Tween-phosphate buffer saline
TTBS	Tween-TRIS-buffer saline
UIPHAR	Union of pharmacology
VIP	Vasoactive intestinal peptide
WB	Western Blot

10 Index of Figures

11 Index of Tables

12 Curriculum vitae

Name Raphaela Elisabeth KAISLER

Born 17th April 1984, Vienna, Austria

Address Rosinagasse 1-3/22, A-1150 Vienna, Austria

e-mail: raphaela.kaisler@aon.at

Tel.: 0043-650-517-04-84 or 0043-1-892-03-88

Nationality Austria

Parents Ing. Rudolf und Roswitha Kaisler

Brother MMag. Rudolf Kaisler

Education

- 1990 – 1994 primary school, A-1130 Vienna
- 1994 – 1998 grammar school BRG XII, A-1120 Vienna
- 1998 – 2003 secondary school, HBLVA for chemical industry,
  Rosensteingasse A-1170 Vienna (5 years duration)
  specialiation: biochemistry, biotechnology and gene technology
  11th June 2003 final exam with diploma project „Core fucosylation in *Caenorhabditis elegans* “
- Oct 2003-Feb 2008 ***Master program „Molecular Biology“*** (10 terms)
  University Vienna, Dr. Bohrgasse 7, A-1030 Vienna
  Specialisation: Cell biology, genetics and neuroscience
  degree: Magistra rerum naturalis (Mag.rer.nat.)

  Diploma thesis at Institute of Cancer Research, Medical University Vienna
  Borschkegasse 8a, A-1090 Vienna
  Supervisor: a.o.Univ.Prof.Dr.Wilhelm Mosgoeller
  Issue: *VPAC receptors as target for anti-cancer drug delivery*
  Duration: March 2007-February 2008
  Methods: western blot (WB), immunocytochemistry (ICC), fluorescent correlation spectroscopy (FCS), ELISA analyses, confocal laser scanning microscopy (CLSM), cell culture, cell proliferation assay (MTT tests), reactive oxygen species (ROS) and photodynamic therapy assays (PDT)
  Diploma student’s stipend by the Institute of Cancer Research Vienna

Projects/ Publications

- *Congress ELSO 2007, Dresden Germany*
  first author poster "VPAC receptors as target for anti-cancer drug delivery"
- *Meeting of the Medical Univiersty of Vienna 21./22.June 2007*
  first author poster "Vasoactive intestinal peptide (VIP) internalisation as strategy for anti cancer drug delivery "

Business practise

- August 2002: ***diploma project for school final exam***
  research project: „Core fucosylation in *Caenorhabditis elegans*"
  University for Bodenkultur (BOKU), A-1190 Vienna, Institute of chemistry, Vienna Glycobiology
  Supervisor: a.o.Univ.Prof.Dr. Iain Wilson and Dipl.Ing. Katharina Paschinger
  Supervisor (internal): Dipl.Ing.Dr. Otto Meixner
  Methods: cloning of plasmids, transformation in E.coli, PCR analysis, HPLC, SDS PAGE, western blot

- Januar 2004-June 2005: ***scientific freelance***
  Clinical Institute of Medical and Chemical Laboratory Diagnostics, Molecular Biology Division, University Vienna Medical School, 1090 Vienna
  Research project: „The influence of platelet separation methods on platelet glycoprotein expression"
  Supervisor: a.o.Univ.Prof. Dr. Christine Mannhalter
  Methods: isolation of platelets from donor blood, extraction of RNA, quality and quantity PCR analysis, electrophoresis

- July 2005 -October 2005: ***Traineeship in Lund*** , Sweden
  University Lund, Department of Cell and Organism Biology, 22362 Lund
  Research project: Molecular genetic of telomeres
  Supervisor: associated professor PhD Marita Cohn
  Responsibility: Electrophoretic mobility shift assay (EMSA), cloning transformation and colony hybridisation, DNA sequencing, genomic DNA

preparation, restriction enzyme cleavage, Southern blot hybridisation, PCR amplification.
Leonardo da Vinci Educational Program fellowship

- June 2006-March 2007: ***scientific freelance***
  Max Perutz Laboratories University Vienna, A-1030 Vienna
  Institute of Cancer Research, Medical University Vienna, A-1090 Vienna
  Supervisor: Prof. Gottfried Koehler, Prof. Wilhelm Mosgoeller
  Project: VIP analogue internalisation studies via VPAC receptors
  Methods: Fluorescence Correlation Spectroscopy (FCS), ELISA analyses, cell culture

- January-March 2007, 2008: ***tutor***
  Tutorium for human anatomy section course for anthropologists
  Department of Anatomy and Cell Biology, Währingerstraße 13, A-1090 Vienna

Speaking language	German native, English fluently, Finnish basics skills
PC knowledge	Microsoft Office (Word, Excel, Power Point, Access, Outlook) Endnote, Sigma Plot, Origin